EARTHQUAKE RESPONSE ANALYSIS OF MULTIPLE TOWERS ON A COMMON PODIUM

by

Cem Tura

B.S., Civil Engineering, Boğaziçi University, 2014

Submitted to the Institute for Graduate Studies in
Science and Engineering in partial fulfillment of
the requirements for the degree of
Master of Science

Graduate Program in Civil Engineering

Boğaziçi University

2017

EARTHQUAKE RESPONSE ANALYSIS OF MULTIPLE TOWERS ON A COMMON PODIUM

APPROVED BY:

Assoc. Prof. Kutay Orakçal (Thesis Supervisor)	. . . . .
Assoc. Prof. Serdar Soyöz	. . . . .
Assoc. Prof. Ufuk Yazgan	. . . . .

DATE OF APPROVAL: 15.08.2017

To my father, Structural Engineer Kemal Tura

ACKNOWLEDGEMENTS

Before everyone else, I would like thank to my mother, Süheyla Tura for her endless support, encouragement and all the sacrifices she made through my life.

I would also like to express my sincere gratitude to my thesis supervisor Associate Professor Kutay Orakçal for his invaluable guidance and support throughout my studies. I am also grateful to him for his endless patience and positive attitude during preparation of this thesis.

Besides, I would like to express my special thanks to Associate Professor Serdar Soyöz and Associate Professor Ufuk Yazgan for accepting to be in my thesis jury and for their valuable comments to my study and suggestions for future works.

Also, I would like to thank Murat Can Tura and Filiz Alpgezmen for their persistent supports at the tough days of preparation period of this study.

Last but not least, I would like to thank from my deep heart to my beloved friend Mine Cetiz for all the patience and tolerances throughout all my studies.

ABSTRACT

EARTHQUAKE RESPONSE ANALYSIS OF MULTIPLE TOWERS ON A COMMON PODIUM

In this study, one of the complex structural systems that requires extra caution during the design process, a tall building structure with multiple towers on a common podium, is analyzed considering effects of interaction between the towers due to connected podium floors. Nonlinear response history analysis is essential for performance-based design of tower structures. However, due to excessive computational demands of nonlinear analysis, using combined models for the multiple towers throughout design process is usually not viable. Therefore, to reduce analysis duration, analyzing separate single-tower models, using assumptions that typically neglect the interaction, is a common industry-standard approach. However, for more reliable response predictions, interaction of the towers with each other must be implemented in the analysis. In the current study, interaction effects of the podium floors are considered in the analyses, first using a simple approach of assigning either fixed or free end restraints at the continuous boundaries of the single-tower models. Responses of the single tower models are then compared with the response obtained using a combined model, which includes both of the towers as well as the common podium and basement floors. Results of various linear and nonlinear analysis methods are compared and the effects of interaction on the structural response are discussed. In addition to important response parameters associated with the tower structures, in-plane tensile and shear force distributions developing in the podium floors are also considered as critical design quantities. Results obtained demonstrate that response spectrum and linear response history analysis methods used for analyzing the combined model provide comparable internal tension and shear force resultants acting on the podium floors. The nonlinear analysis results obtained using the combined model for the tower response quantities are generally closer to those obtained from the single-tower model with free end restraints at the continuous boundaries. In both linear and nonlinear analyses, single-tower models with fixed end restraints overestimate the internal tension and shear forces at the podium floors, although to a reasonable extent.

ÖZET

ORTAK BAZALI ÇOKLU KULE YAPILARININ DEPREM ANALİZİ

Bu çalışmada, tasarım aşamasında özel dikkat gerektiren yapı sistemlerinden biri olan ortak bazalı birden fazla kule içeren bir yüksek bina yapısının deprem davranışı, kulelerin birbirleriyle olan etkileşimi de gözetilerek incelenmiştir. Kule yapılarının performansa dayalı tasarımında, yapının doğrusal olmayan deprem davranışı gözetilmelidir. Fakat, doğrusal olmayan davranış analizi, aşırı hesaplama yükü getirdiğinden, tasarım aşamasında bütün kuleleri içeren modellerin analizleri, projelerin zaman kısıtlaması nedeniyle çoğu zaman mümkün olmamaktadır. Bu nedenle, analiz yükünü azaltmak amacıyla kulelerin bazı varsayımlar çerçevesinde ayrı analiz edilmeleri mühendislik uygulamalarında sıklıkla kullanılan bir yaklaşımdır. Ancak daha güvenilir analiz sonuçları için kulelerin birbirleriyle olan etkileşimleri analizde dikkate alınmalıdır. Bu çalışmada kulelerin birbirleriyle etkileşimleri, basit bir yaklaşımla, en az ve en çok etkiyi gözetecek şekilde tekli modellerde modelin kesildiği ancak bazanın devam ettiği bölgelere tutulu veya hareketli mesnetler atanarak incelenmiştir. Tekli modellerin analiz sonuçları hem her iki kuleyi hem de ortak baza ve bodrum yapısını içeren birleştirilmiş modelin analiz sonuçları ile karşılaştırılmıştır. Kullanılan doğrusal ve doğrusal olmayan analiz yöntemlerinin sonuçları irdelenmiş, kulelerin etkileşiminin yapının deprem davranışına etkileri incelenmiştir. Kulelerin tasarımı için önemli olan davranış büyüklüklerine ek olarak baza döşemelerindeki eksenel çekme ve düzlem içi kesme kuvveti dağılımları da kritik tasarım değerleri olarak dikkate alınmıştır. Analiz sonuçları, birleştirilmiş model ile yapılan doğrusal mod birleştirme ve zaman tanım alanında doğrusal analiz yöntemlerinin baza döşemelerinde birbirine yakın düzlem içi çekme ve kesme kuvveti değerleri verdiğini göstermektedir. Birleştirilmiş modelin zaman tanım alanında doğrusal olmayan analizinden kulelerin davranış büyüklükleri için elde edilen değerlerin genel olarak hareketli mesnetli tekli modelin analiz sonuçlarına yakın mertebede olduğu gözlemlenmiştir. Bütün analiz yöntemlerinde, sabit mesnetli tekli modelin baza katlarındaki eksenel çekme ve kesme kuvvetleri için birleştirilmiş modele kıyasla daha büyük, ancak güvenli tarafta kalacak şekilde makul büyüklükte değerler elde edilmiştir.

TABLE OF CONTENTS

LIST OF FIGURES

LIST OF TABLES

LISY OF SYMBOLS

A_g	Cross-sectional area of column
A_s	Total area of longitudinal reinforcements
A_{sh}	Total cross-sectional area of stirrups and ties in single spacing
a_i	Span length between longitudinal reinforcements for space no *i*
b_0	Width of confined core
b_w	Width of section
D	Over strength factor
d	Effective height of section
E_c	Tangent modulus of elasticity of concrete
E_{ce}	Effective modulus elasticity of concrete
$E_d^{(Z)}$	Earthquake load on Z direction
E_s	Modulus of elasticity of reinforcing steel
E_{sec}	Secant modulus of elasticity of concrete
e_{cc}	Strain at compressive strength of confined concrete
e_{co}	Strain at compressive strength of unconfined concrete
F_1	Local soil effect coefficient for 1s period
F_S	Local soil effect coefficient for short period
f_c	Stress at concrete
f_{cc}	Compressive strength of confined concrete
f_{ce}	Expected compressive strength of concrete
f_{ck}	Characteristic compressive strength of concrete
f_{co}	Compressive strength of unconfined concrete
f_{csd}	Design shear strength of concrete
f_{cse}	Expected shear strength of concrete
f_{ctd}	Design tensile strength of concrete
f_{cte}	Expected tensile strength of concrete

f_e	Effective confining stress
f_{ex}	Effective confinement pressure on X direction
f_{ey}	Effective confinement pressure on Y direction
f_s	Stress at reinforcing steel
f_{su}	Ultimate strength of reinforcing steel
f_{sy}	Yield strength of reinforcing steel
f_{syd}	Design tensile strength of reinforcing steel
f_{sye}	Expected tensile strength of reinforcements
G	Gravitational constant
g	Gravitational constant
G_c	Shear modulus of concrete
G_{ce}	Effective shear modulus of concrete
h	Height of section
h_0	Height of confined core
k_e	Confinement effectiveness factor
L_F	Distance between closest active fault and project site
n	Live load contribution factor
n_B	Live load contribution factor for basement parking garages
n_C	Live load contribution factor for commercial zones
n_R	Live load contribution factor for residential zones
m	Number of ground motion pairs
$m_j^{(s)}$	Seismic mass at node j
P	Maximum compressive load from nonlinear analysis
Q	Capacity
Q_y	Yield capacity
R	Structural behavior factor
R_{JB}	Joyner-Boore distance
r	Parameter defining shape of monotonic stress- strain curve of concrete
S_1	Spectral acceleration coefficient for 1s period

S_S	Spectral acceleration coefficient for short period
S_{aer}	Record spectral elastic acceleration
S_{aet}	Target spectral elastic acceleration
$S_{ae}(T)$	Elastic spectral acceleration at period T
S_{D1}	Design spectral acceleration coefficient for 1s period
S_{DS}	Design spectral acceleration coefficient for short period
s	Spacing between confinements
T	Natural vibration period
T_A	Left corner period for spectrum
T_B	Right corner period for spectrum
T_{ij}	Natural vibration period of tower *i* on *j* direction
T_L	Constant spectral displacement range period limit
T_P	Fundamental period of the structure
V	Maximum shear force from nonlinear analyses
V_{S30}	Shear wave velocity at first 30m of soil
w_i	Weight of period
$w_j^{(s)}$	Seismic weight at node *j*
$w_{G,j}^{(s)}$	Seismic weight at node *j* from dead loads
$w_{Q,j}^{(s)}$	Seismic weight at node *j* from live loads
x	Ratio of strain to strain at compressive strength of confined concrete
a	Hilber-Hughes-Taylor Method coefficient
α_m	Rayleigh damping mass proportional damping coefficient
β_k	Rayleigh damping stiffness proportional damping coefficient
β	Hilber-Hughes-Taylor Method coefficient
Δ	Displacement
ε_s	Strain at reinforcing steel
ε_{sh}	Strain hardening initiation strain
ε_{su}	Ultimate strain capacity

γ	Hilber-Hughes-Taylor Method coefficient
γ_c	Specific weight of concrete
γ_F	Fault distance coefficient
ξ_i	Critical damping ratio for mode *i*
λ_c	Confined concrete strength modifier
ω_i	Natural vibration frequency of mode *i*
ϕ	Diameter of reinforcement
ν_c	Poisson's ratio of concrete
ρ	Ratio of beam bottom reinforcements
ρ'	Ratio of beam top reinforcements
ρ_{bal}	Balanced reinforcement ratio
ρ_S	Ratio of shear reinforcement
ρ_{sh}	Volumetric confinement ratio
ρ_x	Confinement ratio on X direction
ρ_y	Confinement ratio on Y direction
$\sum X$	Total mass participation ratio on X direction
$\sum Y$	Total mass participation ratio on Y direction
θ	Rotation

LIST OF ACRONYMS/ABBREVIATONS

ASCE	American Society of Civil Engineers
ATC	Applied Technology Council
CQC	Complete quadratic combination
CP	Collapse prevention
CSI	Computers and Structures, Inc.
CTBUH	Council on Tall Buildings and Urban Habitat
DOF	Degree of freedom
FEM	Finite element modeling
FEMA	Federal Emergency Management Agency
IO	Immediate occupancy
LATBSDC	Los Angeles Tall Buildings Structural Design Council
LDIRHA	Linear direct integration response history analysis
LMRHA	Linear modal response history analysis
LS	Life safety
MSE	Mean squared error
NLRHA	Nonlinear response history analysis
OCH	Over critical height
PBD	Performance-based design
PEER	Pacific Earthquake Engineering Research Center
PSHA	Probabilistic seismic hazard analysis
RSA	Response spectrum analysis
SEAOC	Structural Engineers Association of California
SRSS	Square root of sum of squares
TBI	Tall Buildings Initiative
TEC	Turkish Earthquake Code
TEHM	Turkish Earthquake Hazard Map
TS	Turkish Standards
UCH	Under critical height

1. INTRODUCTION

1.1. General

Due to recent population increase all around the world, especially on metropolises, to prevent aggressive horizontal growth or due to land scarceness, demand on tall buildings significantly increased. Thanks to developments in structural engineering and the construction industry, number of tall building projects has risen remarkably. On the other hand, since structural design of tall buildings is much more complicated than design of regular structures, requirements for design process also increased correlatively. Furthermore, because of the fact that these skyscrapers are also considered as iconic buildings, modern architectural demands started to cause additional complexities for structural engineers. Structures incorporating multiple towers on common podium are one of these special structures that must be designed with extra attention.

Dynamic behavior of multiple towers on a common base is more complicated than single towers due to interaction at the connecting podium levels. In most projects, dynamic properties of towers are likely to differ from each other. Even though structural properties of the towers are identical, during real seismic events, dynamic behavior of towers may vary due to several reasons like functionality of towers (residential, commercial etc.), possible structural defects during construction, soil conditions, spatial variability of the ground motion, etc. This variance in dynamic behavior of towers may create crucial problems at the podium levels. Possible out of phase response of the towers may create excessive in-plane tensile, compressive, and shear stress demands on the podium floors. Since, concrete is weak under tension, tensile and shear stress resultants acting on podium levels should also be considered as critical design quantities to prevent brittle failure, and design engineers must consider this phenomenon to prevent possible diaphragm failure of the podium slabs. Furthermore, such interaction between the towers may also influence the response parameters (e.g., interstory drifts, story shear forces, story overturning moments, etc.) associated with the design of each individual tower.

For regular structures, linear elastic analysis is sufficient for design. However, for tall buildings, nonlinear response history analysis (NLRHA) is required in the performance-based design (PBD) approach. In PBD, structures are modeled considering nonlinear inelastic behavior of the members and designed according to particular performance criteria based on inelastic deformations on structural members. Computational demand for nonlinear analysis is much more than linear analysis. Besides, a combined nonlinear model of a multiple tower structure demands further computation time due to significant increase in model size. Therefore, in real-life practice, because of time restrictions due to project schedules, as well as other computational demands, analysis of multiple-tower models is typically not preferred. However, interaction effects between the towers, and especially their influence on the diaphragm forces on the podium floors, is not an issue that can be simply be neglected in design.

Based on this shortcoming, in this study, a hypothetical reinforced concrete tall building structure with two towers connected to each other with four podium levels and several basement floors is investigated as a case study. The structure is first analyzed using a simple approach of assigning either fixed or free end restraints at the continuous boundaries of the single-tower models. Responses of the single tower models are then compared with the response obtained using a combined double-tower model, which includes both of the towers as well as the common podium and basement floors. Various linear response analysis methods are first conducted using the finite elements analysis software CSI ETABS. Afterwards, nonlinear models of the structure are generated and the nonlinear seismic performance of the structure is evaluated using the analysis software CSI Perform3D. Results of various linear and nonlinear analysis methods are compared and the effects of interaction on the structural response are discussed. In the response evaluation, in addition to important response parameters associated with the tower structures, in-plane tensile and shear force distributions developing in the podium floors are also considered as critical design quantities.

1.2. Background

1.2.1. Performance-Based Seismic Design of Tall Buildings

PBD is a non-prescriptive design approach that can be adopted for design of tall buildings or special structures. Main objective of the PBD approach is to bypass prescriptive limits of design codes and achieve more cost-efficient structural designs with better seismic performance for complex structures. Since behavior of high rise structures is more complicated than regular buildings, PBD approach is adopted by engineers on design of such buildings considering the nonlinear behavior of the structure. However, nonlinear modeling is a challenging task since it incorporates elaborate simulation of realistic behavior of structural members. Additionally, proper interpretation of nonlinear response parameters are also important. Therefore, guidelines to support design engineers in modeling of the expected behavior of structural members, defining realistic seismic demands, and evaluating seismic performance of such structures with acceptable approaches, are necessary.

Although there were available related background studies, foundation of PBD approach is based on Performance Based Seismic Engineering of Buildings (Vision2000) (Structural Engineers Association of California, SEAOC, 1995). Need of an innovational approach for design in structural engineering is addressed by this work.

Methodological development of PBD began with aid of already existing guidelines for seismic retrofitting like Seismic Evaluation and Retrofit of Concrete Buildings (ATC40) (Applied Technology Council, ATC, 1996), and Standard and Commentary for the Seismic Rehabilitation of Buildings (FEMA356) (American Society of Civil Engineers, ASCE, 2000). During following years, several guidelines have been published by different workgroups. Some of these that are commonly referred to include An Alternative Procedure for Seismic Analysis and Design of Tall Buildings Located in the Los Angeles Region (LATBSDC2015) (Los Angeles Tall Buildings Structural Design Council, LATBSDC, 2015), Recommendations for the Seismic Design of High-Rise Buildings (CTBUH2008) (Council on Tall Buildings and Urban Habitat, CTBUH, 2008), and Guidelines for Performance Based Seismic Design of Tall Buildings (PEER-TBI2010) (Pacific Earthquake Research Center, PEER, 2010). These guidelines include alternative recommendations for

all stages of regular design procedure for tall buildings. However, for detailed modeling of nonlinear behavior of structural members, support documents were found to be necessary. Therefore, simultaneously, in order to aid design engineers for more realistic modeling of structures using state of the art methods, auxiliary documents were developed such as Modeling and Acceptance Criteria for Seismic Design and Analysis of Tall Buildings (ATC72-1) (Applied Technology Council, ATC, 2010).

LATBSDC2015 is the earliest comprehensive guideline for non-prescriptive design of tall buildings. Although the guideline is prepared for the Los Angeles region, it is accepted by design engineers worldwide as a viable document for general practice. The document includes general requirements for a non-prescriptive design approach for buildings higher than 160 feet. Design procedure is addressed for tall buildings for target performance of serviceable behavior under frequent earthquakes and low probability of collapse under extremely rare earthquakes. Design requirements in LATBSDC2015 also state that a peer review process is obligatory for tall building projects.

CTBUH2008 is a valuable document which consists of general recommendations for seismic design and analysis of high rise structures. It covers explanations and recommendations related to the general procedure of PBD for tall buildings, and identifies additional special topics like foundation effects and energy dissipation components.

PEER-TBI2010 is another significant guideline for application of PBD. This guideline is published under the objective of serving as a general resource for PBD for all design engineers. The document includes similar content with LATBSDC2015, yet, stages for procedure is explained in a more detailed way.

ATC72-1 is an extensive report published as a resource document for PEER-TBI2010. The report covers methodology for explicit nonlinear modeling of structural members. In this report, modeling recommendations for structural members are supplied based on latest available studies. The report covers details on modeling of hysteretic behavior for various types of members that are part of a structural system, as well as special topics like damping, p-delta effects, backstay effects, etc.

Similar to the procedure in specified in guidelines mentioned above, design of tall buildings is designated as a separate chapter that embraces PBD approach in the draft version of the new Turkish Earthquake Code, (TEC2017) (Disaster and Emergency Management Presidency, 2017). In TEC2017, a residential building in a highly active seismic zone is evaluated as a tall building if building height exceeds 70 m, and PBD approach with NLRHA is made obligatory.

1.2.2. Interaction of Multiple Towers on a Common Base

Multiple towers on common podium buildings were not very common up to recent years. These types of structures were designed using seismic joints (separations between structures), forcing responses of structures to be independent from each other. Therefore, although there are small number of publications that can be related, interaction of multiple towers on a common base is a subject that is not yet studied in detail. For this reason, comprehensive literature on the subject is not available.

One of the few studies that focus on multiple towers on common base is done by Qi and Chen (1996). Dynamic behavior of two towers connected by typical podium structure is investigated by a parametric study. Towers and podium levels are modeled elastically with lumped mass and stiffness approach (Figure 1.1). A simplified three degree of freedom (DOF) system is analyzed under constant acceleration spectra, considering different mass and stiffness values. This early study identifies effects of towers to response of each other only considering elastic forces. However, this study does not include investigation of diaphragm effects and it is not applicable for nonlinear analysis.

In a more recent study by Behnamfar *et al.* (2015), the importance of interaction effects between two structures with various dynamic properties is addressed. A formulation is developed for simple multi degree of freedom systems to examine the severity of interaction forces on each structure. Linear springs are suggested for separate model analysis. However, these linear springs include only kinematic interaction of the structures and neglect kinetic interaction caused by inertial forces. In addition to this, defining stiffness values for these springs may be tedious in real projects with complex structural configurations, especially projects that contain more than two towers on a single podium. Furthermore, in high rise

structures, kinetic interaction caused by inertial forces can be more effective than kinematic interaction. Although this study provides a valuable information for structures where inertial interaction is not expected to significantly affect the structural response, it is not very suitable for seismic response analysis of structures with high rise towers and connecting podiums.

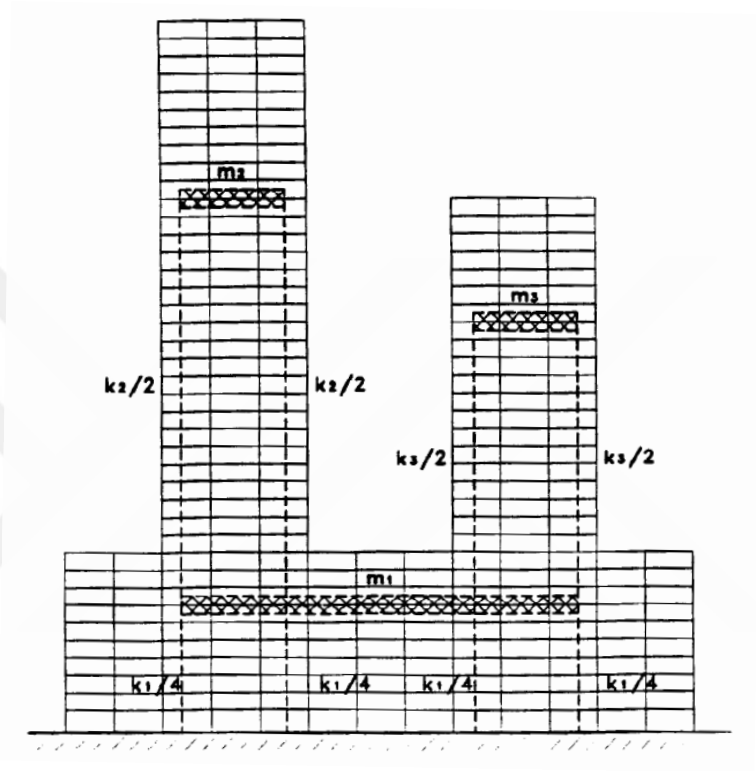

Figure 1.1. Three-DOF model simplification, Qi and Chen (1996).

In addition to the studies above, some of the currently available guidelines also address structures with multiple towers on a common podium. ATC72-1 discusses structures with multiple towers on a common base as a special topic in modeling of podium diaphragms. Interaction problems caused by dynamic variability of towers are clearly identified. Two approaches are suggested as solution strategies. First approach is to apply NLRHA with incoherent ground motions to the combined model. Second approach is to modify mass, stiffness, and other properties of the towers to obtain unsynchronized movements during the analysis. Both of these methods depend on incidental success of catching out of phase response of two towers. In addition to this, both suggestions require analyses on combined models which have excessive computational demands. In addition to these analysis method suggestions, ATC72-1 suggests separations at connecting diaphragms above basement levels

to deal with interaction effects at the first basement floor where backstay effects are already considered. This suggestion can be considered as a last choice design solution if interaction forces at diaphragms are extremely high and efficient design is not possible.

LATBSDC2015 does not suggest any analysis method but mentions multiple towers on a common podium only in the analysis procedure section. Diaphragm in-plane behavior is considered as a force-controlled action, and according to the document, structures in which number of occupants at or below podium level may exceed 5000 persons, design should be performed by reducing the capacity of the structural elements using a risk reduction factor.

Lastly, PEER-TBI2010 considers interaction of two or more towers on a common base as a concept that shows complicated behavior and adds complexity and uncertainty to the analyses. In the document, it is recommended that engineers should avoid design of such structures as much as possible, and stated that more robust analysis is required during the design process for such structures.

1.3. Research Significance

With recent developments in structural engineering, it is generally accepted today that linear elastic analysis is not sufficient for seismic design of tall buildings. Upon recent collaborative research efforts, well established guidelines for PBD of tall buildings are currently made available, and non-prescriptive design of tall buildings using the NLRHA approach is embraced by design engineers worldwide. Yet, computational requirements for NLRHA of tall buildings remains to be a drawback. New improvements in computational capabilities are still necessary for PBD to be an efficient component of the real-life design process. Until then, simplifications in structural models and analysis methods is the only way to address this problem. Structures with multiple towers on common podium are particularly troublesome systems, with a combination of both complex dynamic behavior and large computational demands. The dynamic interaction between the two towers and its effect on the dynamic response of the overall structure and the diaphragm effects on the podium levels is an issue that is explicitly warned against in design guidelines and documents; however, extremely limited literature is available on the subject. There is a clear need for additional analytical studies on this topic, which focus on the nonlinear response of

real-life structural systems. As well, considering computational limitations, there is also a need for development of more practical approaches to be used for analysis and design of such structures.

1.4. Objectives and Scope

In this study, a practical approach is sought to evaluate the seismic response of structures incorporating multiple towers on a single podium, with emphasis on assessment of diaphragm effects at the podium levels. The main motivation is to assess whether critical response quantities for the towers and the podium floors can be approximately obtained within less computation time, by analyzing the towers separately with different assumptions for the end restraints, instead of using a combined model for analysis of the multiple tower structure.

Within the scope of this work, linear and nonlinear models of a hypothetical structure with two towers on a common podium are generated. The structure is analyzed using single-tower and combined double-tower models. The combined double model incorporates the entire structure with including the towers, as well as the connecting podium and basement levels. The single models, created by cutting the double model between the two towers, consist of each individual tower together with the corresponding half of the podium and basement floors. To assess whether the interaction between the two towers can be simulated using a simple methodology, upper bound and lower bound modeling approaches are investigated, by assigning rigid (fixed support) and free (roller support) restraints on the cutting plane in the single tower models. Various linear and nonlinear analyses are conducted on five different model configurations (linear double, linear fixed, nonlinear double, nonlinear fixed, and nonlinear free), using response spectrum, modal time history, direct integration time history, and nonlinear response history analysis methods, and analysis results obtained for important response quantities associated with the tower structures and the podium floors are compared with each other.

1.5. Thesis Outline

In Chapter 1 of this Thesis, general information on the motivation and objective of this study is provided as an introduction. Some of the existing documentation and literature on the topic is addressed and the general scope of the study is described. In Chapter 2, description of the linear and nonlinear modeling procedures employed in this study are presented, with related assumptions and background information. Then, the methods used for the earthquake response analyses are described, and the procedure used for selection and scaling of the ground motion records used in the response history analyses is presented. In Chapter 3, analysis results obtained for critical response quantities are provided and comparison of the results obtained using different analysis methods is presented. Finally, concluding remarks and recommendations for future studies are provided in Chapter 4.

2. METHODOLOGY

2.1. Building Properties

The hypothetical reinforced concrete structure investigated in this study consists of two towers with 44 stories above and five stories below ground level. With 3.2 m typical height of each story, total height of the structure is 156.8 m and clear heights of the towers are 140.8 m (Figure 2.1 and Figure 2.2). An identical structural system for both towers consist of a core wall system connected with coupling beams, T shaped perimeter walls, outrigger beams connecting core wall system to perimeter walls and a perimeter frame along all four edges. Besides, two towers are connected to each other by four floor diaphragms above the ground and five basements surrounded with basement walls. Typical structural plans for basement levels, connected podium floors, and towers are presented in Figure 2.3, Figure 2.4 and Figure 2.5. Architectural properties of the building are assumed such that basement floors are utilized as parking garages, connecting podium floors are utilized as commercial zones and towers are utilized as residential zones.

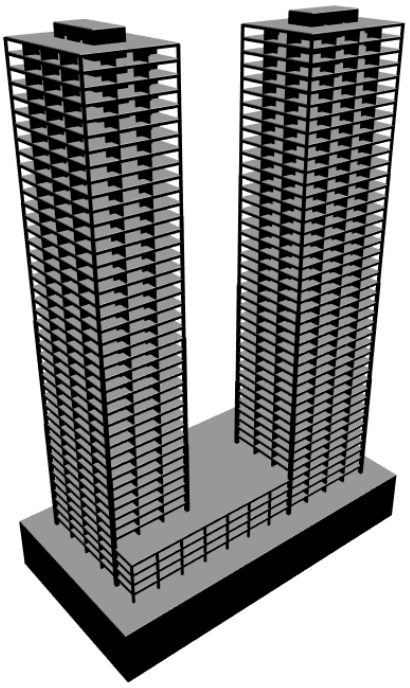

Figure 2.1. 3D view of the structure.

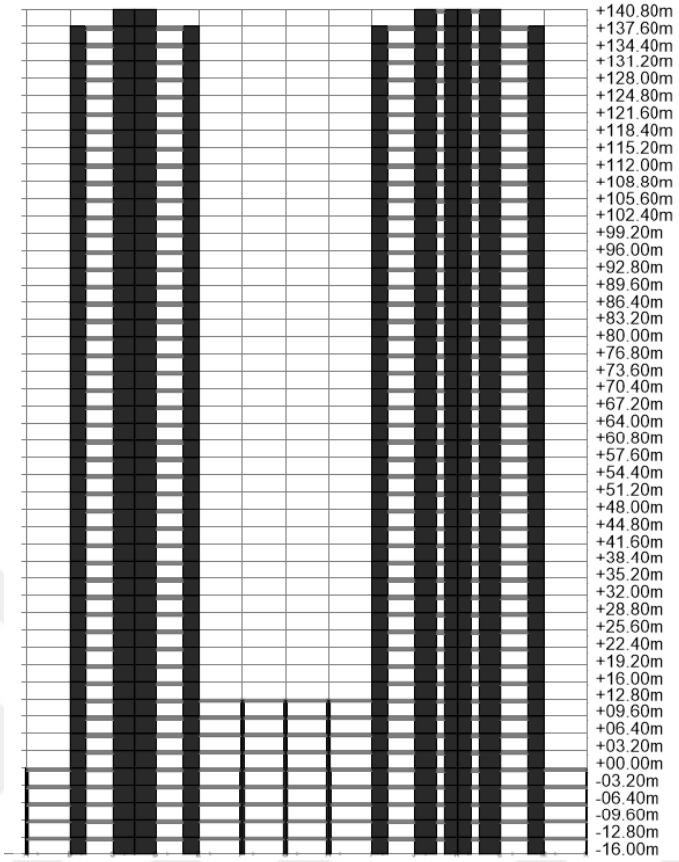

Figure 2.2. Elevation view of the structure.

Based on code-compliant linear elastic design of the structure, thicknesses of all core walls and perimeter walls are 500 mm for wall webs and 400 mm for flanges, up to an elevation of +67.20 m. This thicknesses reduces to 400 mm for webs and 300 mm for flanges beyond that level. Depth of the coupling beams connecting the core wall system is 750 mm throughout the tower height. However, width of these beams are dependent on connecting wall thicknesses. Similarly, depth of the outrigger beams is 700 mm throughout tower height, and width of these beams vary between 300 mm, 400 mm, and 500 mm depending on the thicknesses of structural walls that are connected to the beams at each end. As part of the perimeter frame, all beams have 400 mm x 600 mm cross sections and columns sections vary between 1200 mm x 1200 mm at the base and 600 mm x 600 mm at the top. Besides, on the podium floors and basements, all beams have cross-sections of 400 mm x 600 mm, whereas columns have cross sections of 600 mm x 600 mm, and 800 mm x 800 mm. Lastly, slab thickness throughout the structure is constant and is 20 cm.

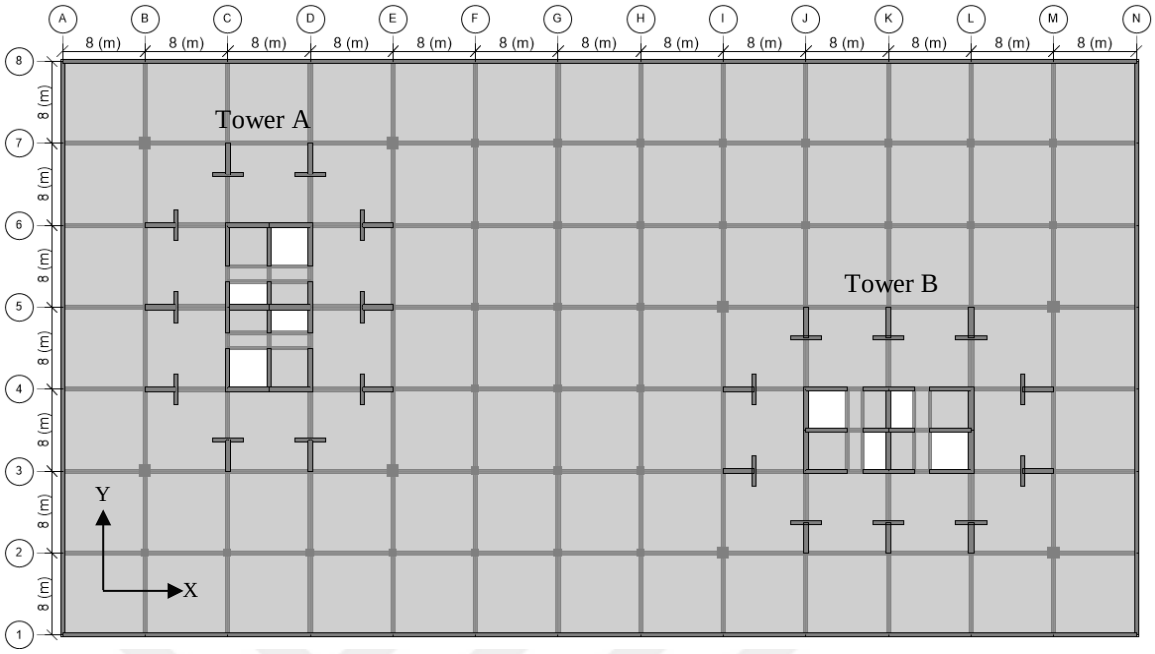

Figure 2.3. Typical plan view for basements.

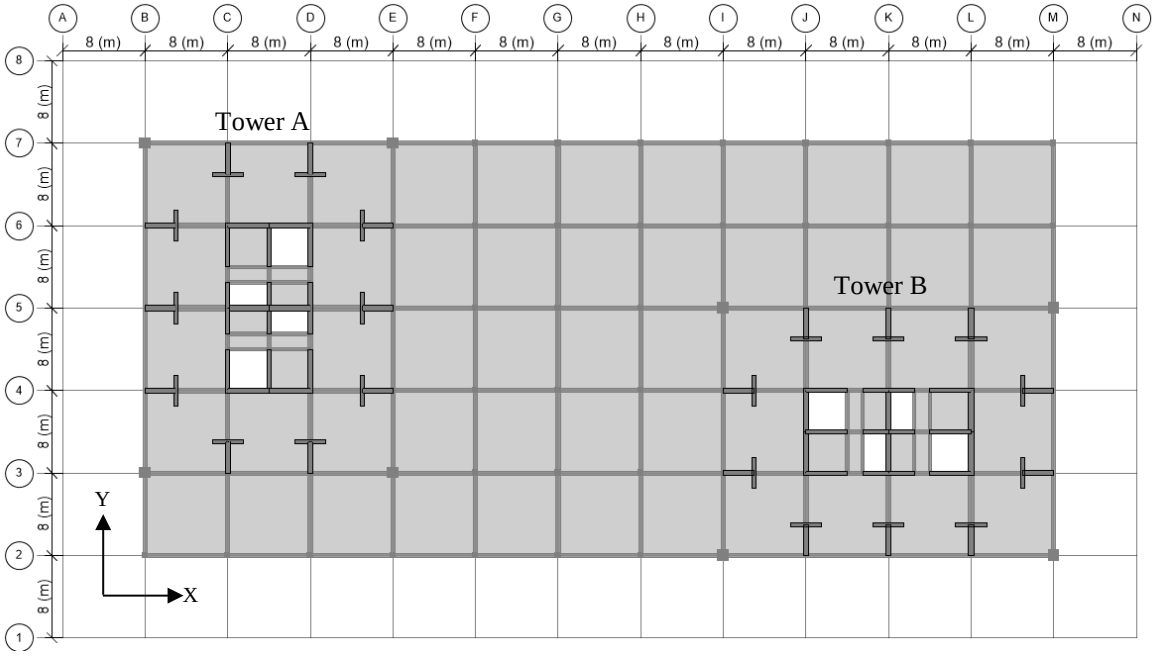

Figure 2.4. Typical plan view for connected podium floors.

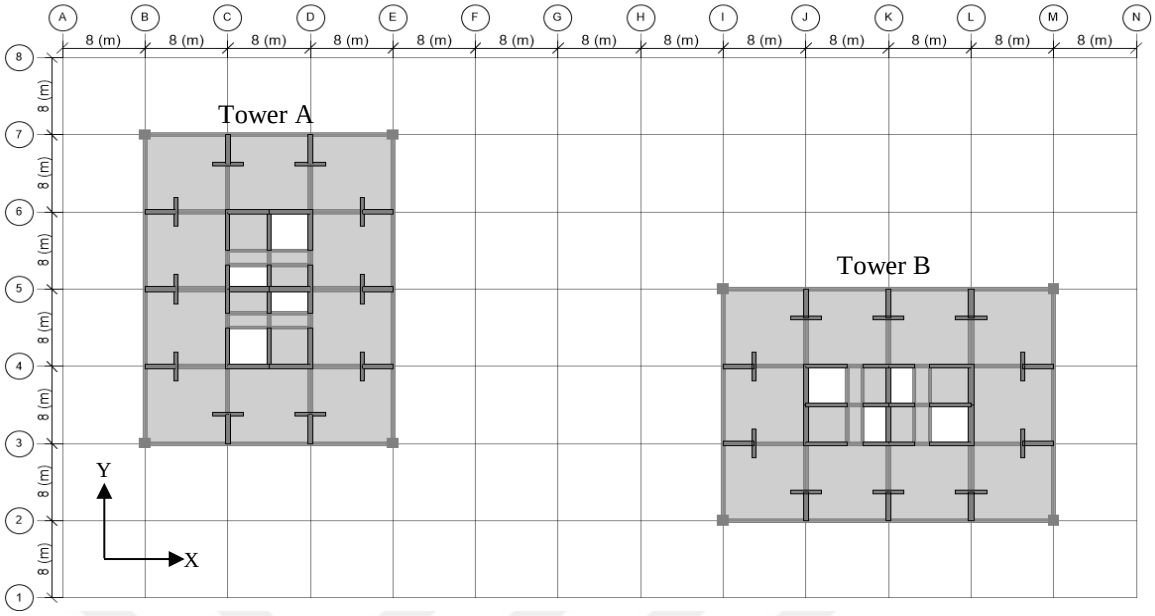

Figure 2.5. Typical plan view for towers.

2.2. Interaction Behavior

Interaction between two towers can be classified as kinematic interaction and kinetic interaction. Kinematic interaction is effect of a tower to nearby towers due to its stiffness properties. This type of interaction can be modeled with linear springs with constant stiffness. Second type of interaction is kinetic interaction. Kinetic interaction is effect of a tower to nearby towers due to its inertia. This type of interaction cannot be simply modeled using linear springs with stiffness values obtained from static analysis, since stiffness of the springs would change depending on relative motions (deformed shape) of the towers at the podium levels.

In this study, interaction between the towers during earthquake response are modeled using upper bound and lower bound approaches, where the lower bound approach simply neglects the interaction and the upper bound approach can be interpreted to represent the interaction to the full extent. Prior to conducting analyses using a double (combined two tower) model, single (one tower) models are generated, by cutting the double model at the centerline of the podium structure between the two towers (Figure 2.6). For the case when the response of two towers completely out of phase, fixed supports are assigned to the joints where double model is cut. With this approach, the single models are analyzed assuming that

there is an identical tower with completely symmetric response on other side of the cutting plane. On the other hand, for the case when response of two towers are completely in phase, no horizontal restraint (roller supports) are assigned to the joints where the double model is cut. Using this approach, the single models are analyzed assuming that there is an identical adjacent tower, with an identical response on other side of the cutting plane. Depending on these extreme assumptions, linear and nonlinear analysis results obtained using single fixed and single free models for both towers are compared with analysis results of the combined double tower model.

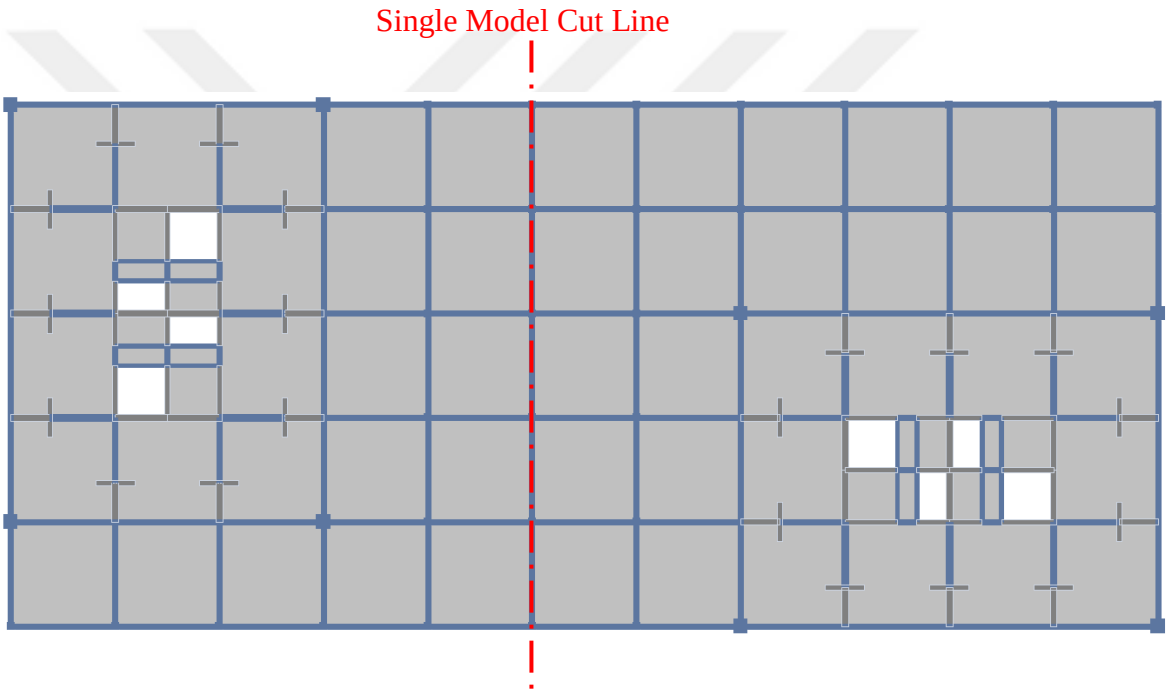

Figure 2.6. Cutting plane of double model for preparation of single models.

2.3. Linear Elastic Modeling

Linear elastic models of the structure are generated using CSI-ETABS software for linear analyses. In linear elastic modeling, mechanical properties of materials, cross sectional properties of the structural members, and model geometry are needed for assemblage of stiffness matrix of the structure. For dynamic properties of the structure, masses are defined according to existing loads considering live load contribution factors and energy dissipation is modeled using viscous damping. For linear modeling, material properties are defined

according to Requirements for Design and Construction of Reinforced Concrete Structures (TS500) (Turkish Standards Institute, 2000). Effective rigidity of structural members, masses and damping characteristics are defined according to TEC2017. Besides, for general modeling assumptions, criteria in TEC2017 is complied with. Finally, loads corresponding to different architectural utilization properties are defined according to Design Loads for Buildings (T498) (Turkish Standards Institute, 1997).

2.3.1. Materials

Mechanical properties of reinforced concrete structures are modeled linear elastically by considering material properties of concrete only. Because of the fact that effect of reinforcements are neglected, definition of a steel material is not required for linear analysis. In this structure, C50 concrete class is used with characteristic compressive strength $f_{ck} = 50$ MPa. For C50 class concrete, Modulus of Elasticity of concrete is defined as $E_c = 37000$ MPa using Equation 2.1 (TS500). Shear Modulus of concrete is defined as $G_c = 15417$ MPa using Equation 2.2 (TS500) by taking Poisson Ratio of concrete $\nu_c = 0.2$ (TS500). Besides, for dead load calculations, specific weight of the concrete is assumed as $\gamma_c = 25\ \text{kN/m}^3$ in accordance with common practice.

$$E_c = 3250\sqrt{f_{ck}} + 14000 \tag{2.1}$$

$$G_c = \frac{E_c}{2(1+\nu_c)} \tag{2.2}$$

2.3.2. Structural Elements

In compliance with the Finite Element Modeling (FEM) method, structural members are defined using different types of elements in modeling. Choice of types of the elements depend on the criterion that the behavior of the members are represented acceptably well, requiring as less computational demand as possible. Therefore, based on this approach, beams and columns are typically modeled as frame elements which are straight lines connecting two joints, resisting axial load, biaxial bending, torsion and biaxial shear. Slab

and walls are generally defined as shell elements which are three or four node area objects that combine membrane and plate behavior.

Moreover, for reinforced concrete structures, rigidities of structural members must be modified with stiffness modifiers to obtain effective rigidities considering cracking of concrete under tension. To consider cracked behavior of reinforced concrete sections, effective rigidities are defined using the coefficients listed in Table 2.1. (TEC2017). In addition to this, even though there is no stiffness modifier for axial behavior of beams defined in TEC2017, axial rigidity of critical beams between two towers on connecting floors is reduced using 0.25 stiffness modifier similar to slab in plane axial behavior in order to achieve a more realistic stress distribution on the slab elements.

Table 2.1. Reinforced concrete sections stiffness modifiers.

Reinforced Concrete Structural Elements	Stiffness Modifiers	
Walls-Slab (In-Plane)	Axial	Shear
Structural Walls	0.50	0.50
Basement Walls	0.80	0.50
Slab	0.25	0.25
Walls-Slab (Out of Plane)	Bending	Shear
Structural Walls	0.25	1.00
Basement Walls	0.50	1.00
Slab	0.25	1.00
Frame Elements	Bending	Shear
Coupling Beams	0.15	1.00
Moment Frame Beams	0.35	1.00
Moment Frame Columns	0.70	1.00

2.3.3. Gravity Loads

Decision on magnitudes of gravity loads is an important part of the modeling and analysis process. Models should be loaded with realistic distribution and magnitudes to achieve reliable results. Gravity loads are classified as dead loads for permanent loads and live loads for temporary loads. For dead loads, magnitudes are dependent on self-weights of materials used for both structural and non-structural elements. On the other hand,

magnitudes of live loads are defined considering functionality of the building with a probabilistic approach since live loads on a structure is variable throughout its life span. In this study, self-weights of structural members are included in analysis model by ETABS automatically. Remaining part of the dead loads are assigned as uniform loads on floor slabs with magnitudes in accordance with common practice. Live loads are also assigned as uniform loads on floor slabs and magnitudes are defined according to TS498. Uniform load values are tabulated in Table 2.2.

Table 2.2. Uniform loads.

Load Type	Uniform Load (kN/m^2)
Partition Walls	1.00
Floor finishes and ceiling plaster	1.50
Live load Residential	2.00
Live Load Commercial	5.00
Live Load Basement	5.00
Live Load Stairs	5.00

2.3.4. Seismic Masses

Since dynamic behavior of structures depend directly on mass magnitude and distribution, realistic definition of masses is crucial on the reliability of the analytical response. Differently from regular design loads, contribution of dead loads to mass of the structure is not factored. On the other hand, since probability of having nominal live load at the same time with an earthquake event is low, to achieve more realistic dynamic properties, live loads are reduced using live load contribution factors in definition of seismic masses. These live load contribution factors are defined according to occupancy of the building described with a probabilistic approach. In this study, live load contribution factors are defined according to TEC2017 (Table 2.3).

Seismic masses are assembled by ETABS automatically as concentrated joint masses in compliance with corresponding distributed mass inside tributary area of each joint.

Contributions to seismic masses from dead and live loads are combined at each node *j* using Equation 2.3 and 2.4 (TEC2017).

Table 2.3. Live load mass contribution factors.

Load Type	Live Load Contribution Factor
Live Load Residential	0.3
Live Load Commercial	0.6
Live Load Parking Garage	0.3
Live Load Stairs	0.6

$$w_j^{(s)} = w_{G,j}^{(s)} + n w_{Q,j}^{(s)} \tag{2.3}$$

$$m_j^{(S)} = \frac{w_j^{(S)}}{g} \tag{2.4}$$

2.3.5. Assembled Model

Based on the procedure described above, a linear elastic model of the structure is generated (Figure 2.7). Additional commonly-employed assumptions are made regarding foundation flexibility of the structure, diaphragm assignments, and beam column intersections during the modeling process. In compliance with common practice, foundation of the structure is not modeled explicitly. Instead, fixed supports are assigned to joints at the foundation level. Additionally, since TEC2017 requires inclusion of additional accidental eccentricity on analyses, semi-rigid diaphragms are assigned to each floor slab, and 5% accidental eccentricity is applied by ETABS automatically. Finally, rigid end zones are assigned to beam column intersections since frame elements are connected to each other at intersection joints and modeling of these regions should consider frame element overlaps near intersection joints to obtain more precise mass and rigidity properties for the structure.

After the structural model is completed, natural vibration periods and corresponding mode shapes of the structure are obtained with eigenvalue analysis. According to free vibration analysis of the double model, fundamental periods of the towers are $T_{AX} = 5.200$ s

, $T_{AY} = 4.287$ s for Tower A, and $T_{BX} = 4.080$ s, $T_{BY} = 5.410$ s for Tower B (Table 2.5). These periods decrease to $T_{AX} = 4.880$ s, $T_{AY} = 4.081$ s for Tower A, and $T_{BX} = 3.963$ s, $T_{BY} = 5.119$ s for Tower B according to single-fixed models. On the other hand, these periods increase to $T_{AX} = 5.441$ s, $T_{AY} = 4.330$ s for Tower A, and $T_{BX} = 4.291$ s, $T_{BY} = 5.479$ s for Tower B according to single-free models (Table 2.4). Corresponding mode shapes for first four fundamental periods of double model are presented in Figure 2.8. The double model reaches 90% mass participation ratio, which is a limit value for acceptability of analyses in TEC2017, in both directions, at its 48th mode. However, once eigenvalue analysis is done for single towers considering only tower masses, it is observed that single towers reach 90% of mass participation ratio at their 8th mode. In linear dynamic analyses of the double model, first 120 vibration modes are included to achieve higher mass participation. Correlatively, first 60 vibration modes are included in analysis of the single tower models.

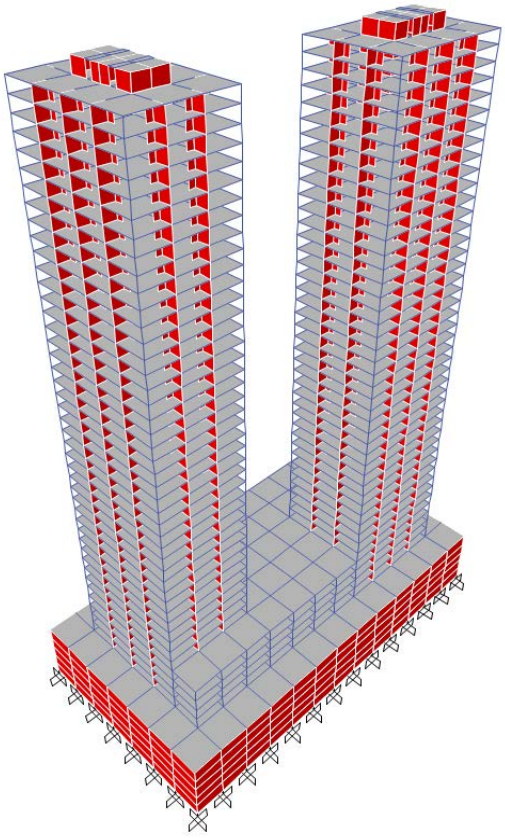

Figure 2.7. ETABS model of the structure.

Table 2.4. Fundamental vibration periods of towers for fixed, double and free models.

	Tower A Periods (s)			Tower B Periods (s)		
	Fixed	Double	Free	Fixed	Double	Free
X Direction	4.880	5.200	5.441	3.963	4.080	4.291
Y Direction	4.081	4.287	4.330	5.119	5.410	5.479

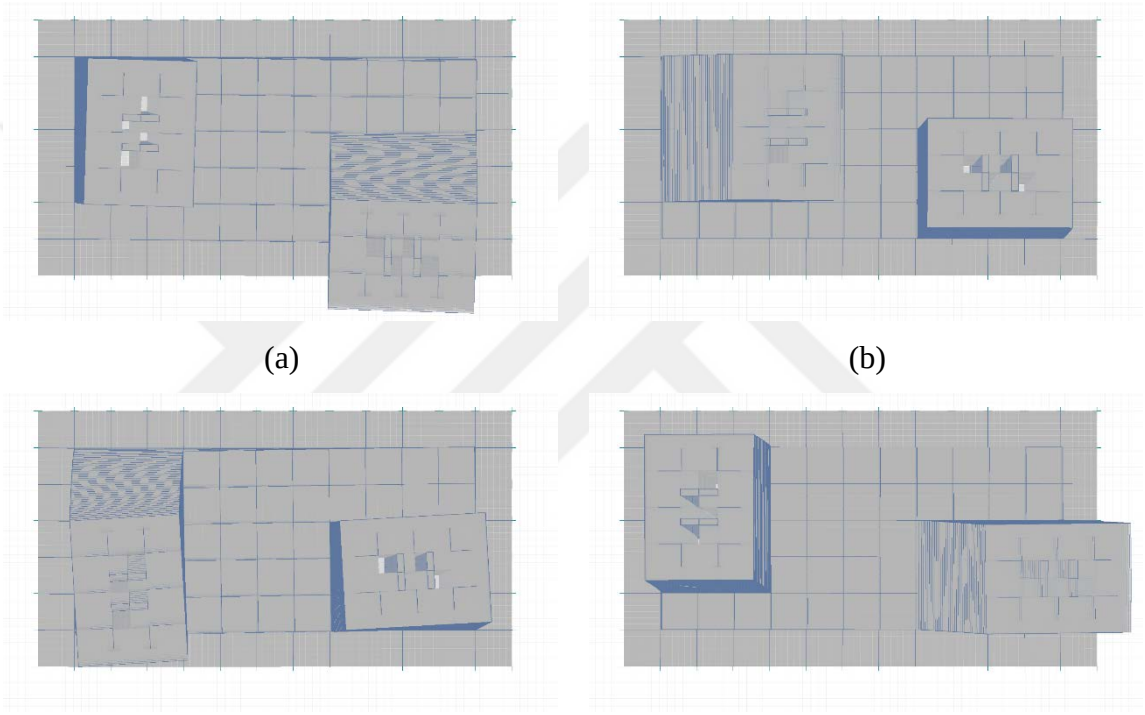

(a) (b)

(c) (d)

Figure 2.8. Mode shapes corresponding to fundamental periods (a) T_{BY}, (b), T_{AX}, (c) T_{AY}, (d) T_{BX}.

Table 2.5. Natural vibration periods and corresponding mass participation factors for double model.

Mode Number	Period (s)	Mass Participation on X direction	Mass Participation on Y direction	$\sum X$	$\sum Y$
1	5.410	0.006	0.259	0.006	0.259
2	5.200	0.316	0.009	0.322	0.267
3	4.287	0.008	0.215	0.330	0.482
4	4.080	0.149	0.005	0.479	0.487

Table 2.5. Natural vibration periods and corresponding mass participation factors for double model (cont.).

Mode Number	Period (s)	Mass Participation on X direction	Mass Participation on Y direction	$\sum X$	$\sum Y$
5	3.220	0.000	0.000	0.479	0.487
6	3.217	0.000	0.000	0.479	0.488
7	1.384	0.001	0.088	0.480	0.575
8	1.326	0.108	0.003	0.588	0.578
9	1.193	0.002	0.055	0.590	0.633
10	1.092	0.025	0.001	0.615	0.634
11	1.054	0.000	0.000	0.615	0.634
12	1.045	0.000	0.001	0.615	0.635
13	0.636	0.000	0.071	0.615	0.706
14	0.614	0.064	0.001	0.679	0.707
15	0.599	0.002	0.011	0.682	0.718
16	0.569	0.000	0.000	0.682	0.718
17	0.554	0.000	0.001	0.682	0.719
18	0.526	0.001	0.000	0.682	0.719
⋮	⋮	⋮	⋮	⋮	⋮
46	0.136	0.000	0.000	0.879	0.915
47	0.132	0.007	0.002	0.886	0.916
48	0.130	0.014	0.003	0.900	0.919
49	0.128	0.011	0.002	0.911	0.920
⋮	⋮	⋮	⋮	⋮	⋮
116	0.064	0.000	0.000	0.960	0.972
117	0.064	0.001	0.000	0.960	0.972
118	0.064	0.000	0.001	0.960	0.972
119	0.063	0.000	0.000	0.961	0.972
120	0.063	0.001	0.001	0.961	0.973

2.3.6. Damping

For energy dissipation during linear dynamic analysis, equivalent viscous damping is defined in accordance with common practice. For response spectrum analysis (RSA), 5% modal damping ratio is defined according to requirements of TEC2017. 5% modal damping

was also used for the linear modal response history analyses (LMRHA). Since modal damping for linear direct integration response history analysis (LDIRHA) is not defined, Rayleigh damping is defined for the LDIRHA using ETABS. Rayleigh damping is defined based on criteria that natural vibration modes with higher mass participations are neither overdamped nor underdamped as much as possible. Therefore, mass and stiffness proportional damping coefficients are defined as $\alpha_m = 0.112$ rad^2/s^2 and $\beta_k = 0.011$ s/rad using Equation 2.5 (Chopra, 2015) to satisfy 5% damping ratio at periods T=4.76 s and T=0.85 s (Figure 2.9). Longer period T=4.76 s is average of first two fundamental periods of each tower considering only tower masses (5.41 s, 5.20 s, 4.32 s, 4.11 s). Shorter period T=0.85 s is average of four periods of the two towers where total mass participation nearly reaches to 90% on both directions, considering only tower masses (1.08 s, 1.06 s, 0.64 s, 0.62 s). Corresponding damping ratios for all natural vibration periods included in analyses are presented in Table 2.6.

$$\begin{bmatrix} \xi_i \\ \xi_j \end{bmatrix} = \frac{1}{2} \begin{bmatrix} \frac{1}{\omega_i^2} & \omega_i \\ \frac{1}{\omega_j^2} & \omega_j \end{bmatrix} \begin{bmatrix} \alpha_m \\ \beta_k \end{bmatrix} \tag{2.5}$$

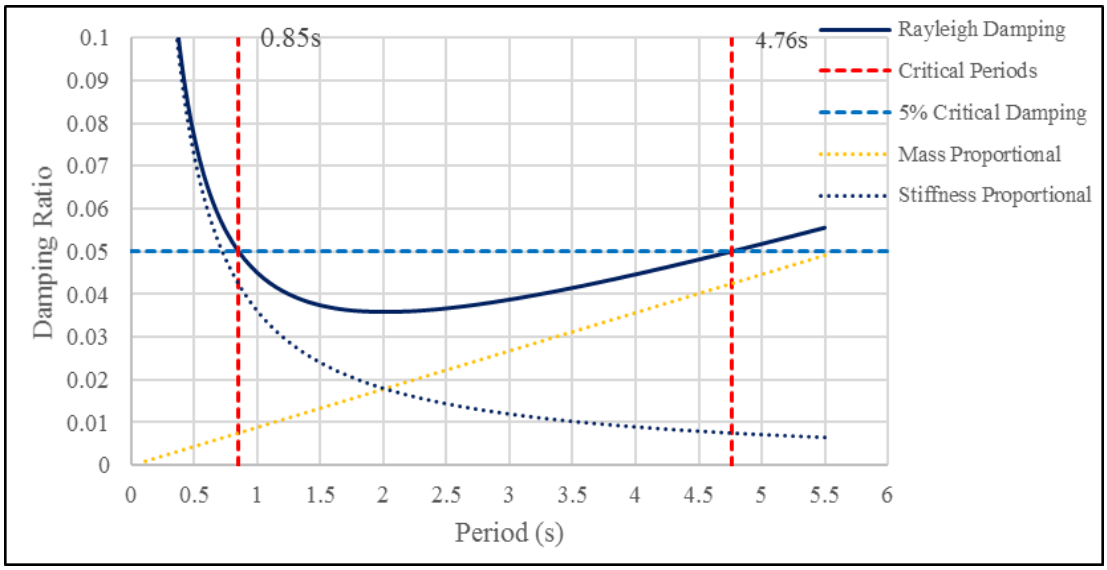

Figure 2.9. Distribution of Rayleigh damping.

Table 2.6. Rayleigh damping ratios corresponding to natural vibration periods of the structure.

Mode Number	Period (s)	Rayleigh Damping Ratio
1	5.410	0.05
2	5.200	0.05
3	4.287	0.05
4	4.080	0.05
5	3.220	0.04
6	3.217	0.04
7	1.384	0.04
8	1.326	0.04
9	1.193	0.04
10	1.092	0.04
11	1.054	0.04
12	1.045	0.04
13	0.636	0.06
14	0.614	0.06
15	0.599	0.07
16	0.569	0.07
17	0.554	0.07
18	0.526	0.07
⋮	⋮	⋮
45	0.140	0.26
46	0.136	0.27
47	0.132	0.27
48	0.130	0.28
49	0.128	0.28
⋮	⋮	⋮
116	0.064	0.56
117	0.064	0.56
118	0.064	0.56
119	0.063	0.57
120	0.063	0.57

2.4. Nonlinear Modeling

Modeling nonlinear behavior of structural members is a complicated task. Individual behavior of each member that contributes to the seismic response of the structure should be included in the nonlinear model. Compared to uncertainty in ground motions and soil behavior, even though nonlinear behavior characteristics of structural members are more easily defined, it is still not possible to accurately represent the real seismic response characteristics of complex structural systems. However, due to recent research advancements on characterization of the nonlinear behavior of individual members, it is possible to obtain reasonably reliable results using nonlinear analysis.

In addition to complexities in nonlinear modeling, nonlinear analysis of structures is computationally demanding task. Therefore, only primary structural members that affect the nonlinear seismic response of structures are typically included with nonlinear behavior in the model. This primary member assignment can be made considering whether nonlinearity is expected on the member or not. In this study, based on state of the art design guidelines, behavior of primary members (walls, beams, columns, coupling beams) are modeled nonlinearly, whereas the behavior of secondary members (slabs, basement walls, partition walls, etc.) are modeled elastically or not even included in analysis models.

Furthermore, differently from linear modeling, expected strengths for materials are used instead of characteristic or reduced design strength values in nonlinear modeling, in order to predict the behavior more realistically in analysis. Therefore, throughout nonlinear modeling, expected compressive strength of concrete is defined as $f_{ce} = 65$ MPa and expected yield strength of reinforcing steel is defined as $f_{sye} = 504$ MPa, according to TEC2017.

Nonlinear models of the structure are generated using the commonly-used software Perform3D. Through the modeling process, modeling assumptions are referred to TEC2017, LATBSDC2015, and ASCE41-13.

2.4.1. Materials

2.4.1.1. Elastic Material for Fiber Sections. Since nonlinearity under axial or flexural behavior is not expected in the basement walls, axial and flexural behavior of these elements are modeled by the linear elastic material named as Elastic Material for Fiber Sections in Perform3D. Effective elastic modulus for this material is defined as $E_{ce} = 33678$ MPa using Equations 2.6 and 2.7 (LATBSDC2015).

$$E_{ce} = 4733.6\sqrt{f_{ce}} \qquad f_{ce} \le 41.4MPa \tag{2.6}$$

$$E_{ce} = 3321.8\sqrt{f_{ce}} + 6896.6 \qquad f_{ce} > 41.4MPa \tag{2.7}$$

2.4.1.2. Elastic Shear Material for Walls. Since structural walls are designed with adequate shear capacity, nonlinearity under shear force is not expected. Therefore, shear behavior of the walls are modeled by material named Elastic Shear Material for Walls in Perform3D. Effective shear modulus of this material is defined as $G_{ce} = 14032$ MPa by Equation 2.8 with Poisson ratio $\nu_c = 0.2$.

$$G_{ce} = \frac{E_{ce}}{2(1+\nu_c)} \tag{2.8}$$

2.4.1.3. Concrete Material. Concrete stress-strain relationships are defined according to concrete model developed by Mander *et al.* (1988). This model is also recommended in TEC2017 for modeling nonlinear behavior of concrete. Both confined and unconfined concrete stress-strain relationships are obtained by Equation 2.21 and modeled in Perform3D with appropriate linearization. However, tensile strength and cyclic degradation of concrete is neglected in the model.

Since effect of confinement varies depending on amount of confining reinforcement and confined core geometry, different concrete materials are defined considering effectiveness of different confinement details. To represent confinement, effects, confined concrete material properties in the structure are classified according to varying confinement

details in wall boundary regions, which change with wall thickness and the critical height of the walls. According to this classification, confined concrete materials are defined as:

- 30 cm over critical height (30 cm OCH)
- 40 cm over critical height (30 cm OCH)
- 50 cm over critical height (30 cm OCH)
- 40 cm under critical height (30 cm UCH)
- 50 cm under critical height (30 cm UCH).

To obtain the stress-strain relationship of confined concrete, first, confinement effectiveness coefficient k_e is calculated using Equation 2.9.

$$k_e = \left(1 - \frac{\sum a_i^2}{6 b_0 h_0}\right)\left(1 - \frac{s}{2 b_0}\right)\left(1 - \frac{s}{2 h_0}\right)\left(1 - \frac{A_s}{b_0 h_0}\right)^{-1} \tag{2.9}$$

Then, effective confining pressures in two perpendicular directions f_{ex}, f_{ey} are calculated using Equation 2.10 and Equation 2.11.

$$f_{ex} = k_e \rho_x f_{sye} \tag{2.10}$$

$$f_{ey} = k_e \rho_y f_{sye} \tag{2.11}$$

Next, confined concrete compressive strengths modifier λ_c is calculated using Equation 2.12 and Equation 2.13.

$$\lambda_c = 2.254\sqrt{1 + 7.94\frac{f_e}{f_{co}}} - 2\frac{f_e}{f_{co}} - 1.254 \tag{2.12}$$

where

$$f_e = \frac{f_{ex} + f_{ey}}{2} \tag{2.13}$$

and modified compressive strength of confined concrete is calculated using Equation 2.14.

$$f_{cc} = \lambda_c f_{co} \tag{2.14}$$

On the other hand, strain corresponding to compressive strength of concrete is calculated using Equations 2.15 and Equation 2.16.

$$e_{cc} = e_{co}\left[1+5\left(\lambda_c - 1\right)\right] \tag{2.15}$$

where

$$e_{co} = \frac{\left(f_{co}\right)^{0.25}}{1150} \tag{2.16}$$

Modulus of elasticity of concrete for unconfined concrete is defined using Equation 2.17

$$E_c = 5000\sqrt{f_{co}} \tag{2.17}$$

and secant modulus of elasticity for confined concrete is defined using Equation 2.18.

$$E_{sec} = \frac{f_{cc}}{e_{cc}} \tag{2.18}$$

Additionally, parameters required for function of stress-strain curve are calculated using Equations 2.19 and 2.20.

$$x = \frac{e_c}{e_{cc}} \tag{2.19}$$

$$r = \frac{E_c}{E_c - E_{sec}} \tag{2.20}$$

Finally, stress-strain relationships for confined concrete are plotted using Equation 2.21.

$$f_c = \frac{f_{cc} x r}{r - 1 + x^r} \tag{2.21}$$

In addition, to prevent sudden stress drop at possible high compressive strains, post peak behavior of materials are modified such that stress-strain relationship is linear until stress values reach to 20% of peak strength. Linearized stress-strain relationship and Perform3D modeling parameters can be observed in Figure 2.10 and Table 2.7, respectively.

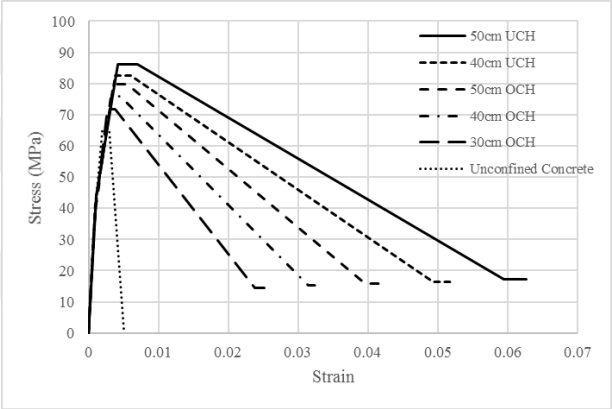

Figure 2.10. Linearized concrete material stress-strain relationships.

Table 2.7. Concrete material Perform 3D modeling parameters.

Concrete Type	DY	DU	DL	DR	DX	FY	FU	FL	FR	FX
Unconfined Concrete	0.0009	0.0020	0.0030	0.0050	0.0053	36.4	65.0	65.0	1.0	1.0
30 cm OCH	0.0009	0.0027	0.0038	0.0238	0.0251	37.3	71.7	71.7	14.3	14.3
40 cm OCH	0.0010	0.0032	0.0046	0.0314	0.0331	39.0	75.9	75.9	15.2	15.2
50 cm OCH	0.0010	0.0036	0.0056	0.0396	0.0417	40.8	79.7	79.7	15.9	15.9
40 cm UCH	0.0010	0.0039	0.0060	0.0493	0.0520	42.3	82.5	82.5	16.5	16.5
50 cm UCH	0.0011	0.0042	0.0070	0.0594	0.0626	44.2	86.0	86.0	17.2	17.2

2.4.1.4. Reinforcing Steel Material. Characteristic properties of steel reinforcement include modulus of elasticity E_s, expected yield strength f_{sye}, strain hardening initiation strain ε_{sh},

ultimate strain capacity ε_{su} and strain hardening ratio f_{su}/f_{sye}. Steel reinforcement in structural walls (Figure 2.11) is modeled using Equations 2.22 to 2.24, also using the properties presented in Table 2.8 (TEC2017). Buckling and cyclic degradation of reinforcement is neglected in reinforcing steel model.

$$f_s = E_s \varepsilon_s \qquad \left(\varepsilon_s \le \varepsilon_{sy}\right) \tag{2.22}$$

$$f_s = f_{sy} \qquad \left(\varepsilon_{sy} < \varepsilon_s \le \varepsilon_{sh}\right) \tag{2.23}$$

$$f_s = f_{su} - \left(f_{su} - f_{sy}\right)\frac{\left(\varepsilon_{su} - \varepsilon_s\right)^2}{\left(\varepsilon_{su} - \varepsilon_{sh}\right)^2} \qquad \left(\varepsilon_{sh} < \varepsilon_s \le \varepsilon_{su}\right) \tag{2.24}$$

Table 2.8. Properties for steel reinforcements.

Steel Grade	E_s	f_{sye}	ε_{sh}	ε_{su}	f_{su}/f_{sy}
S420	200GPa	504MPa	0.008	0.08	1.2

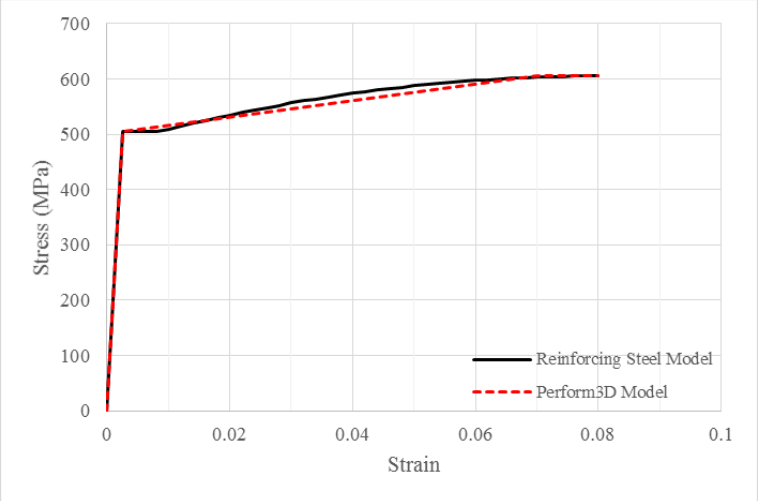

Figure 2.11. Reinforcing steel stress-strain relationship.

2.4.2. Modeling of Structural Members

As mentioned before, to decrease computational demands, only the behavioral characteristics of the primary members (where nonlinearity is expected) are included explicitly in nonlinear model. Secondary members that are expected to remain linear elastic are included in the nonlinear model using linear elastic material properties. In addition to these, elements that are expected to contribute negligibly to the overall seismic response (tower slabs, infill walls etc.) are not included in the nonlinear model, as is typical. In this study, structural elements included in the nonlinear model consist of structural walls, frame beams, coupling beams, columns, and podium slabs.

In Perform 3D, nonlinear behavior of structural members can be modeled using two different approaches, using lumped plasticity (plastic hinge model) or distributed plasticity (fiber model). In the lumped plasticity approach, nonlinearity in member behavior is included in the model using concentrated hinges at possible inelasticity regions. Monotonic force-deformation relationships of sections are defined as backbone curves and these backbone curves are further calibrated to represent hysteretic degradation. In the distributed plasticity approach, the geometry of cross-section is defined by dividing the section into fibers. For nonlinear flexural behavior of fiber sections, uniaxial stress-strain relationships and hysteretic behavior for different materials are defined explicitly and assigned to each fiber. In this study, the nonlinear flexural behavior of structural walls is modeled using the distributed plasticity approach, whereas the nonlinear flexural behavior of beams and columns are modeled using lumped plasticity approaches.

2.4.2.1. Structural Walls. Structural walls are crucial part of the lateral stiffness and lateral load-carrying capacity of tall building structures. Hence, nonlinear behavior of these members have significant effect on structural response. Therefore behavior of these members should be included in analysis explicitly, with appropriate modeling and acceptance criteria.

In Perform3D, in order to define fiber cross sections, two different methods are available. The first method is “Auto Section”, where the tributary area and coordinates of the concrete and steel fibers in the cross section are defined by the software automatically.

However, using the auto section method, only one type of concrete material can be used in a single cross-section. Therefore, to be able to model confined concrete (in boundary regions) and unconfined concrete (in the web) in a wall section, web and boundary regions of all walls must be defined as separate elements. As a result of this, computational demand increases excessively due to increase on number of nonlinear wall elements in the model. On the other hand, in the second method named as “Fixed Sections”, area, coordinate, and material type of each fiber are defined manually. Thus, different material types can be used in single section and elements are not needed to be further meshed. In this study, Fixed Sections method of Perform3D is used for fiber section modeling of structural walls in the building (Figure 2.12 and Figure 2.13).

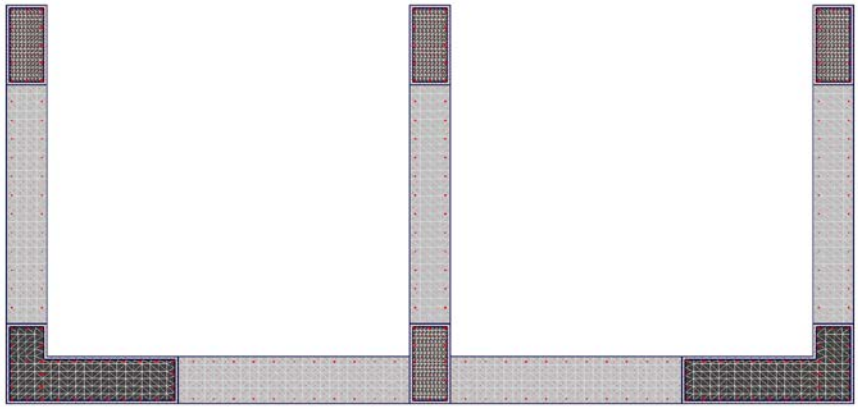

Figure 2.12 Cross section of a structural wall.

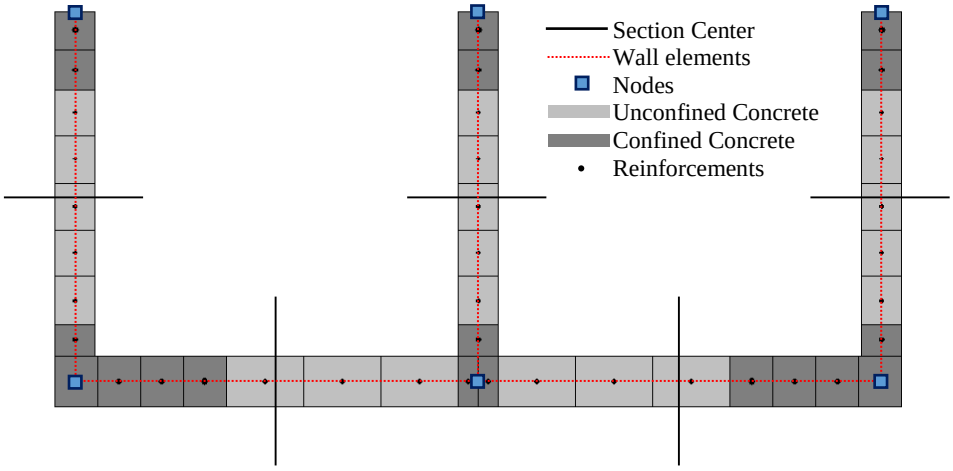

Figure 2.13 Fiber modeling of a structural wall in Perform3D.

Performance criteria for nonlinear behavior of structural walls is defined as strain limits for concrete and reinforcements in TEC2017. Therefore, to evaluate the performance levels of the structural walls, strain gage elements are included in the nonlinear model of the structure. Strain gages are defined at both ends of each structural wall component in the model.

2.4.2.2. Beams. In this study, beams are classified as frame beams, outrigger beams, and coupling beams. Frame beams are the beams that are only part of the perimeter frame. Outrigger beams span along the interior axes of the building, and since they are connected to structural walls at one end, they have a more pronounced effect on the lateral stiffness of the tower structures and contribute to hysteretic energy dissipation more than frame beams. Coupling beams are beams with smaller span-to-depth ratios that connect structural walls to each other and create a coupling action between the walls they connect by transferring axial forces on the individual wall segments.

Nonlinearity in the flexural behavior of the beams is modeled with the lumped plasticity approach. In the lumped plasticity approach, nonlinear behavior of a member is concentrated at localized region using plastic hinges. The beams in the structure with conventional (top and bottom longitudinal) reinforcement are modeled using moment-rotation plastic hinges. On the other hand, coupling beams with diagonal reinforcement are modeled using plastic shear hinges. Rotational capacities and acceptance criteria of the beams are defined as shown in Figure 2.14, Table 2.9, and Table 2.10, per ASCE41-13 recommendations.

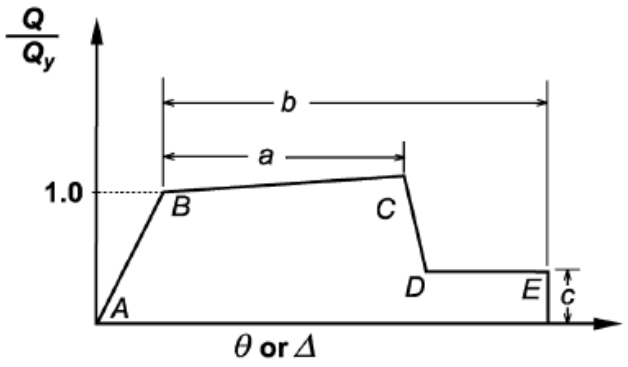

Figure 2.14 Backbone curve for modeling of beams.

Table 2.9 Modeling parameters and acceptance criteria for coupling beams.

Conditions		Plastic Rotation (rad)		Strength Loss Ratio	Performance Criteria (rad)		
Reinforcement Type	$\frac{V}{b_w h\sqrt{f_{ce}}}$	a	b	c	IO	LS	CP
Conventional longitudinal reinforcement with conforming transverse reinforcement	≤ 0.25	0.025	0.050	0.75	0.010	0.025	0.050
	≥ 0.50	0.020	0.040	0.50	0.005	0.020	0.040
Conventional longitudinal reinforcement with nonconforming transverse reinforcement	≤ 0.25	0.020	0.035	0.50	0.006	0.020	0.035
	≥ 0.50	0.010	0.025	0.25	0.005	0.010	0.025
Diagonal Reinforcement	-	0.030	0.050	0.80	0.006	0.030	0.050

Table 2.10 Modeling parameters and acceptance criteria for frame and outrigger beams.

Conditions			Plastic Rotation (rad)		Strength Loss Ratio	Performance Criteria (rad)		
$\frac{\rho-\rho'}{\rho_{bal}}$	Transverse Reinforcement	$\frac{V}{b_w h\sqrt{f_{ce}}}$	a	b	c	IO	LS	CP
≤ 0.0	Conforming	≤ 0.25	0.025	0.050	0.20	0.010	0.025	0.050
≤ 0.0	Conforming	≥ 0.5	0.020	0.040	0.20	0.005	0.020	0.040
≥ 0.5	Conforming	≤ 0.25	0.020	0.030	0.20	0.005	0.020	0.030
≥ 0.5	Conforming	≥ 0.5	0.015	0.020	0.20	0.005	0.015	0.020
≤ 0.0	Nonconforming	≤ 0.25	0.020	0.030	0.20	0.005	0.020	0.030
≤ 0.0	Nonconforming	≥ 0.5	0.010	0.015	0.20	0.0015	0.010	0.015
≥ 0.5	Nonconforming	≤ 0.25	0.010	0.015	0.20	0.005	0.010	0.015
≥ 0.5	Nonconforming	≥ 0.5	0.005	0.010	0.20	0.0015	0.005	0.010

In the structure, all coupling beams are reinforced with diagonal reinforcement bars. Therefore, all coupling beams are modeled using shear hinges. In Perform3D, coupling beams are modeled as a frame member compound components. This compound component

consists of a shear hinge between two elastic sections with effective flexural rigidities (Figure 2.15).

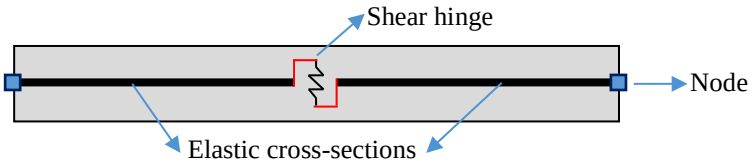

Figure 2.15 Modeling of coupling beams with diagonal reinforcements.

On the other hand, all frame and outrigger beams are modeled such that an elastic cross section between two plastic moment-rotation hinges (Figure 2.16). Note that, in modeling of these beams, rigid end zones (ends of the beam that are within stiff beam-column intersection zones) and plastic hinge length of the section is neglected. In other words, moment-rotation hinges are defined adjacent to end nodes, as done typically.

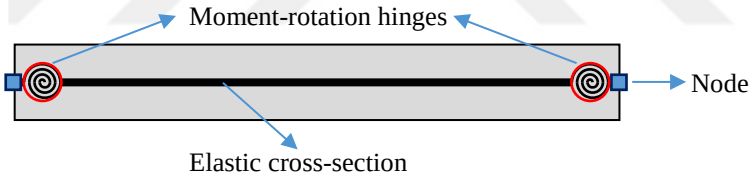

Figure 2.16 Modeling of frame and outrigger beams.

Besides the backbone curves, hysteretic behavior of beams may also be affected by hysteretic strength and stiffness degradation. In hysteretic strength degradation, moment capacity of a beam is reduced during each loading cycle. In stiffness degradation, stiffness of the hysteresis loop is reduced depending on the rotation level. In this study, strength degradation is neglected, as is typical in performance-based design applications, and stiffness degradation is represented using energy factors suggested by Naish *et al.* (2009).

2.4.2.3.Columns. Differently from the beams, hysteretic behavior of the columns are dependent on the level of axial force on the section, since expected axial force levels are significant in these elements. Hence, plastic hinges considering biaxial bending under axial

load (PMM hinges) are used to model column nonlinear behavior in the model. Yield surface for plastic deformation initiation is defined carrying out sectional analysis. Backbone curves for nonlinear behavior and plastic rotation capacities are defined per ASCE 41-13 recommendations, as listed in Table 2.11.

Table 2.11 Modeling parameters and acceptance criteria for columns.

Conditions			Plastic Rotation (rad)		Strength Loss Ratio	Performance Criteria (rad)		
$\frac{P}{A_g f_{ce}}$	$\rho_{sh}=\frac{A_{sh}}{b_w s}$	$\frac{V}{b_w h\sqrt{f_{ce}}}$	a	b	c	IO	LS	CP
≤ 0.10	≥ 0.0060	≤ 0.25	0.032	0.060	0.20	0.005	0.045	0.060
≤ 0.10	≥ 0.0060	≥ 0.50	0.025	0.060	0.20	0.005	0.045	0.060
≥ 0.60	≥ 0.0060	≤ 0.25	0.010	0.010	0	0.003	0.009	0.010
≥ 0.60	≥ 0.0060	≥ 0.50	0.008	0.008	0	0.003	0.007	0.008
≤ 0.10	≤ 0.0005	≤ 0.25	0.012	0.012	0.20	0.005	0.010	0.012
≤ 0.10	≤ 0.0005	≥ 0.50	0.006	0.006	0.20	0.004	0.005	0.006
≥ 0.60	≤ 0.0005	≤ 0.25	0.004	0.004	0	0.002	0.003	0.004
≥ 0.60	≤ 0.0005	≥ 0.50	0.0	0.0	0	0.0	0.0	0.0

To model columns in Perform3D, frame member compound components are defined as shown in Figure 2.17. PMM hinges are assigned to each end of the elastic column elements, with the above-mentioned nonlinear properties. An elastic cross-section with effective rigidity is defined between these two hinges. In addition, rigid end zones are assigned to two ends of members to include the relatively stiffer region of beam-column connections in the analysis model.

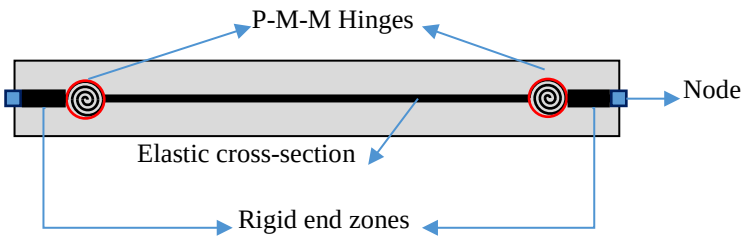

Figure 2.17 Modeling of columns.

2.4.2.4. Floor Slabs. Floor slabs that are components of the towers are not included in the model. Since the structural system includes frame and outrigger beams, effect of slabs to total response of the towers can be neglected. Instead, rigid diaphragms are assigned to the model at floor elevations of the tower structures However, to observe critical response quantities associated with diaphragm effects at the podium levels and include flexible podium slab behavior, slabs between the two towers are modeled using elastic shell elements at the connected floor levels. For effective rigidities of shell elements, stiffness modification factors given at Table 2.1 are used.

2.4.3. Gravity Loads

In linear analysis, gravity loads do not have any direct effect on the lateral response of the structure, other than indirect second-order effects. However, in nonlinear analysis, since behavior of columns and structural walls are modeled as axial load dependent, the lateral response of the structure is also greatly affected by gravitational forces. Therefore, gravity loads defined in the analysis model must be assigned realistic values. In other words, expected load effects should be incorporated in the analysis as realistically as possible. The expected gravity loads consist of dead loads and reduced live loads. As dead loads, self-weight of the structural members, architectural finishes (infill walls, cladding, floor finishing etc.) and, if exists, mechanical equipment, should be included in the model. As reduced live loads, live loads included in linear design stage are reduced by a factor and included in the analysis model. The reason behind reduction of the live loads is the fact that conservatively-defined design values of live loads are not likely to coincide with rare seismic events in reality. Therefore, during application of gravitational loads on the nonlinear model, live load reduction factors are defined as $n_B = 0.6$ for basement parking lots, $n_C = 0.6$ for commercial zones and $n_R = 0.3$ for residential zones.

2.4.4. Masses

Masses of the structure are defined in compliance with definition of dead and reduced live loads. Assembled point masses automatically calculated by ETABS are imported to the nonlinear model in Perform3D. Masses are defined only in X and Y directions, as is typical. Dynamic response of structure to vertical components of ground motions is included in

analyses with an implicit method suggested in TEC2017. Instead of modeling masses in Z (vertical) direction and including dynamic behavior explicitly, effects of dead loads are magnified by a factor calculated using Equation 2.25 (TEC2017).

$$E_d^{(Z)} \approx (2/3) S_{DS} G \tag{2.25}$$

2.4.5. Damping

Majority of energy dissipation sources are included in nonlinear analysis by modeling hysteretic behavior of the structural members. These members absorb seismic energy by taking damage in the inelastic range. On the other hand, there may be other sources that are not included in the model like non-structural elements, soil structure interaction etc. To also consider these non-modeled energy dissipation sources in analyses, additional viscous damping is introduced to the model. In TEC2017, 2.5% viscous damping ratio is suggested for nonlinear analysis of high-rise structures. This damping ratio is introduced into model as 2.4% modal damping and 0.1% Rayleigh damping to also damp out higher mode shapes, as suggested by Powell (2006).

2.4.6. Model Geometry

Since modeling of structural system geometry in Perform3D is troublesome, an ETABS model is first prepared, which is suitable to nonlinear model geometry, and this model is exported into Perform3D (Figure 2.18). In the nonlinear model, explicit modeling of the foundation and soil structure interaction is not included, as is typical for tall buildings that do not incorporate pile foundations. Instead, the structure is assumed to rest on fixed supports. To reduce the number of degrees of freedom and therefore the size of stiffness matrix, podium slabs are explicitly modeled only at the topmost four connecting podium level elevations (+12.80, +09.60, +06.40, +03.20) and at critical regions (Figure 2.19). Since the effect of tower floor slabs to the nonlinear seismic response of the towers is neglected (as significant seismic actions are not expected to develop on the slabs), tower and basement

floor slabs are assumed to have adequate in plane rigidities and are modeled using the rigid diaphragm assumption, as typically indicated in performance-based design guidelines.

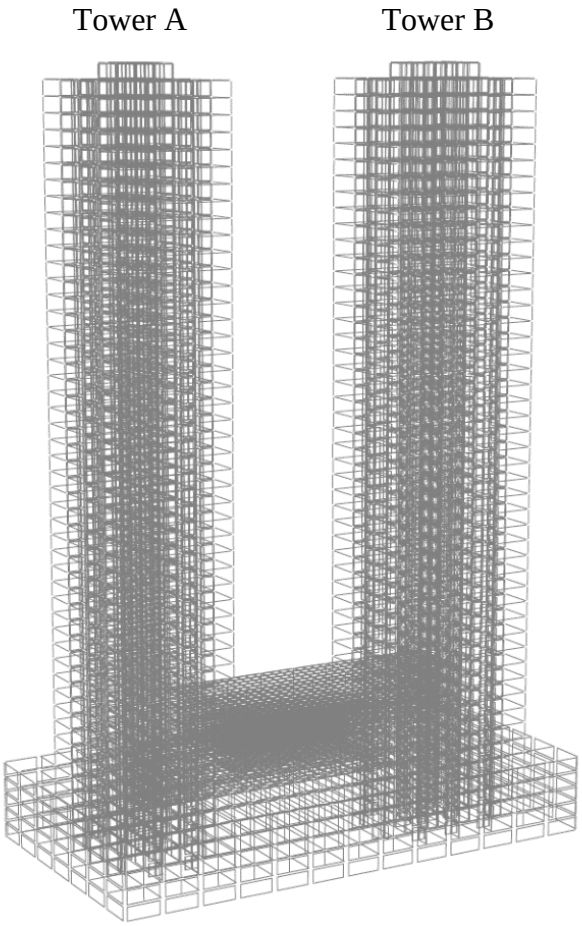

Figure 2.18 Perform 3D model geometry of double model.

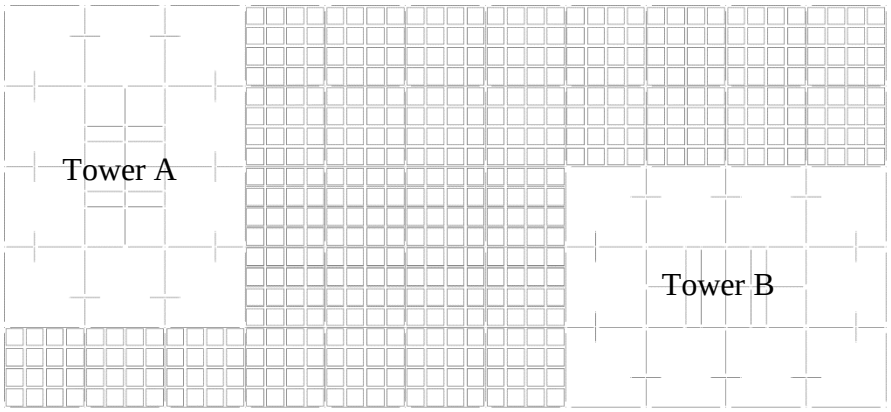

Figure 2.19 Modeling of podium slabs at critical floors.

2.5. Analysis Methods

To evaluate the seismic response of the structure, various analysis methods that are commonly used in real practice are adopted. These methods are linear modal response history analysis (LMRHA), linear direct integration response history analysis (LDIRHA), response spectrum analysis (RSA) and nonlinear response history analysis (NLRHA).

2.5.1. Linear Direct Integration Response History Analysis

LDIRHA is a dynamic analysis method, in which equations of motion of the structure subjected to ground motion time history are integrated directly within each time step. In LDIRHA, mass, stiffness, and damping matrices of the structure are formed and the differential equation of motion is solved using numerical methods, by applying the ground motion time history at small time intervals. In this study, Hilber-Hughes-Taylor Method is used with coefficients $\alpha = 0$, $\beta = 0.25$ and $\gamma = 0.5$ as numerical integration method.

2.5.2. Linear Modal Response History Analysis

LMRHA is a more computationally efficient dynamic time history analysis method. In LMRHA, uncoupled modal equations of motion are solved step by step separately, and responses of each natural vibration mode to applied ground motion time history are combined by direct summation within each time increment.

2.5.3. Response Spectrum Analysis

RSA is the most commonly used analysis method for strength-based linear elastic design of structures. In RSA, seismic demand is defined using a design spectrum (which is inherently a design-basis constant ductility acceleration response spectrum that is defined in seismic codes) instead of time histories. Spectral response quantities for each mode are obtained using this spectrum and the total response of the structure is calculated using a modal combination rule, which is typically complete quadratic combination (CQC) or square root of sum of squares (SRSS).

2.5.4. Nonlinear Response History Analysis

Analysis engine of Perform3D is used in NLRHA. In Perform 3D, NLRHA is conducted with Constant Average Acceleration as a step by step numerical integration method. Perform 3D is based on event to event solution strategy. In event to event solution strategy, time steps of ground motions are divided into sub steps when a nonlinear event occurs, in other words, when stiffness of the structure changes.

2.6. Seismic Hazard Definition and Ground Motion Record Selection

Ground motions of past earthquakes are recorded at numerous station points all around the world. These records are stored at ground motion databases after they are classified according to their properties such as local soil condition, distance between epicenter and source fault, fault mechanism etc. In this study, ground motion records are selected from NGAWest2 Ground Motion Database (PEER, 2013).

2.6.1. Definition of Target Spectra

Ground motions are selected by matching acceleration spectra of the motions with a target spectrum. This spectrum is defined as 1.3 times the design spectrum in TEC2017. To define the spectra, characteristic spectral accelerations coefficients, S_S and S_1 are needed. S_S and S_1 are spectral acceleration coefficients corresponding to the so-called short natural vibration period and the 1.0 second (or long period) natural vibration period, respectively.

For the short and long period spectral acceleration coefficients, ground motion levels are quantified considering their probability of exceedance values within a specific time interval, which is typically interpreted as the operating life of the structure. In TEC2017, ground motion levels to obtain these spectral acceleration coefficients are defined using four levels:

- DD1 level corresponds to ground motions with probability of exceedance of 2% in 50 years, with recurrence period of 2475 years.

- DD2 level corresponds to ground motions with probability of exceedance of 10% in 50 years, with recurrence period of 475 years.
- DD3 level corresponds to ground motions with probability of exceedance of 50% in 50 years, with recurrence period of 72 years.
- DD4 level corresponds to ground motions with probability of exceedance of 50% in 30 years, with recurrence period of 43 years.

In this study, the structure is analyzed under DD1 and DD2 level design earthquakes. Hence, target spectra corresponding to these seismic hazard levels are required. Short period and long period spectral acceleration coefficients required for these target spectra can be obtained from probabilistic seismic hazard analysis (PSHA).

In PSD, earthquake hazard levels at a construction site are typically obtained using a probabilistic approach, considering all of the seismic sources that are expected to create earthquakes in the region of the specified site location. Seismic sources are modeled as linear sources for well-known active faults and area sources for background seismicity. Seismic hazard analysis is not included within the scope of this study. Therefore, spectrum parameters at a hypothetical project site coordinates (40˚58’39.1”N, 28˚48’52.1”E) required to define the target spectrum are obtained from the draft Turkish Earthquake Hazard Map (TEHM) website (2017) released by the Disaster and Emergency Management Presidency (Table 2.12).

Table 2.12. Short and long period spectral acceleration at the project site.

	S_S	S_1
DD1	2.165	0606
DD2	1.244	0.338

In sites close to active faults, effect of earthquakes on structures with relatively long periods may magnify because of directivity effects. Therefore, spectral acceleration coefficients must be magnified with a fault distance coefficient if project site is close to an active fault. Distance between closest active fault and the hypothetical project site is

measured as $L_F = 11.2\ km$ from the TEHM maps (Figure 2.20). Therefore, the fault distance coefficient is calculated as $\gamma_F = 1.2$, as defined in Equations 2.26 and 2.27 (TEC2017).

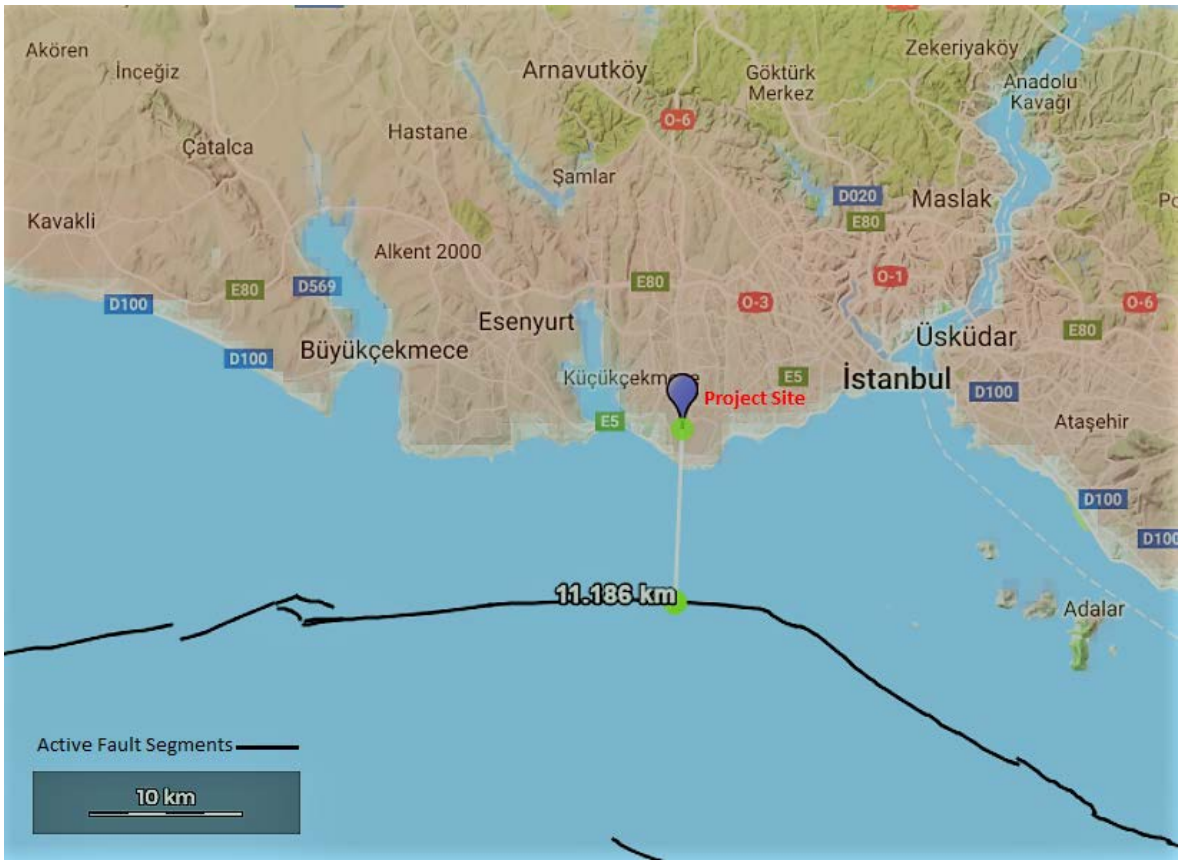

Figure 2.20 Distance between closest active fault and project site.

$$\gamma_F = 1.2 \qquad L_F \le 15\ km \tag{2.26}$$

$$\gamma_F = 1.2 - 0.02\left(L_F - 15\right) \qquad 25\ km \le L_F \le 15\ km \tag{2.27}$$

Spectral acceleration coefficients obtained from TEHM are defined for a reference soil condition of ZB-ZC boundary with first 30 meter shear wave velocity V_{S30} of 760 m/s. Therefore, these coefficients must be modified considering local soil conditions at the project site. Local soil effect coefficients are selected for the hypothetical project as $F_S = 1.2$ for short period and $F_1 = 1.4$ for 1 second period, according to TEC2017 (Table 2.13 and Table 2.14).

Table 2.13. Local soil effect coefficients for short period.

Local Soil Class	Short Period Local Soil Effect Coefficient, F_S					
	$S_S \leq 0.25$	$S_S = 0.50$	$S_S = 0.75$	$S_S = 1.00$	$S_S = 1.25$	$S_S \geq 1.50$
ZA	0.8	0.8	0.8	0.8	0.8	0.8
ZB	0.9	0.9	0.9	0.9	0.9	0.9
ZC	1.3	1.3	1.2	1.2	1.2	1.2
ZD	1.6	1.4	1.2	1.1	1.0	1.0
ZE	2.4	1.7	1.3	1.1	0.9	0.8
ZF	Site specific soil survey shall be done.					

Table 2.14. Local soil effect coefficients for long period.

Local Soil Class	Long Period Local Soil Effect Coefficient, F_1					
	$S_1 \leq 0.25$	$S_1 = 0.50$	$S_1 = 0.75$	$S_1 = 1.00$	$S_1 = 1.25$	$S_1 \geq 1.50$
ZA	0.8	0.8	0.8	0.8	0.8	0.8
ZB	0.8	0.8	0.8	0.8	0.8	0.8
ZC	1.5	1.5	1.5	1.5	1.5	1.4
ZD	2.4	2.2	2.0	1.9	1.8	1.7
ZE	4.2	3.3	2.8	2.4	2.2	2.0
ZF	Site specific soil survey shall be done.					

Considering hazard levels at the site, distance between project site and closest active fault, as well as local soil conditions, design spectral acceleration coefficients are defined (Table 2.15) according to Equations 2.28 and 2.29.

$$S_{DS} = S_S F_S \tag{2.28}$$

$$S_{D1} = S_1 F_S \gamma_F \tag{2.29}$$

Table 2.15. Design spectral acceleration coefficients.

	S_{DS}	S_{D1}
DD1	2.598	1.018
DD2	1.493	0.608

Finally, the design spectra are generated as shown in Figure 2.21 and Figure 2.22, using Equations 2.30 to 2.33.

$$S_{ae}(T) = \left(0.4 + 0.6\frac{T}{T_A}\right) S_{DS} \qquad (0 \le T \le T_A) \qquad (2.30)$$

$$S_{ae}(T) = S_{DS} \qquad (T_A \le T \le T_B) \qquad (2.31)$$

$$S_{ae}(T) = \frac{S_{D1}}{T} \qquad (T_B \le T \le T_L) \qquad (2.32)$$

$$S_{ae}(T) = \frac{S_{D1} T_L}{T^2} \qquad (T_L \le T) \qquad (2.33)$$

where corner periods T_A, T_B and constant spectral displacement range period limit T_L are defined by Equation 2.34

$$T_A = 0.2\frac{S_{D1}}{S_{DS}} \qquad T_B = \frac{S_{D1}}{S_{DS}} \qquad T_L = 6s \qquad (2.34)$$

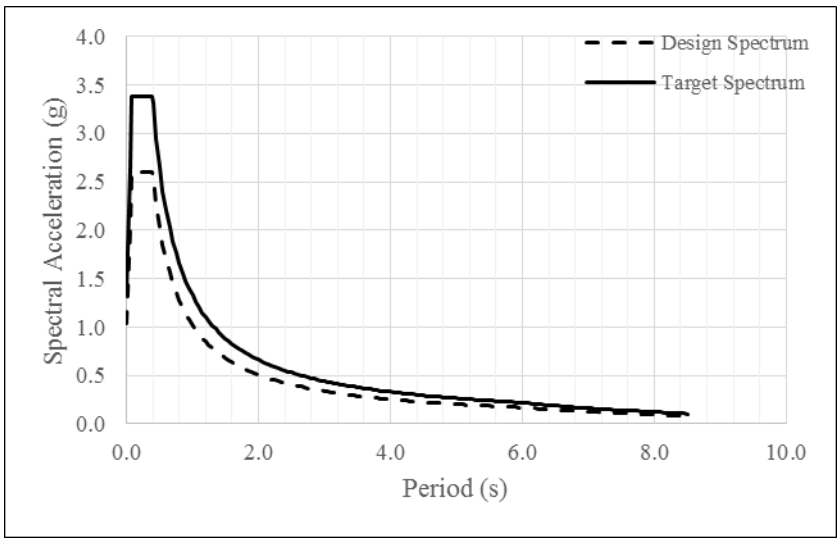

Figure 2.21. Design and target spectra for DD1 level earthquake.

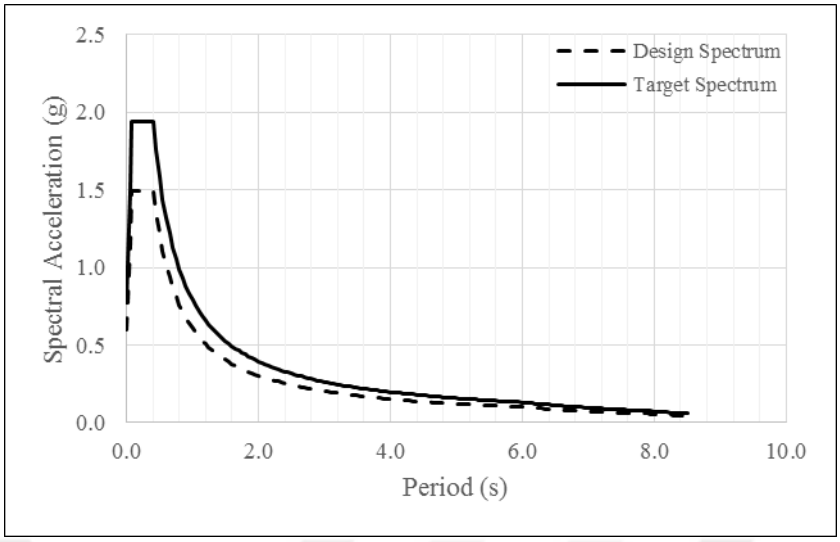

Figure 2.22. Design and target spectra for DD2 level earthquake

2.6.2. Selection and Scaling of Ground Motion Records

Ground motion records to be used in linear and nonlinear response history analyses of the structure should be selected with inherent properties similar to the type of earthquakes expected at the project site as much as possible. Therefore, parameters considered in filtering of candidate ground motion records during the selection process should be defined in a sensible range. Main properties considered in selection of ground motion records are:

- source type
- magnitude
- shear wave velocity, V_{S30}
- distance between project site and closest active fault, R_{JB}

Ground motion records are categorized and listed in databases, based on acceptable ranges of these parameters. Then, suitable records are selected using Mean Squared Error (MSE) method from this list. In the MSE method, mean error is quantified by calculating differences between spectral acceleration values of a record and target spectrum at specified periods of vibration of the structure using Equation 2.35

$$MSE = \frac{1}{m}\sum_{i=1}^{m} w_i \left(S_{aet} - S_{aer}\right)^2 \tag{2.35}$$

Suitable ground motions are linearly scaled to match the target spectrum. For the sake of not exceedingly deviating from the inherent characteristics of the original record, the maximum scale factor to be applied on a selected ground motion record is typically limited to 10. Furthermore, the records are selected such that the amplitudes of the two horizontal components of the record are not widely different. Pronounced difference between the amplitudes of the two horizontal components may not significantly influence linear response history analysis results. However, during nonlinear response history analysis, a component with disproportionally large amplitude may result in unrealistically large response quantities (e.g., interstory drift).

According to TEC2017, spectral acceleration values for mean resultant spectrum of selected records must not be lower than the target spectrum between $0.2\,T_P$ and $1.5\,T_P$ where T_P is fundamental natural vibration period of the structure. In addition to that, spectral acceleration values for mean components spectrum of selected records must not be lower than the design spectrum between period values of $0.2\,T_P$ and $1.5\,T_P$.

2.6.2.1. DD1 Level Earthquake Ground Motions. For DD1 level earthquake ground motions, specified filtering properties for selection of the ground motion records for nonlinear response history analyses conducted in this study are:

- Strike slip fault mechanism
- 6.9-7.4 magnitude range
- 360-760 m/s V_{S30}
- 5-65 km R_{JB}

Acceleration and displacement response spectra obtained for individual components, as well as SRSS spectra of the selected and scaled ground motion records are compared with selection criteria of TEC2017 in Figure 2.23 to Figure 2.26. Furthermore, properties of the selected and scaled ground motions are presented in Table 2.16.

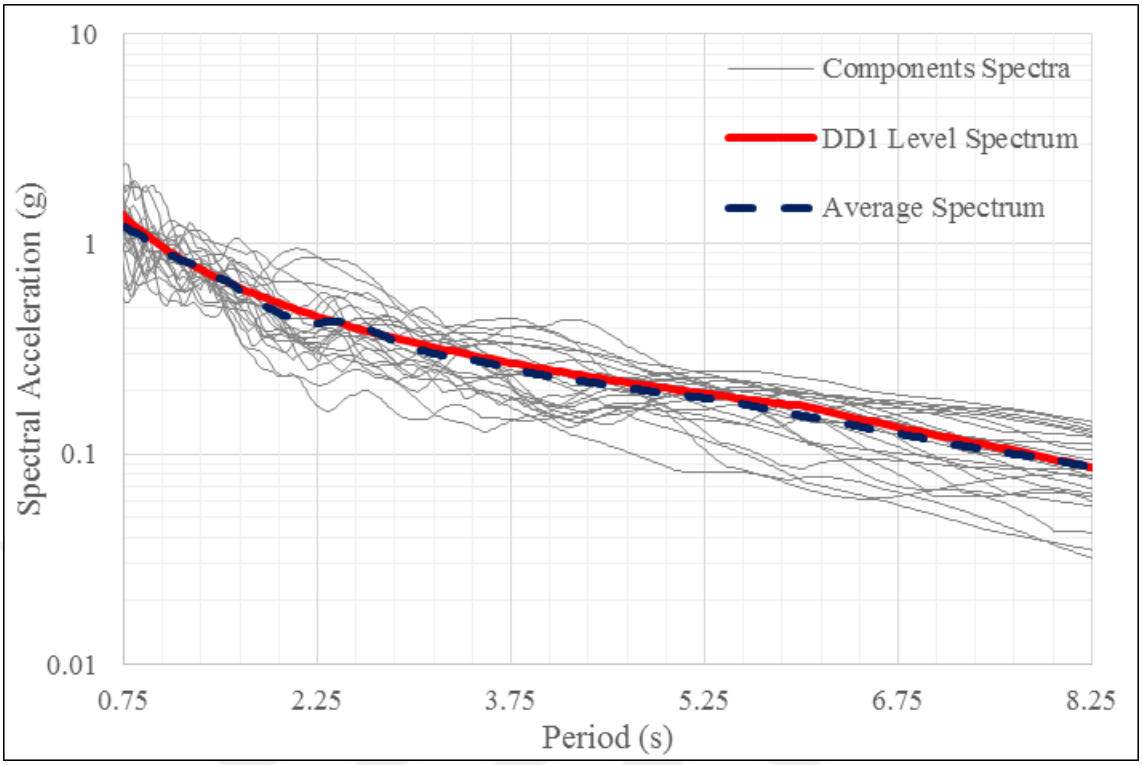

Figure 2.23. DD1 level acceleration response spectra of selected ground motions.

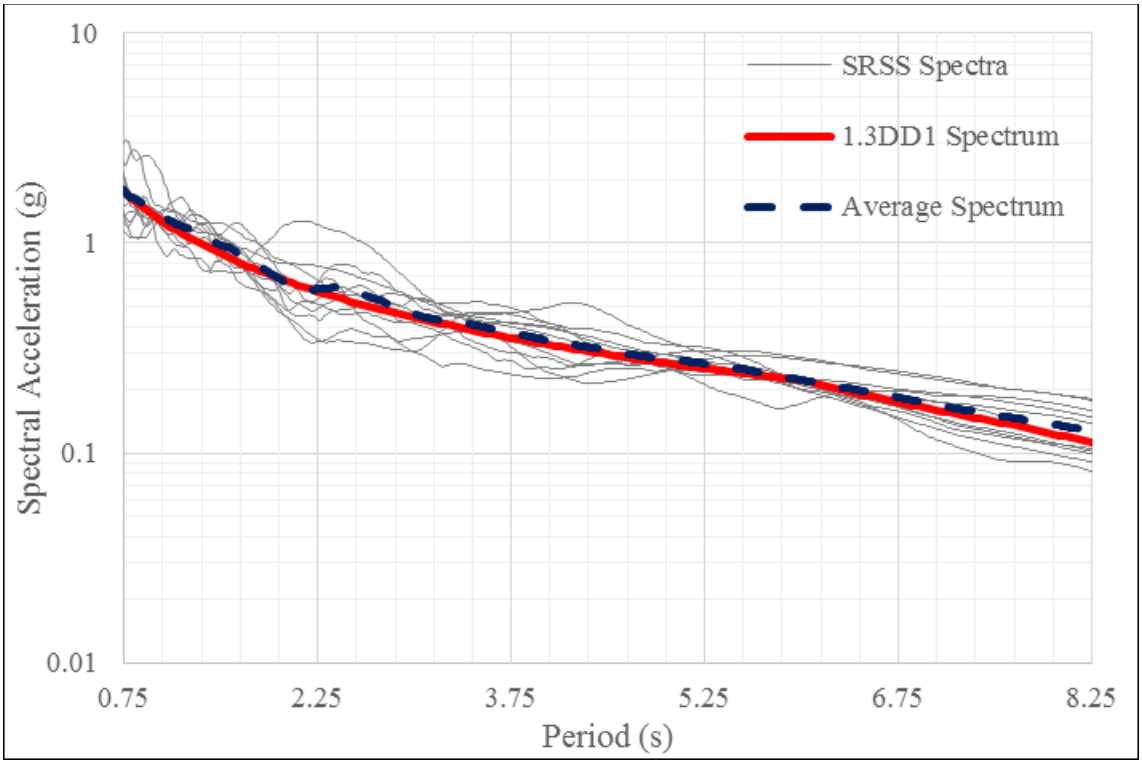

Figure 2.24. DD1 level SRSS acceleration spectra of selected ground motions.

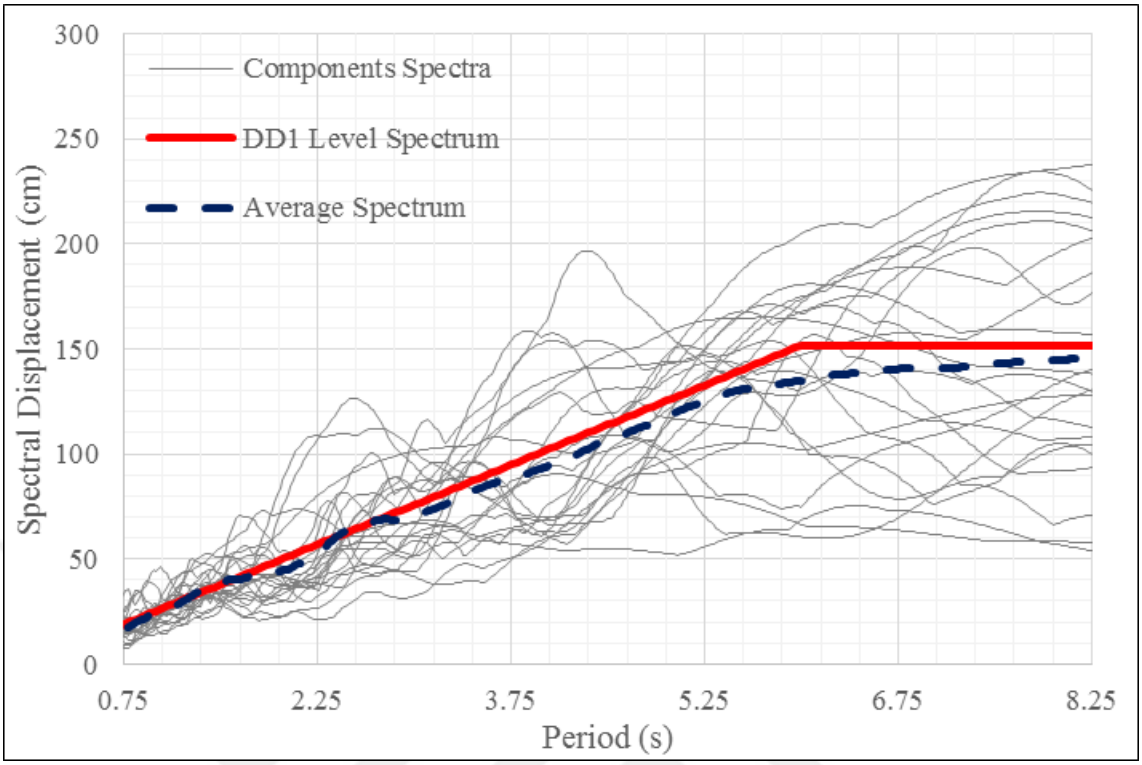

Figure 2.25. DD1 level displacement response spectra of selected ground motions.

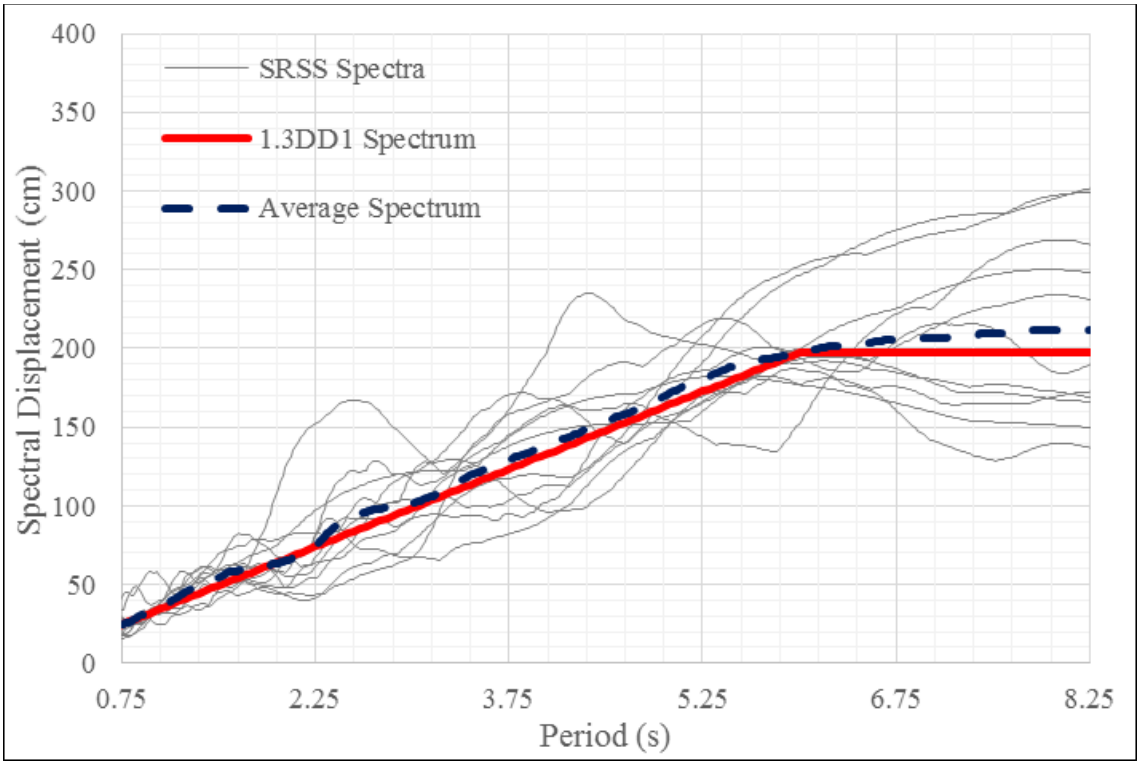

Figure 2.26. DD1 level SRSS displacement spectra of selected ground motions.

Table 2.16. Properties of selected ground motion records for DD1 level earthquakes.

Record ID	Earthquake Name	Scale Factor	Magnitude	Mechanism	R_{JB} (km)	V_{S30} (m/s)
RSN15	Kern County	6.327	7.36	Reverse	38.4	385
RSN746	Loma Prieta	9.406	6.93	Reverse Oblique	53.5	391
RSN762	Loma Prieta	8.695	6.93	Reverse Oblique	39.3	368
RSN802	Loma Prieta	2.465	6.93	Reverse Oblique	7.6	381
RSN838	Landers	4.837	7.28	Strike Slip	34.9	370
RSN900	Landers	2.107	7.28	Strike Slip	23.6	354
RSN1144	Gulf of Aqaba	9.421	7.20	Strike Slip	43.3	355
RSN1762	Hector Mine	3.326	7.13	Strike Slip	41.8	383
RSN1770	Hector Mine	8.119	7.13	Strike Slip	61.9	407
RSN3744	Cape Mendocino	2.207	7.01	Reverse	8.5	566
RSN6948	Darfield New Zealand	8.403	7.00	Strike Slip	30.6	482

2.6.2.2. DD2 Level Earthquake Ground Motions. For DD2 level earthquake ground motions, filtering properties for selection of the ground motion records for linear response history analyses are:

- Strike slip fault mechanism
- 6.2-7.3 magnitude range
- 360-760 m/s V_{S30}
- 10-55 km R_{JB}

Acceleration response spectra, displacement response spectra, and the SRSS spectra for the selected records are compared with the target spectrum in Figure 2.27 to Figure 2.30. Properties of selected and scaled ground motions for the DD2 earthquake level are presented in Table 2.17.

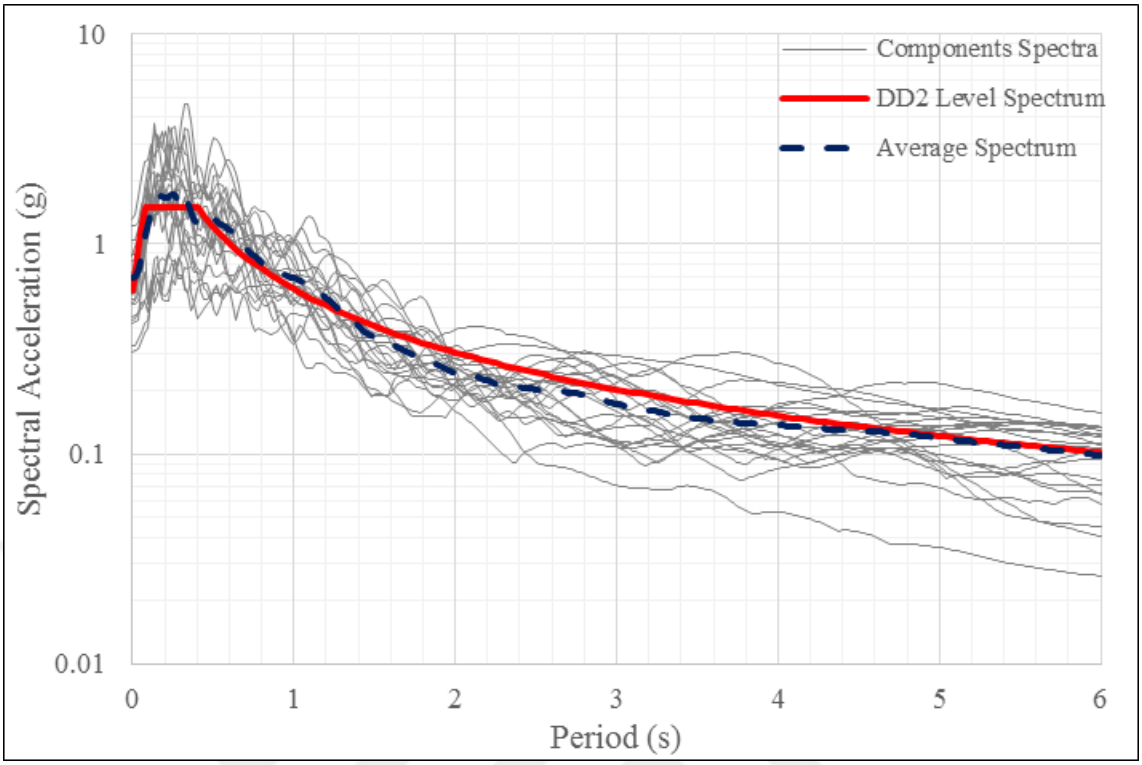

Figure 2.27. DD2 level acceleration response spectra of selected ground motions.

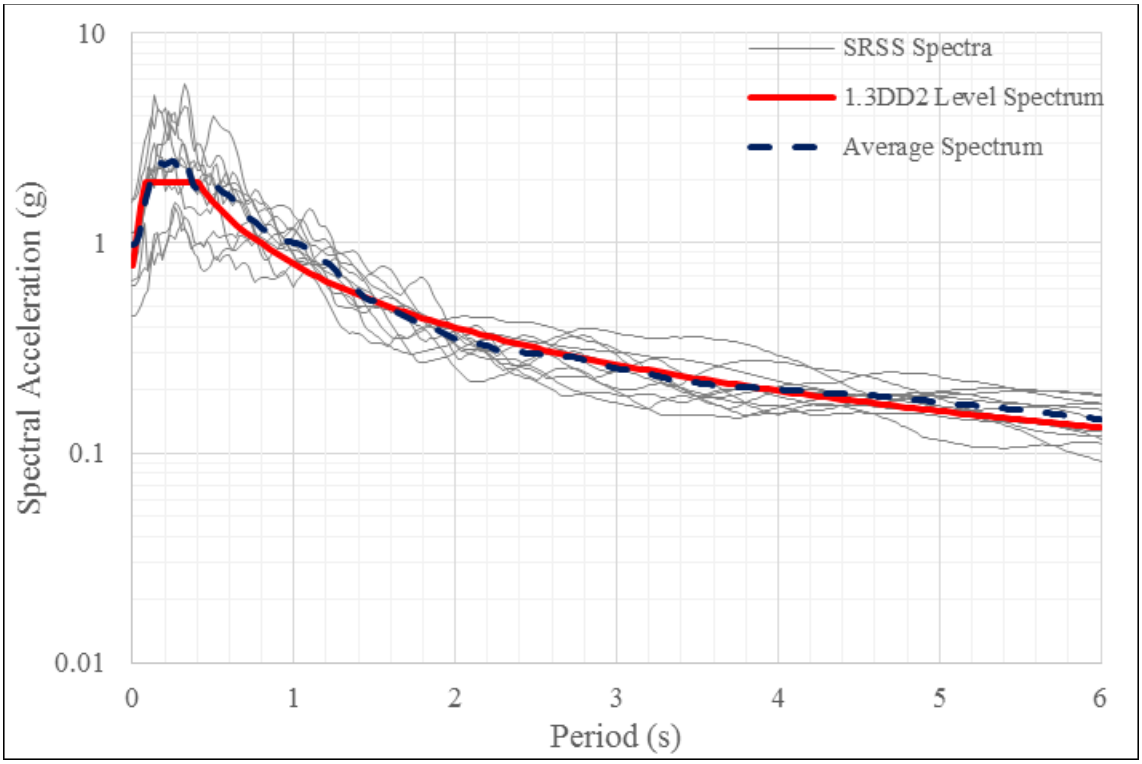

Figure 2.28. DD2 level SRSS acceleration spectra of selected ground motions.

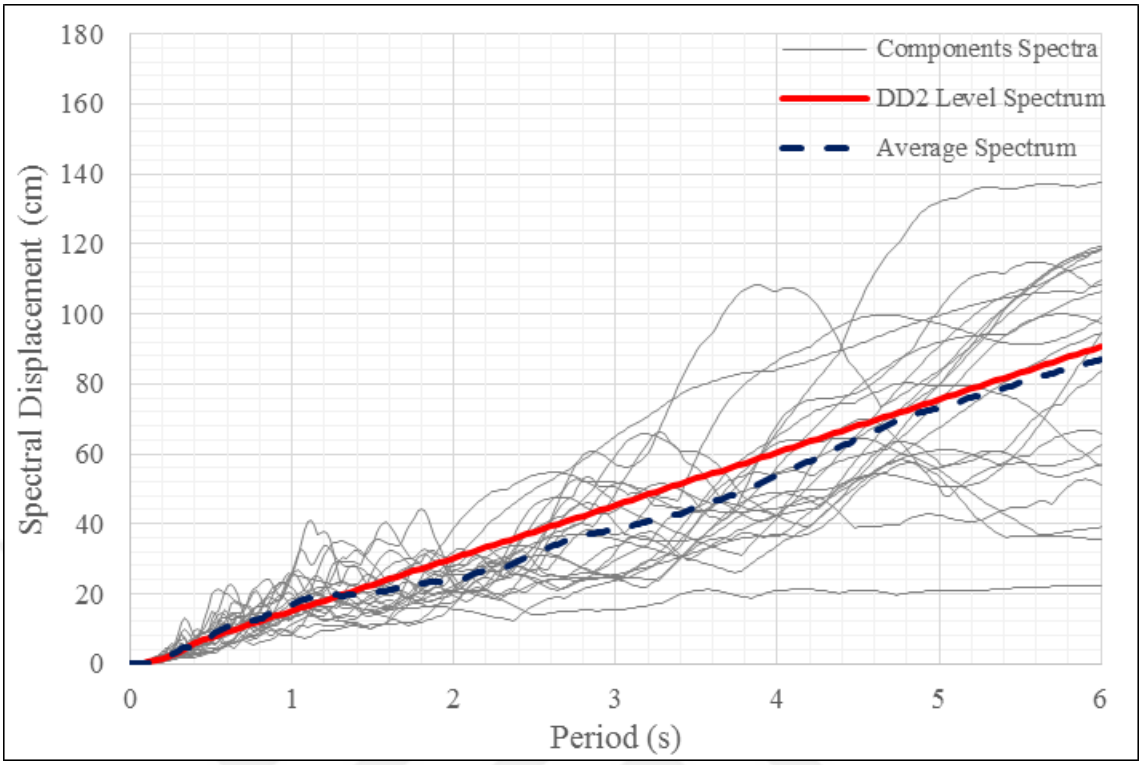

Figure 2.29. DD2 level displacement response spectra of selected ground motions.

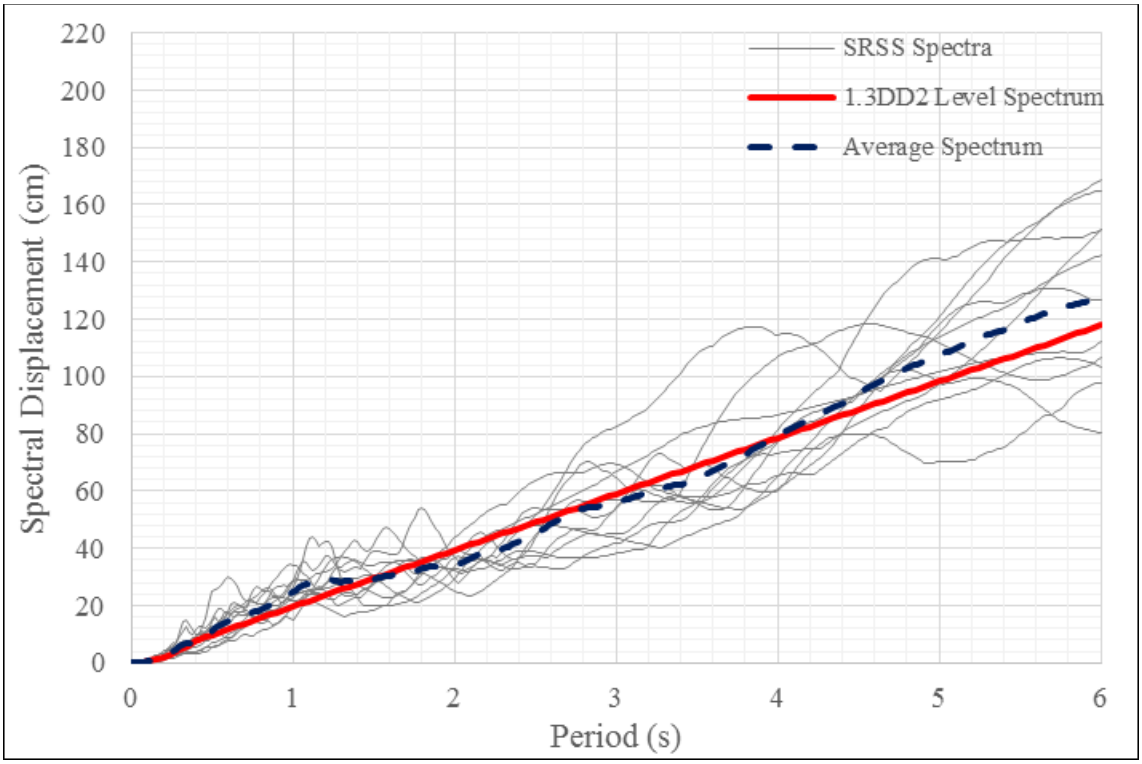

Figure 2.30. DD2 level SRSS displacement spectra of selected ground motions.

Table 2.17. Properties of selected ground motion records for DD2 level earthquake.

Record ID	Earthquake Name	Scale Factor	Magnitude	Mechanism	R_{JB} (km)	V_{S30} (m/s)
RSN164	Imperial Valley	3.436	6.53	Strike Slip	15.2	472
RSN838	Landers	3.302	7.28	Strike Slip	34.9	370
RSN1614	Duzce	6.780	7.14	Strike Slip	11.5	481
RSN1785	Hector Mine	8.398	7.13	Strike Slip	54.7	389
RSN1795	Hector Mine	9.498	7.13	Strike Slip	50.4	686
RSN2699	Chi-Chi Taiwan	4.455	6.2	Strike Slip	19.7	428
RSN2893	Chi-Chi Taiwan	4.399	6.2	Strike Slip	23.1	475
RSN3752	Landers	5.979	7.28	Strike Slip	45.3	436
RSN3760	Landers	6.340	7.28	Strike Slip	45.5	430
RSN6928	Darfield New Zealand	3.641	7.00	Strike Slip	25.2	650
RSN6948	Darfield New Zealand	4.908	7.00	Strike Slip	30.6	482

3. ANALYIS RESULTS

In the following sections, analysis results related to tensile and in-plane shear force resultants at connected podium floors as well as the seismic performance assessment of Tower A, obtained using the double tower model are presented. Furthermore, differences in response quantities obtained using the double tower model and single tower models are identified. To resist the diaphragm forces at podium floors, the required additional reinforcement in the diaphragms are calculated based on results of the different analyses. In all analyses, in-plane tensile and shear forces are obtained at section cuts defined adjacent to the tower edges (Figure 3.1).

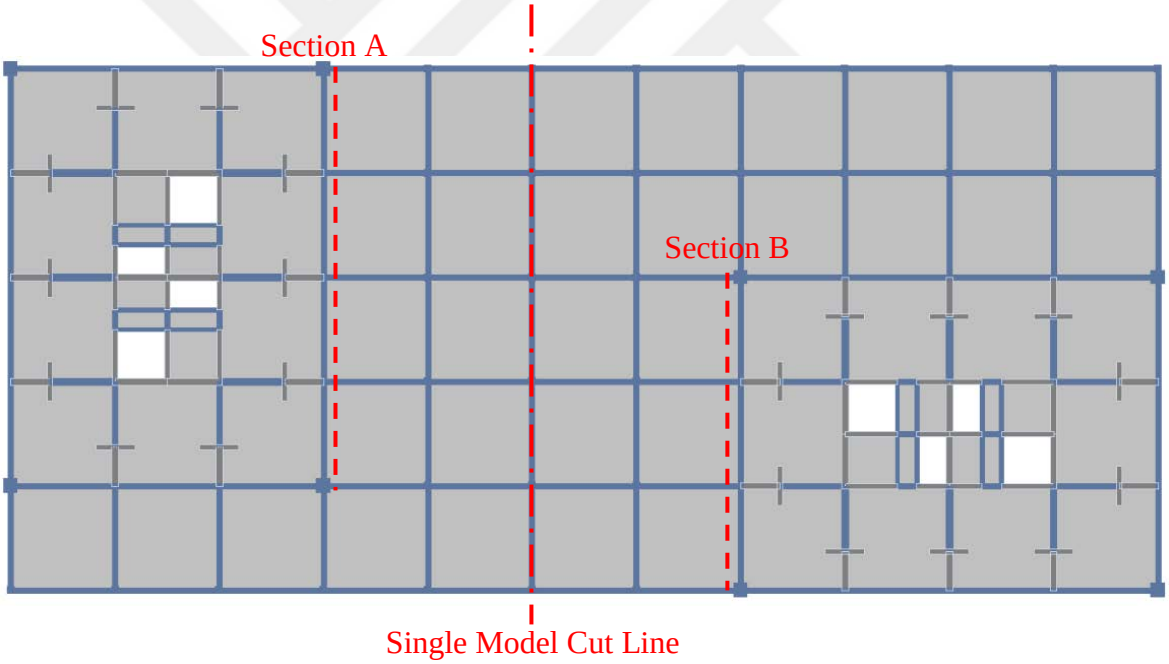

Figure 3.1. Section cut and single model cut line locations.

Since stress distribution differs between top and bottom face of slab elements due to out of plane bending behavior, in plane response of diaphragm is evaluated using force resultants (per unit slab thickness) instead of stresses. In addition, in plane behavior of floor diaphragms are considered as force-controlled elements in TEC2017, In other words, these elements are not allowed to exhibit inelastic deformation on in-plane behavior under seismic

loads. Therefore, during evaluation of analysis results of linear analysis, earthquake effects are magnified using the over-strength factor $D = 2.5$, as it is obligated by TEC2017.

Seismic demands for analyses are defined according to Section 2.6. In linear analyses, design spectrum of DD2 level seismicity (Figure 2.22) is used for RSA and 11 pairs of ground motion records selected for the target spectrum of DD2 level seismicity (Figure 2.28) are used for LMRHA and LDIRHA. Furthermore, seismic demand is defined for linear analyses using a structural system behavior factor $R = 6$ for structural systems where all seismic demand is resisted by uncoupled structural walls according to TEC2017. On the other hand, 11 pairs of ground motion records selected for target spectrum of DD1 level seismicity are used for NLRHA. In all response history analyses, total of 22 analyses are conducted, first by applying 11 ground motion record pairs, and secondly by reapplying the records at 90 degree rotated state. P-Delta effects are included in all analyses conducted using ETABS and Perform3D.

For interpretation of cracking in concrete, average tensile stresses at critical sections are compared with tensile strength. During calculations, total cross-sectional area of beams and slabs cut by sections are defined as $7.2\ m^2$ for section A and $5.44\ m^2$ for section B. Design tensile strength of concrete is calculated as 1.65 MPa using Equation 3.1 and expected tensile strength of concrete is calculated as 2.82 MPa using Equation 3.2 for C50 class concrete (TEC2017). These stress values correspond to cracking limit resultant tensile force magnitudes of 330 kN/m for design strength and 564 kN/m for expected strength.

$$f_{ctd} = \frac{0.35\sqrt{f_{ck}}}{1.5} \tag{3.1}$$

$$f_{cte} = 0.35\sqrt{1.3 f_{ck}} \tag{3.2}$$

For interpretation of the requirement for additional reinforcement against diaphragm shear forces, average shear stresses are compared with the shear strength of concrete. During calculations, total cross-sectional area cut by the sections are defined as $6.4\ m^2$ for Section A and $4.8\ m^2$ for Section B, considering only slab area. Design shear strength of concrete

is calculated as 1.07 MPa and expected shear strength of concrete is calculated as 1.83 MPa using Equation 3.3 and 3.4 for C50 class concrete (TEC2017). These stress values correspond to resultant shear force magnitudes of 214 kN/m for design strength and 366 kN/m for expected strength. Furthermore, required amount of additional reinforcement to resist in-plane shear forces at critical sections is calculated by Equation 3.5 and 3.6 (TEC2017).

$$f_{csd} = 0.65 f_{ctd} \tag{3.3}$$

$$f_{cse} = 0.65 f_{cte} \tag{3.4}$$

$$\tau_{rd} = 0.65 f_{ctd} + \rho_s f_{syd} \tag{3.5}$$

$$\tau_{re} = 0.65 f_{cte} + \rho_s f_{sye} \tag{3.6}$$

3.1. Response Spectrum Analysis Results

In plane distribution of resultant tensile forces (per unit slab thickness) in the floor diaphragm at +12.80 m elevation is presented in Figure 3.2 for RSA using the double model. From the figure, stress concentration between the two towers due to interaction at the podium floors can be observed clearly. Resultant tensile force magnitudes in slab elements reach up to 600 kN/m at locations where stiff structural walls and floor slab are connected. In addition, due to beam action in the podium diaphragm, stress concentrations at upper and lower edges of the critical zone are noted. From design perspective, when resultant tensile forces are compared with limit 330 kN/m corresponding to design tensile strength of concrete, it is clear that concrete cracks under tension and additional diaphragm reinforcement is required for code-compliant behavior.

Resultant tensile force distribution between connected diaphragms is presented in Table 3.1 and Figure 3.3 for RSA using double and single models. As it is expected, interaction effects are much more critical at first connected diaphragm than diaphragms at lower stories. Once results of total tensile forces at critical section cuts are evaluated, it is

clear that single models with fixed end restraints overestimate the in-plane response at critical zones. According to section cut results of the double model for RSA, average tensile stresses are calculated as 2.68 MPa for Section A and 2.75 MPa for Section B of the diaphragm at +12.80 m elevation. Total cross-sectional area of the additional reinforcement required for design strength are 52890 mm^2 for Section A and 41040 mm^2 for Section B at this level. In addition, axial loads on beams range between 800 kN and 1000 kN with total of 4420 kN for Section A and 3540 kN for Section B. Considering this distribution, additional diaphragm reinforcement can be designed as $\phi 16/300\ mm$ (1340 mm^2/m) top and bottom reinforcement in slabs and $8\phi 20$ (2512 mm^2) skin reinforcement in beams at Section A, and $\phi 16/300\ mm$ (1340 mm^2/m) top and bottom reinforcement in slabs and $8\phi 20$ (2512 mm^2) skin reinforcement in beams at Section B. Furthermore, when average stresses at lower podium levels are evaluated (1.36 MPa for Section A, 1.41 MPa for Section B), it is noted that concrete at these levels does not crack under axial tension; therefore, no additional reinforcement is required.

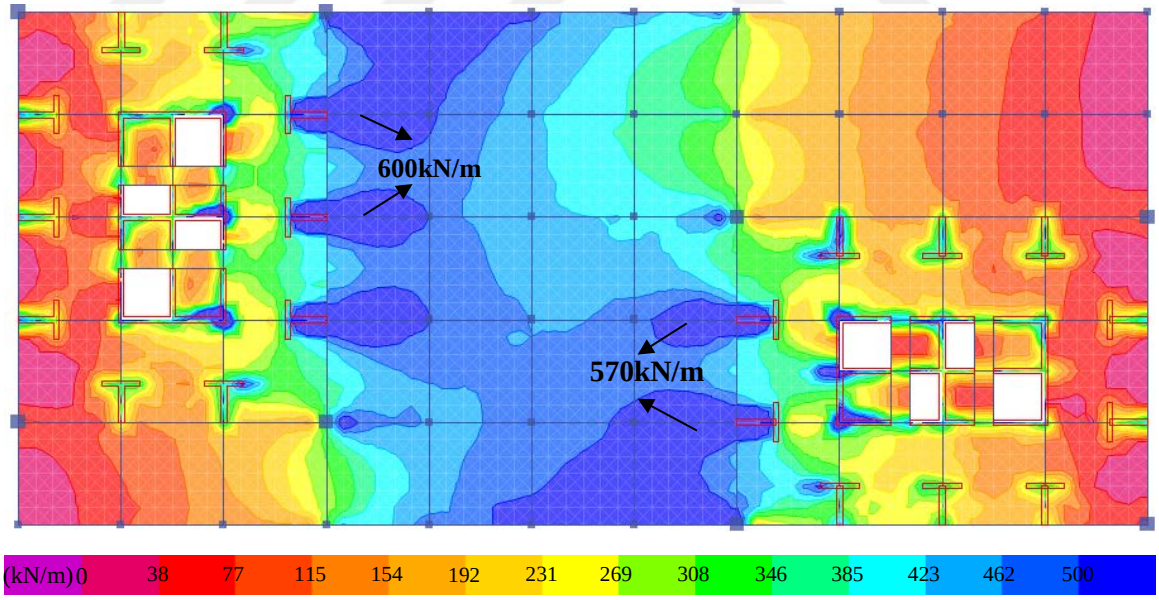

Figure 3.2. RSA resultant tensile force diagram at +12.80 m elevation of double model.

On the other hand, if fixed model analysis results are used in design, reinforcement amounts calculated for double model increase up to $\phi 16/200\ mm$ (2010 mm^2/m) and $8\phi 26$ (4248 mm^2) for Section A, $\phi 16/175\ mm$ (2297 mm^2/m) and $8\phi 26$ (4248 mm^2) for

Section B. Besides, according to fixed model results, the diaphragm at +09.60 m elevation also cracks and it can be designed with $\phi 12/200\ mm$ ($1130\ mm^2/m$) top and bottom reinforcement in slabs and $6\phi 22$ ($2280\ mm^2$) skin reinforcement in beams at Section A, and $\phi 12/175\ mm$ ($1291\ mm^2/m$) top and bottom reinforcement in slabs and $8\phi 20$ ($2512\ mm^2$) skin reinforcement in beams at Section B.

Table 3.1. RSA section cut tensile force resultants (kN).

	Tower A				Tower B			
	+03.20m	+06.40m	+09.60m	+12.80m	+03.20m	+06.40m	+09.60m	+12.80m
Double	5770	7052	9814	19305	2957	4322	7650	14980
Tower A	9484	11500	17532	32603	#N/A	#N/A	#N/A	#N/A
Tower B	#N/A	#N/A	#N/A	#N/A	8678	10452	14701	26388

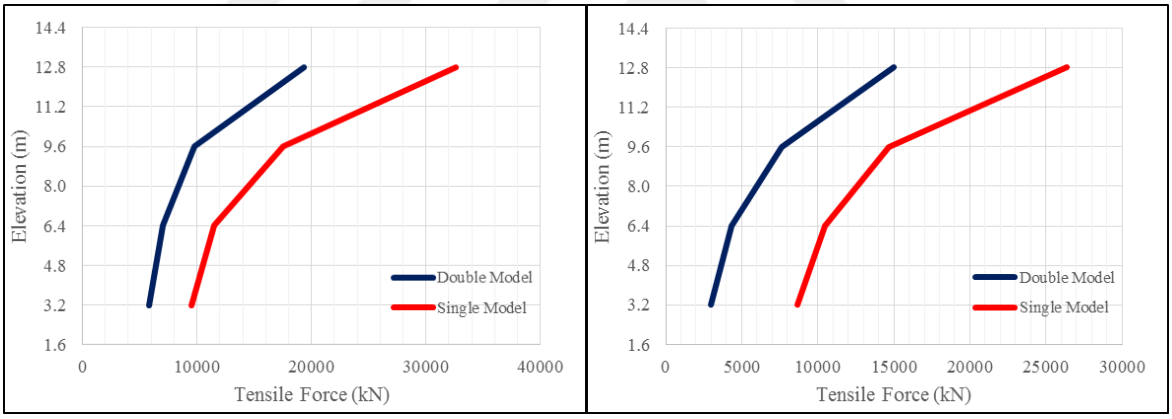

(a) (b)

Figure 3.3. RSA section cut tensile force distributions at (a) Section A, (b) Section B.

In-plane distribution of resultant shear forces (per unit slab thickness) in the podium floor diaphragm at +12.80 m elevation is presented in Figure 3.4 for RSA using the double model. Resultant shear forces in slab elements vary between 200 kN/m and 250 kN/m at regions between the two towers. Comparing these magnitudes with a resultant shear force capacity 214 kN/m, corresponding to concrete shear strength 1.07 MPa, it is observed that diaphragm shear forces are as not critical as tensile forces for this structure.

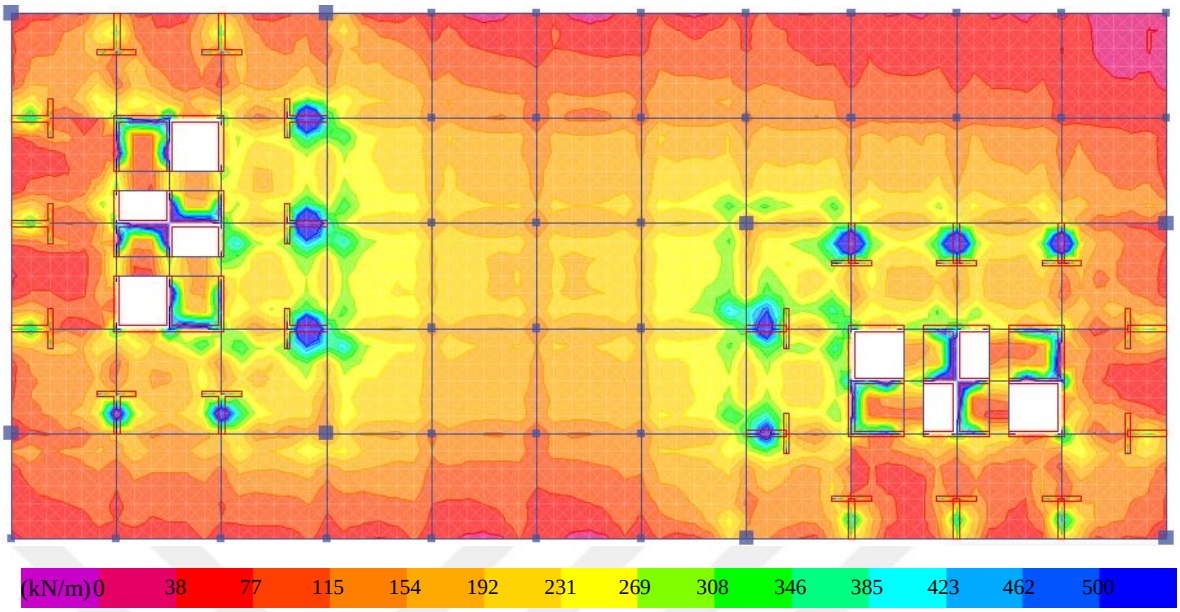

Figure 3.4. RSA resultant shear force diagram at +12.80 m elevation of double model.

Resultant shear force distribution between connected diaphragms is presented in Table 3.2 and Figure 3.5 for RSA using double and single models. Similar to tensile force distributions, total shear forces are highest at top connecting diaphragm as 7046 kN for Section A and 5542 kN for Section B, and diminish throughout lower stories down to 3785 kN for Section A and 2778 kN for Section B. Besides, resultant shear forces obtained using double and fixed models differ significantly, similar to tensile force resultants. According to the section cut results of the double model for RSA, average shear stresses are calculated as 1.10 MPa for Section A and 1.15 MPa for Section B, in the diaphragm at +12.80 m elevation. Since these stress levels are very close to the concrete design shear strength 1.07 MPa, the required amounts of additional reinforcement, which is 16 mm^2/m for Section A and 44 mm^2/m for Section B, are negligible for both sections.

On the other hand, if analysis results using the fixed model are used in design, average shear stress values increase up to 2.27 MPa for Section A and 2.41 MPa for Section B. Therefore, the required amount of additional reinforcement for design increases up to 658 mm^2/m for Section A and 734 mm^2/m for Section B. Based on these demands, reinforcement can be designed as $\phi 12/350\ mm$ (646 mm^2/m) top and bottom bars at Section A and $\phi 12/300\ mm$ (753 mm^2/m) top and bottom bars at Section B. Additionally,

according to section cut results of the fixed model under RSA, average shear stresses in the diaphragm at +09.60 m elevation are calculated as 1.29 MPa for Section A and 1.35 MPa for Section B. Since these stress levels are very close to the concrete design shear strength of 1.07 MPa, the required amount of additional reinforcement (121 mm^2/m for Section A and 153 mm^2/m for Section B), are also negligible for design purposes.

Table 3.2. RSA section cut shear force resultants (kN).

	Tower A				Tower B			
	+03.20m	+06.40m	+09.60m	+12.80m	+03.20m	+06.40m	+09.60m	+12.80m
Double	3785	4117	4549	7046	2778	2772	2983	5542
Tower A	4618	5688	8241	14548	#N/A	#N/A	#N/A	#N/A
Tower B	#N/A	#N/A	#N/A	#N/A	3759	4553	6467	11567

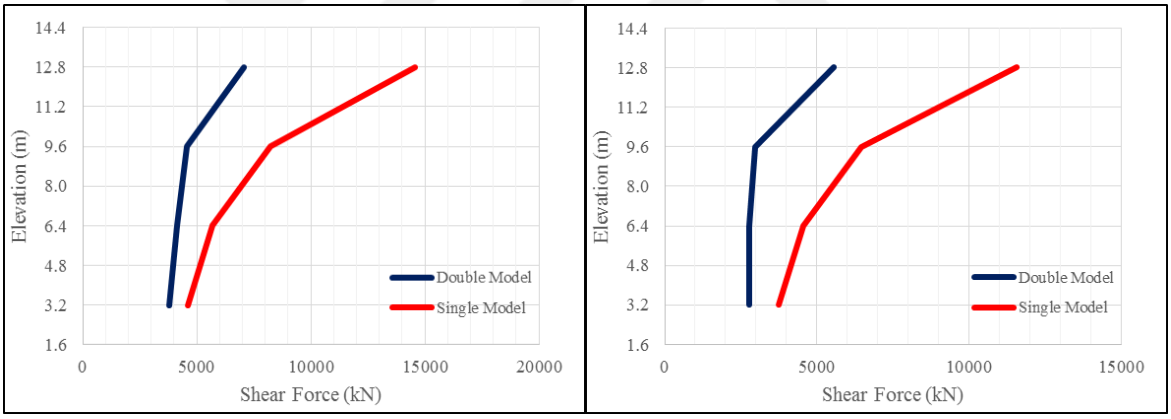

(a) (b)

Figure 3.5. RSA section cut shear force distributions at (a) Section A, (b) Section B.

3.2. Linear Modal Response History Analysis Results

Distribution of resultant tensile forces (per unit slab thickness) in the floor diaphragm at +12.80 m elevation is presented in Figure 3.6 for LMRHA using the double model. When LMRHA and RHA distributions are compared, it is observed that LMRHA gives similar resultant tensile force magnitudes and distributions compared to RHA results. The only difference noted is barely smaller magnitudes at critical regions of the diaphragm.

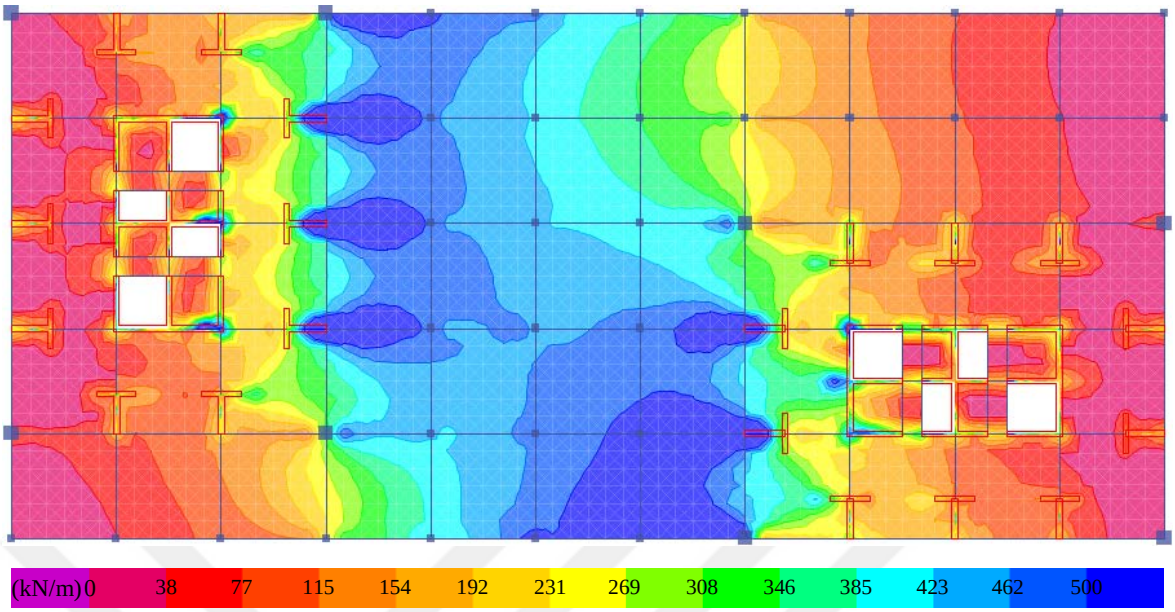

Figure 3.6. LMRHA with 5% modal damping resultant tensile force diagram at +12.80 m elevation of double model.

Resultant tensile force distribution throughout the connected podium stories is presented in Table 3.3 and Figure 3.7 for LMRHA using double and single models. To be consistent with RSA, mean results of 22 analyses are presented in the table and figure. Similar to RSA, analysis results of the fixed model overestimate the double model results. According to the average of 22 analyses, maximum resultant tensile force values obtained in the first connecting diaphragm are 18024 kN for Section A and 14322 kN for Section B. These resultants corresponds to average tensile stresses 2.50 MPa for Section A and 2.63 MPa for Section B. Since these stress levels are close to results of RSA, the same reinforcement design is applicable to resist the diaphragm forces.

Table 3.3 LMRHA with 5% modal damping section cut tensile force resultants (kN).

	Tower A				Tower B			
	+03.20m	+06.40m	+09.60m	+12.80m	+03.20m	+06.40m	+09.60m	+12.80m
Double	3259	4383	8017	18024	1903	3577	7180	14322
Tower A	5012	8092	15404	30863	#N/A	#N/A	#N/A	#N/A
Tower B	#N/A	#N/A	#N/A	#N/A	4584	7036	12041	22759

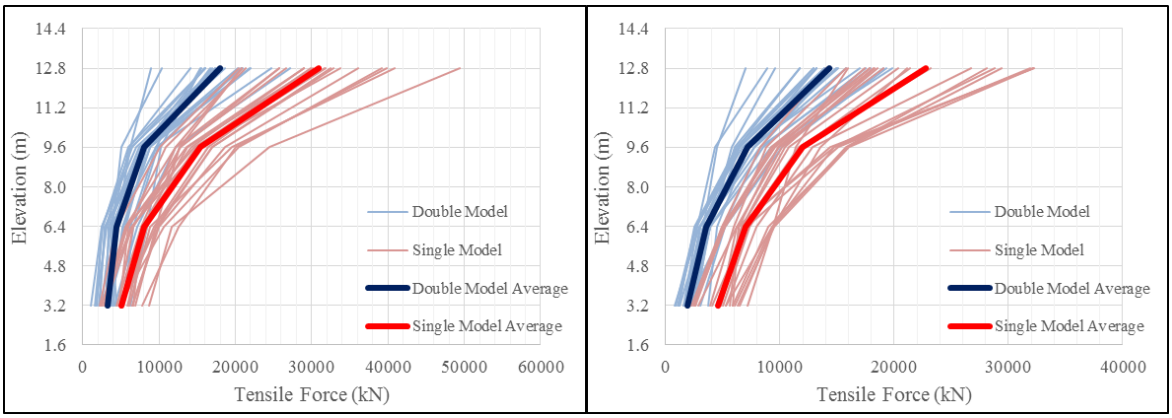

(a) (b)

Figure 3.7. LMRHA with 5% modal damping section cut tensile force distributions at (a) Section A, (b) Section B.

In-plane distribution of resultant shear forces in the floor diaphragm at +12.80 m elevation is presented in Figure 3.8 for LMRHA using the double model. Similar to tensile forces, distribution of resultant shear forces are also similar to RSA results. As was the case in RHA, resultant shear forces (per slab thickness) in the slabs vary between 200 kN/m and 250 kN/m in the region between the two towers.

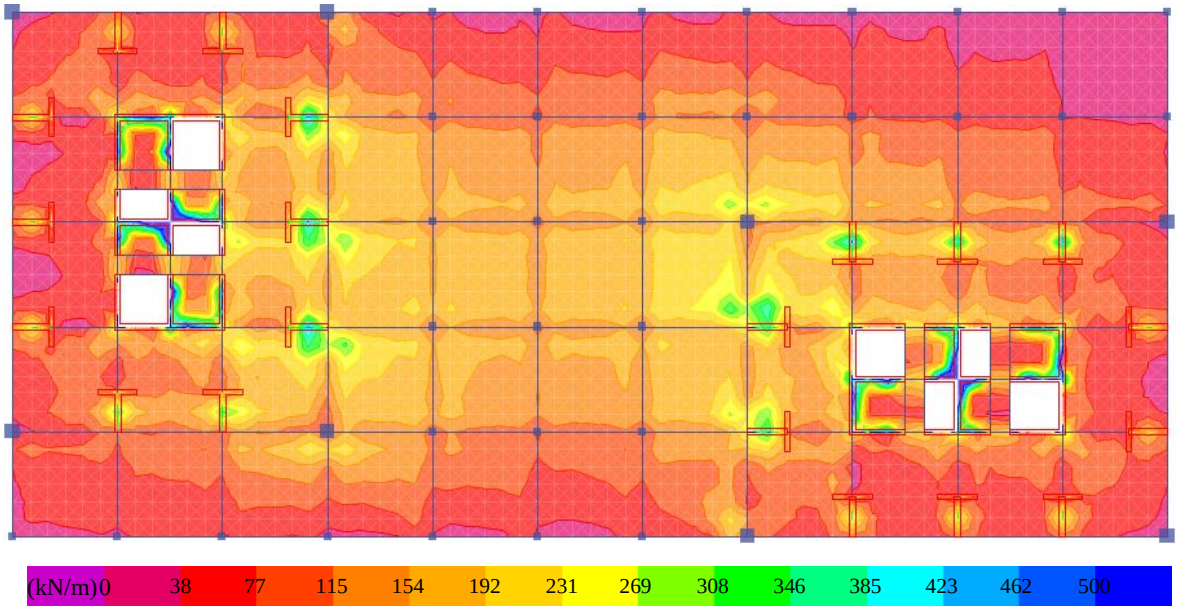

Figure 3.8. LMRHA with 5% modal damping resultant shear force diagram at +12.80 m elevation of double model.

Resultant shear force distribution along the connected podium floors is presented in Table 3.4 and Figure 3.9 for LMRHA using single and double models. Similar to RSA, analysis results obtained using the fixed model overestimate the double model results. According to average of 22 analyses, maximum resultant shear forces developing in the topmost connecting diaphragm are 5359 kN at Section A and 4324 kN at Section B. These resultants correspond to average tensile stresses of 0.84 MPa at Section A and 0.90 MPa at Section B. Since these stress levels are smaller than the concrete design shear strength of 1.07 MPa, no additional diaphragm shear reinforcement is required.

On the other hand, if fixed model analysis results are used in design, average shear stresses increase up to 2.27 MPa at Section A and 2.18 MPa at Section B. Since these stresses exceed the design shear strength of concrete 1.07 MPa, the required amount of additional reinforcement for design increases up to 658 mm^2/m for Section A and 608 mm^2/m for Section B at this level. According to these amounts, slab reinforcement can be designed as $\phi 12/350\ mm$ (646 mm^2/m) top and bottom bars at Section A, and $\phi 12/350\ mm$ (646 mm^2/m) top and bottom bars at Section B. In addition, according to section cut results of the fixed model under LMRHA, average shear stresses in the diaphragm of +09.60 m elevation are calculated as 1.34 MPa at Section A and 1.29 MPa at Section B. Since these stress levels are very close to the concrete design shear strength of 1.07 MPa, the required amount of additional slab reinforcement (148 mm^2/m for Section A and 120 mm^2/m for Section B), is negligible in design.

Table 3.4. LMRHA with 5% modal damping section cut shear force resultants (kN).

	Tower A				Tower B			
	+03.20m	+06.40m	+09.60m	+12.80m	+03.20m	+06.40m	+09.60m	+12.80m
Double	2829	2809	3438	5359	2034	1826	2147	4324.
Tower A	4103	5665	8585	14507	#N/A	#N/A	#N/A	#N/A
Tower B	#N/A	#N/A	#N/A	#N/A	3240	4231	6195	10485

In the following figures, comparison of distributions of resultant tensile and shear forces obtained from RSA and LMRHA of the single and double models, throughout the connected podium floors are presented. According to Figure 3.10, LMRHA consistently

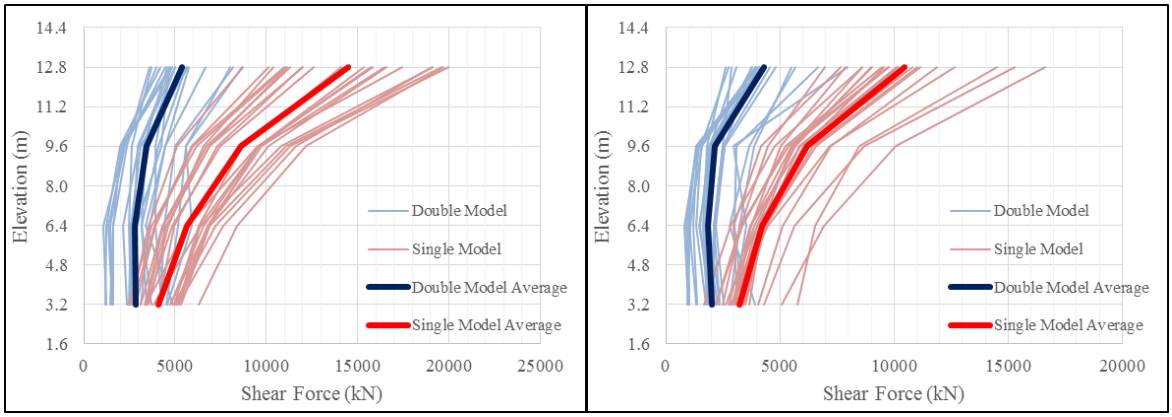

Figure 3.9. LMRHA with 5% modal damping section cut shear force distributions at (a) Section A, (b) Section B.

gives smaller tensile force values with respect to RSA. Resultant tensile forces at critical sections are very close to each other at the topmost connecting diaphragm, except for the single model results obtained for Tower B. Furthermore, differences in results of the two analysis methods are more significant at lower diaphragm levels. Similarly, according to Figure 3.11, shear force resultants obtained by LMRHA are generally smaller than RSA results. The only exception is the fixed model results for the section cut at +09.60 m elevation of Tower A. At this section, the result of LMRHA is barely higher than the RSA result.

The reason behind obtaining slightly different responses from RSA and LMRHA is the approach used in obtaining the design-level response quantities in the two analysis methods. In RSA, seismic demand is defined as a design spectrum, which represents a response spectrum obtained by applying ground motions to single degree of freedom systems with different periods and recording corresponding peak responses for all period values. During analysis of multi degree of freedom structures, peak modal response corresponding to each natural vibration period is obtained from the spectrum and contribution of each mode to a response quantity is calculated using the statistical modal combination rule CQC, in order to obtain total response of the structure. On the other hand, in LMRHA, ground motions are applied directly to the structural model for dynamic analysis. Modal response corresponding to each natural vibration period is obtained as a response history function and these response histories are summed directly without using any modal combination rule.

Since the peak response of each natural vibration period does not coincide at a specific time of the ground motion, LMRHA inherently gives different, and in general slightly smaller design-level response quantities compared with RSA, also depending on the selection and scaling of the ground motion records used. Since, in the analyses presented, LMRHA and RSA results are comparable, with RSA results being slightly larger, the ground motion selection and scaling approach used in this study can be deemed reliable for the structure investigated.

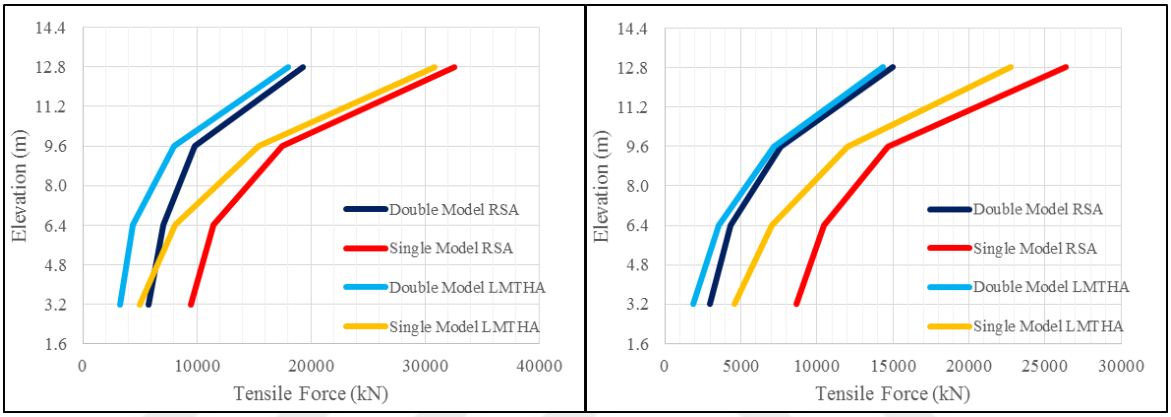

(a) (b)

Figure 3.10. Comparison of LMRHA and RSA tensile force distributions at (a) Section A, (b) Section B.

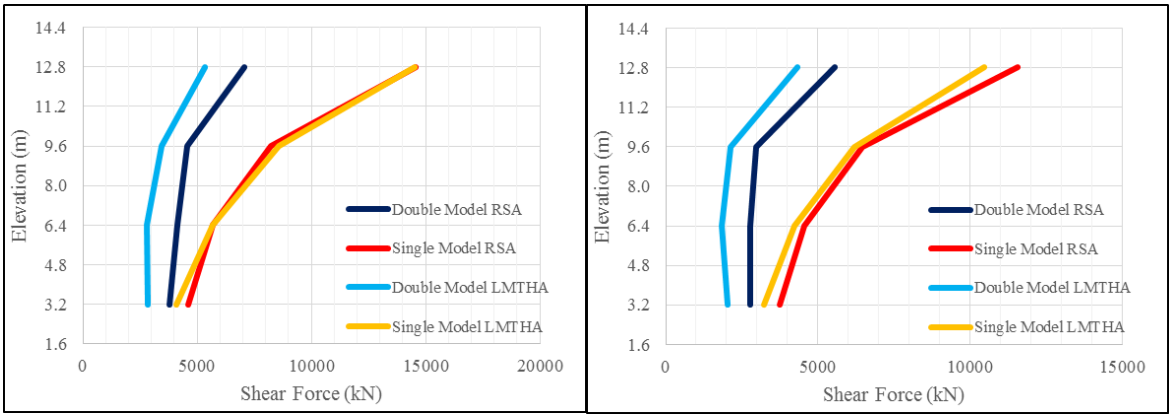

(a) (b)

Figure 3.11. Comparison of LMRHA and RHA shear force distributions at (a) Section A, (b) Section B.

3.3. Linear Direct Integration Response History Analysis Results

Due to its computational demands, LDIRHA is still not widely-used as a viable method for analysis and design of tall building structures. However, in this study, in order to compare results of LDIRHA and LMIRHA and identify possible differences, this analysis method is also applied for analyzing the double model of the structure. Comparisons of resultant tensile force and resultant shear force distributions throughout the connected podium diaphragms of the double model are presented in Figure 3.12 and Figure 3.13, respectively. Note that, for consistence between the two analysis methods, 5% Rayleigh damping is defined in both LMIRHA and LDIRHA models presented in this section. LMIRHA results presented in previous sections were obtained using 5% modal damping defined for all modes.

As shown in Figure 3.12, diaphragm tensile force resultants obtained from LDIRHA are moderately smaller compared to LMIRHA results. At the topmost diaphragm, resultant tensile force magnitudes are 15229 kN from LDIRHA and 17726 kN from LMIRHA at Section A, and 12331 kN from LDIRHA and 14324 kN from LMIRHA at Section B. Considering these magnitudes, LDIRHA results at most critical sections are lower than LMRHA results by 15% at Section A, and 14% at Section B. However, results of two analyses converge to each other at lower diaphragm levels. On the other hand, when diaphragm shear force resultants are compared, it is observed that two analysis methods provide approximately identical results, as shown is Figure 3.13. It can be deduced that the two analysis methods provide comparable results for the diaphragm forces developing at the connecting podium levels of the structure investigated.

3.4. Nonlinear Response History Analysis (NLRHA) Results

In the previous section, the diaphragm forces developing in the connecting podium floors of the two tower structure were evaluated using response spectrum and linear response history analysis methods, and using double and single tower models, in compliance with force-based design requirements under the DD2 design level earthquake. An earthquake load reduction factor (corresponding a behavior coefficient of R=6) and an over strength factor (D=2.5) was used in the analyses, as described in TEC2007. In this section, the diaphragm forces at the connecting podium levels are evaluated with a performance-based approach,

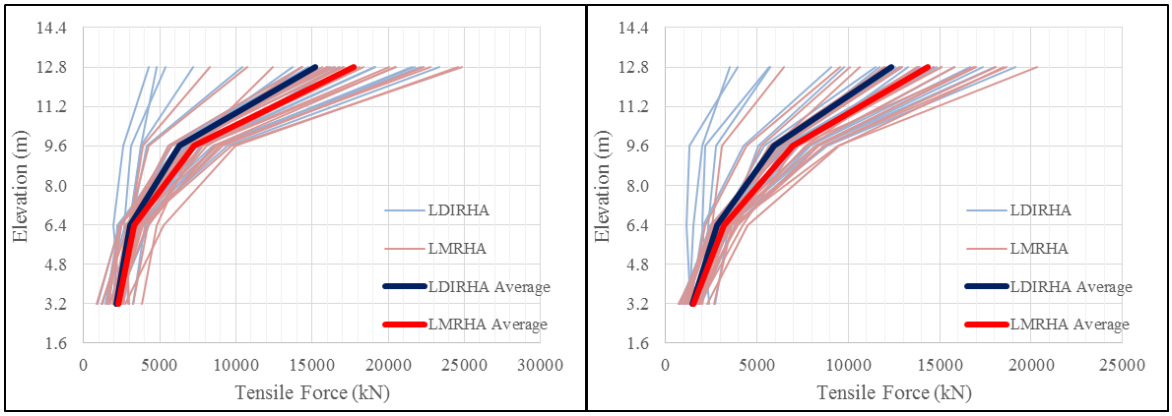

Figure 3.12. Comparison of LDIRHA and LMRHA tensile force distributions for double model at (a) Section A, (b) Section B.

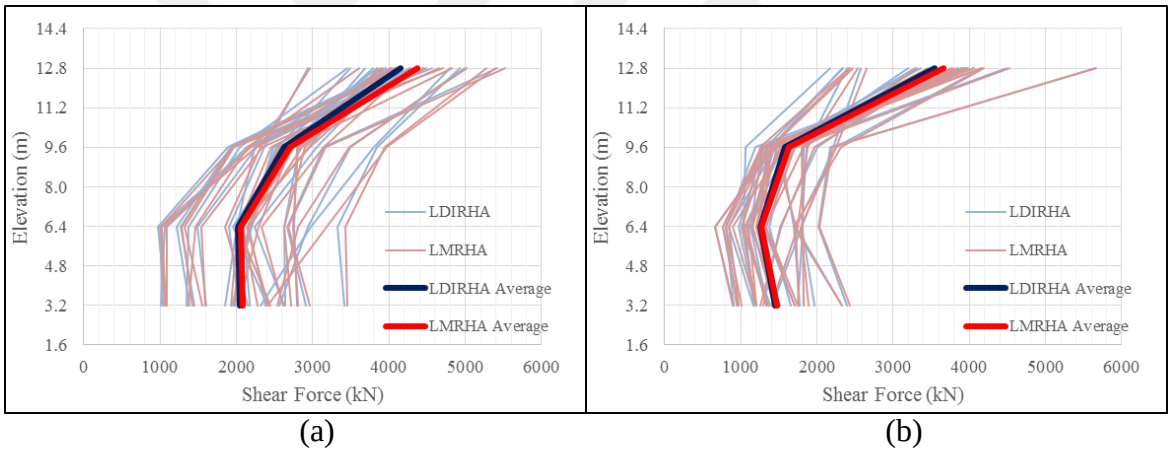

Figure 3.13. Comparison of LDIRHA and LMRHA shear force distributions for double model at (a) Section A, (b) Section B.

using NLRHA of the structure under the DD1 level earthquake, again using both double and single tower models. Required amounts of diaphragm reinforcement obtained from LHRHA results to reach sufficient diaphragm strength are compared with reinforcement amounts obtained using linear analysis results under the design-level earthquake. As well, the expected seismic performance of one of the towers (Tower A) under DD1 level ground motion is evaluated, based on analysis results obtained using the double tower model. Furthermore, performance predictions obtained for Tower A using the double tower model

are compared with predictions obtained using a single tower model, with both free and fixed end restraints at the connecting podium levels.

3.4.1. Podium Diaphragm Force Resultants

With the objective of reducing analysis time, compared to linear elastic models, podium diaphragms are modeled with shell elements with relatively larger size in the nonlinear Perform3D model of the structure. However, even though local stresses are not easily captured since the diaphragms are more crudely-meshed, reliable values for diaphragm force resultants can still be obtained from the analyses. Because NLRHA of the double model required weeks of analysis time, analysis under different ground motion records were run in parallel, using separate models running on separate computers. Therefore, graphical representation of the distribution of the diaphragm forces obtained from all 22 analyses is not available. However, for illustrative purposes, distribution of the diaphragm tension force (per unit slab thickness) developing in the topmost podium floor is illustrated in Figure 3.14, for a representative ground motion record RSN1762_0, which produces similar diaphragm force resultant magnitudes compared with the average of all 22 analyses. Differently from linear analysis results, due to the crude meshing, local stress concentrations in the slab at the structural wall connections are not recognizable. However, the overall distribution of the diaphragm tension forces is clearly shown in the figure. Tension force concentrations between the two towers as well as at top and bottom edges of the connecting podium can be identified, similarly to the results of linear analysis.

Tension force resultant distribution along connected podium floors is presented in Table 3.5 and Figure 3.15, for the average of 22 NLRHA cases (corresponding to 22 ground motions). Compared to results of RSA and NLRHA, force resultant distribution along the podium floor elevations shows a similar pattern. However, there is 18% increase at Section A and 31% increase at Section B, in the total tension force resultants at the floor with +12.80 m elevation, compared to RSA. This percent difference reaches to 48% increase at Section A and 35% increase at Section B, when analysis results using the fixed models are considered.

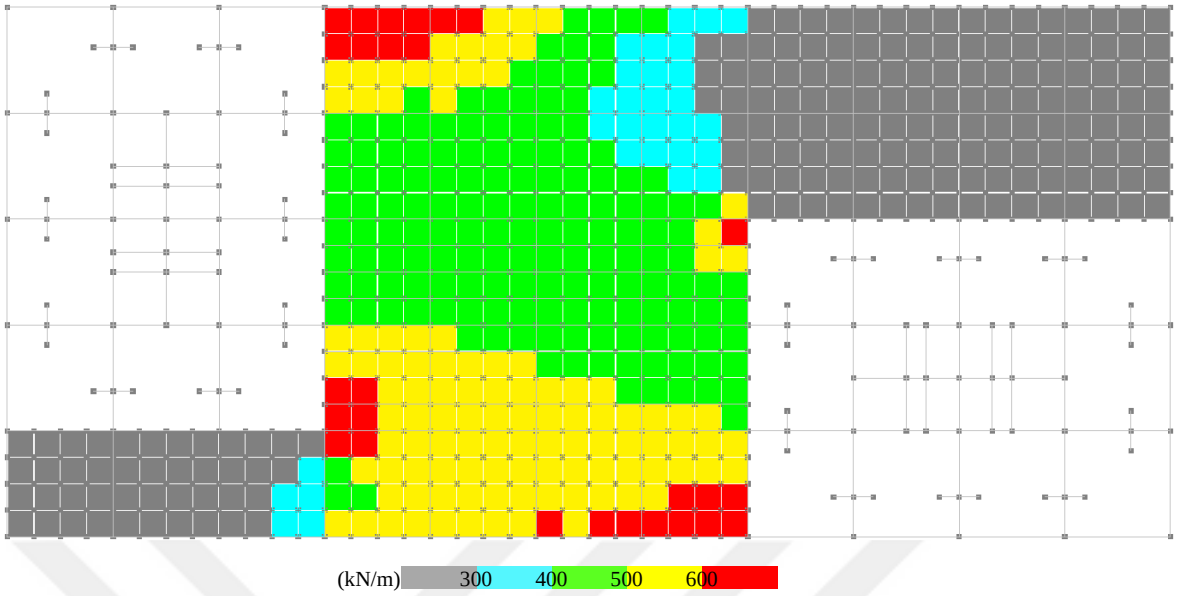

Figure 3.14. NLRHA RSN1762_0 resultant tensile force diagram (kN/m) at +12.80 m elevation of double model.

Considering mean analysis results (average of 22 ground motions) obtained using the double model, average tensile stresses developing at the topmost podium diaphragm are calculated as 3.17 MPa at Section A and 3.60 MPa at Section B. Comparing these stress levels with the expected tensile strength of concrete 2.82 MPa, it is clear that concrete cracks in tension and additional reinforcement is required in these regions, similarly to linear analysis results. Using expected yield strength, total amounts of required slab reinforcement are calculated as 45339 mm^2 for Section A and 38813 mm^2 for Section B. Furthermore, contribution of beams to the total tensile force resultant is obtained as 6762 kN at Section A and 5243 kN at Section B. Note that, percentages corresponding to contribution of beams to the total diaphragm tension force are 30% for Section A and 27% for Section B, whereas they were obtained as 23% for Section A and 24% for Section B from RSA. Taking into account all the information mentioned above, the required additional reinforcement can be designed as $\phi 14/300\ mm$ (1027 mm^2/m) top and bottom bars in the slabs and $9\phi 20$ (2826 mm^2) skin reinforcement in the beams at Section A, and $\phi 14/250\ mm$ (1232 mm^2/m) top and bottom bars in slabs and $7\phi 22$ (2660 mm^2) skin reinforcement in the beams at Section B. Average tensile stress levels at lower podium floors, which are 1.79 MPa at Section A and 1.88 MPa at Section B, are lower than the expected tensile strength of concrete.

Therefore, no additional reinforcement is required to resist diaphragm tension at lower podium floors.

On the other hand, when fixed model results are taken into account, average tensile stresses developing in the slabs at the topmost podium floor increase to 6.70 MPa at Section A and 6.82 MPa at Section B. Correspondingly, total amounts of required tension reinforcement increases up to 95655 mm^2 at Section A and 70687 mm^2 at Section B. According to these amounts, the required additional reinforcement can be designed as $\phi 18/250\ mm$ (2032 mm^2/m) top and bottom bars in slabs and $8\phi 30$ (5656 mm^2) skin reinforcement in beams at Section A, and $\phi 20/300\ mm$ (2093 mm^2/m) top and bottom bars in slabs and $8\phi 28$ (4928 mm^2) skin reinforcement in beams at Section B. Additionally, average tensile stress levels at the podium floor of +09.60 m elevation increases to 3.41 MPa at Section A and 3.29 MPa at Section B. Therefore, concrete at this floor also cracks and additional tension reinforcement is required. Required additional reinforcement at this elevation can be designed as $\phi 14/300\ mm$ (1027 mm^2/m) top and bottom bars in slabs and $8\phi 22$ (3040 mm^2) skin reinforcement in beams at Section A, and $\phi 14/300\ mm$ (1027 mm^2/m) top and bottom bars in slabs and $8\phi 20$ (2512 mm^2) skin reinforcement in beams at Section B.

Table 3.5. NLRHA section cut tension force results (kN).

	Tower A				Tower B			
	+03.20m	+06.40m	+09.60m	+12.80m	+03.20m	+06.40m	+09.60m	+12.80m
Double	4527	7800	12869	22851	2884	5634	10259	19562
Tower A	7557	12865	24550	48210	#N/A	#N/A	#N/A	#N/A
Tower B	#N/A	#N/A	#N/A	#N/A	3118	8441	17873	35626

In plane distribution of diaphragm shear forces (per unit slab thickness) in the podium floor slab at +12.80 m elevation is presented in Figure 3.16 for the RSN1762_0 ground motion analysis case of NLRHA using the double model. Similar to tensile forces, despite crude meshing, diaphragm tension effects are clearly shown in the figure. The in-plane shear force distribution is similar to linear analysis results.

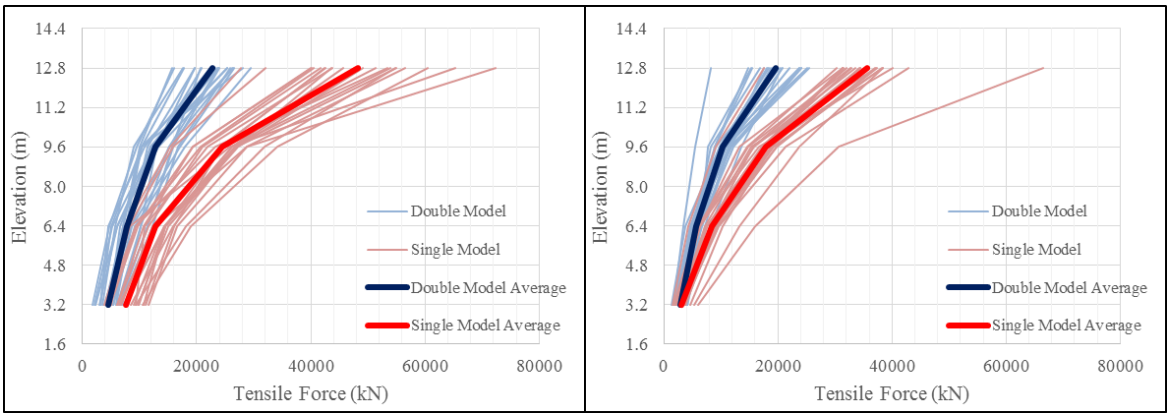

(a) (b)

Figure 3.15. NLRHA section cut tensile force distributions at (a) Section A, (b) Section B.

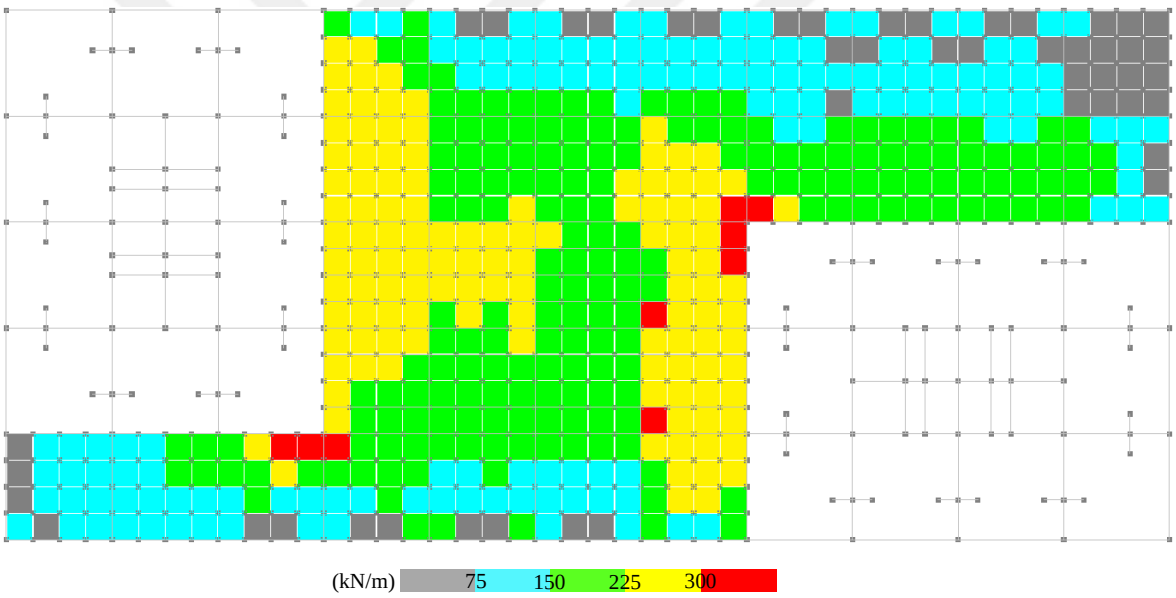

Figure 3.16. NLRHA RSN1762_0 resultant shear force diagram (kN/m) at +12.80 m elevation of double model.

Diaphragm shear force distribution along the connected podium floors is presented in Table 3.6 and Figure 3.17, as average of 22 load cases used in NLRHA. Comparing results of RSA and NLRHA, the distribution along the floors show similar patterns in single models, and slightly different patterns in double models. Furthermore, there is a 91% increase at Section A and an 87% increase at Section B in the total diaphragm shear force acting on the podium floor with +12.80 m elevation in the double model, compared to RSA. This percent

increase changes to 109% increase at Section A and 81% increase at Section B, when RSA and NLRHA results using fixed models are considered.

Considering mean response quantities of double model, average diaphragm shear stress values at the topmost podium floor are calculated as 2.10 MPa at Section A and 2.16 MPa at Section B. Since these stress levels are very close to the concrete design shear strength 1.83 MPa, the required amounts of additional diaphragm shear reinforcement, which is 107 mm^2/m for Section A and 131 mm^2/m for Section B, are negligible amounts for design purposes. Furthermore, analysis results show that the contribution of beams to diaphragm shear forces is negligible, as is typical.

On the other hand, if fixed model analysis results are considered in design, average diaphragm shear stress values at the topmost podium floor increase to 4.76 MPa at Section A and 4.37 MPa at Section B. Therefore, required amount of additional slab reinforcement increases up to 1163 mm^2/m at Section A and 1008 mm^2/m at Section B, at this elevation. Corresponding reinforcement can be designed as $\phi 14/250\ mm$ (1232 mm^2/m) top and bottom bars at Section A and $\phi 14/300\ mm$ (1027 mm^2/m) top and bottom bars at Section B. Again, diaphragm shear forces in the beams are negligible. Additionally, based on section cut results from NLRHA of the fixed models, average diaphragm shear stresses at the floor with +09.60 m elevation are calculated as 2.75 MPa at Section A and 2.64 MPa at Section B. Considering these stress levels, the floor slab at this elevation can be designed using $\phi 10/400\ mm$ (393 mm^2/m) top and bottom bars at Section A and $\phi 10/500\ mm$ (314 mm^2/m) top and bottom bars at Section B.

Table 3.6. NLRHA section cut shear force results (kN).

	Tower A				Tower B			
	+03.20m	+06.40m	+09.60m	+12.80m	+03.20m	+06.40m	+09.60m	+12.80m
Double	5224	7655	8294	13471	4121	5828	6407	10374
Tower A	8010	11502	17591	30442	#N/A	#N/A	#N/A	#N/A
Tower B	#N/A	#N/A	#N/A	#N/A	6877	9065	12675	20991

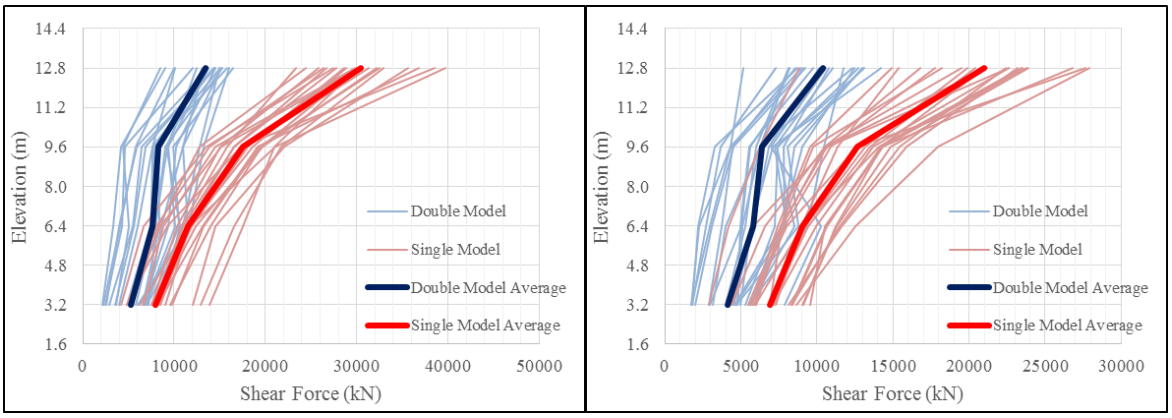

(a) (b)

Figure 3.17. NLRHA section cut shear force distributions at (a) Section A, (b) Section B

Finally, comparisons of diaphragm reinforcement required at critical sections, obtained using RSA (under DD2 level earthquake considering load reduction factor and over strength coefficient) and NLRHA (under DD1 level earthquake), are presented in Table 3.7 for Section A and Table 3.8 for Section B. According to the results listed in the tables, the amount of reinforcement required for design against diaphragm effects, obtained from RSA and NLRHA of the double model, are very close to each other. On the other hand, when fixed models are used for the analysis, the required amount diaphragm reinforcement obtained from NLRHA is moderately larger than that obtained using RSA. It is also interesting to observe that the amount of diaphragm reinforcement obtained from NLRHA of the double model under the DD1 level earthquake, which is the most robust and reliable analysis approach, is less than the reinforcement amount obtained from RSA of the single fixed model under the DD2 level earthquake, which is the simplest analysis approach that can be used for diaphragm design. This happens mostly because the fixed model overestimates the diaphragm effects in the connecting podium floors, as previously discussed in detail, and also because the design based on NLRHA uses expected material strengths, rather than reduced design strength values for the materials. Overall, this is a comforting result, since it implies that diaphragm design of connecting podium floors based on simple RSA of a fixed single tower model under the design level earthquake can potentially satisfy the required performance criteria of the double tower structure under the maximum considered earthquake level.

Table 3.7. Comparison of additional reinforcement at Section A for RSA and NLRHA.

Section A			RSA		NLRHA	
			+12.80 m	+09.60 m	+12.80 m	+09.60 m
Double Model	Tension	Beams	$2512\,mm^2$	0	$2826\,mm^2$	0
		Slab	$1340\,mm^2/m$	0	$1027\,mm^2/m$	0
	Shear	Slab	0	0	0	0
Fixed Model	Tension	Beams	$4248\,mm^2$	$2280\,mm^2$	$5656\,mm^2$	$3040\,mm^2$
		Slab	$2010\,mm^2/m$	$1130\,mm^2/m$	$2032\,mm^2/m$	$1027\,mm^2/m$
	Shear	slab	$646\,mm^2/m$	0	$1232\,mm^2/m$	$393\,mm^2/m$

Table 3.8. Comparison of additional reinforcement at Section B for RSA and NLRHA.

Section B			RSA		NLRHA	
			+12.80 m	+09.60 m	+12.80 m	+09.60 m
Double Model	Tension	Beams	$2512\,mm^2$	0	$2660\,mm^2$	0
		Slab	$1340\,mm^2/m$	0	$1232\,mm^2/m$	0
	Shear	slab	0	0	0	0
Fixed Model	Tension	Beams	$4248\,mm^2$	$2512\,mm^2$	$4928\,mm^2$	$2512\,mm^2$
		Slab	$2297\,mm^2/m$	$1291\,mm^2/m$	$2533\,mm^2/m$	$1027\,mm^2/m$
	Shear	slab	$753\,mm^2/m$	0	$1027\,mm^2/m$	$314\,mm^2/m$

3.4.2. Performance Assessment of Tower A using Double Model

In this section, seismic performance assessment of Tower A is performed, under the DD1 earthquake level, using NLRHA results. Interstory drifts, beam plastic rotations, structural wall shear forces, and structural wall longitudinal strains in concrete and reinforcing steel are evaluated as critical structural response parameters, as is typical in performance based design of tall buildings. Response quantities for Tower A are first obtained from the double model analyses, under the objective of achieving CP performance level under DD1 level earthquake hazard, based on TEC2017 and LATBSDC2015 requirements. It should be noted that response quantities obtained from RSA and LRHA (using double, fixed, or free models) for the towers were not compared in this study, since design of the towers is ultimately based on the performance based design approach using results of NLRHA. As well, the seismic performance of the tower is not evaluated and discussed in detail, since the scope of this study is to assess the effect of dynamic interaction

in the seismic response structures with multiple towers on a common podium. Comparison of performance analysis results for the tower using double, fixed and free model formulations are presented in the following section.

Interstory drift ratios are controlled at geometric centroid of each floor (Figure 3.18) on two principal directions of structural system. Performance limits for interstory drift ratios are defined in TEC2017 as 0.02 for LS and 0.03 for CP. Interstory drift ratios obtained for all 22 analyses, as well as their average in X and Y directions are presented in Figure 3.19 for Tower A. From the figure, it is observed that mean values reach maximum drift values of 0.023 in positive X direction, 0.022 in negative X direction, 0.014 in positive Y direction, and 0.014 in negative Y direction. According to these results, Tower A satisfies CP performance criteria considering interstory drift ratios.

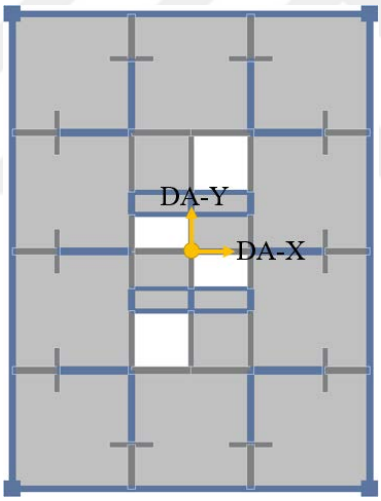

Figure 3.18. Interstory drift ratio control location for Tower A.

Plastic rotations obtained for all beams are presented in Figure 3.20. In the figure, average of 22 analysis is plotted as one data point for each beam. Performance limits for plastic rotations are defined as 0.025 rad and 0.05 rad for LS and CP of outrigger and perimeter beams, 0.03 rad and 0.05 rad for LS and CP of coupling beams, as defined in LATBSDC2015, according to Table 2.9 and Table 2.10. As can be observed in the figure, coupling beams of Tower A satisfy CP performance level. However, some of the outrigger beams fails to satisfy CP limits. Therefore, revisions on capacities of these beams are required to achieve CP performance criteria.

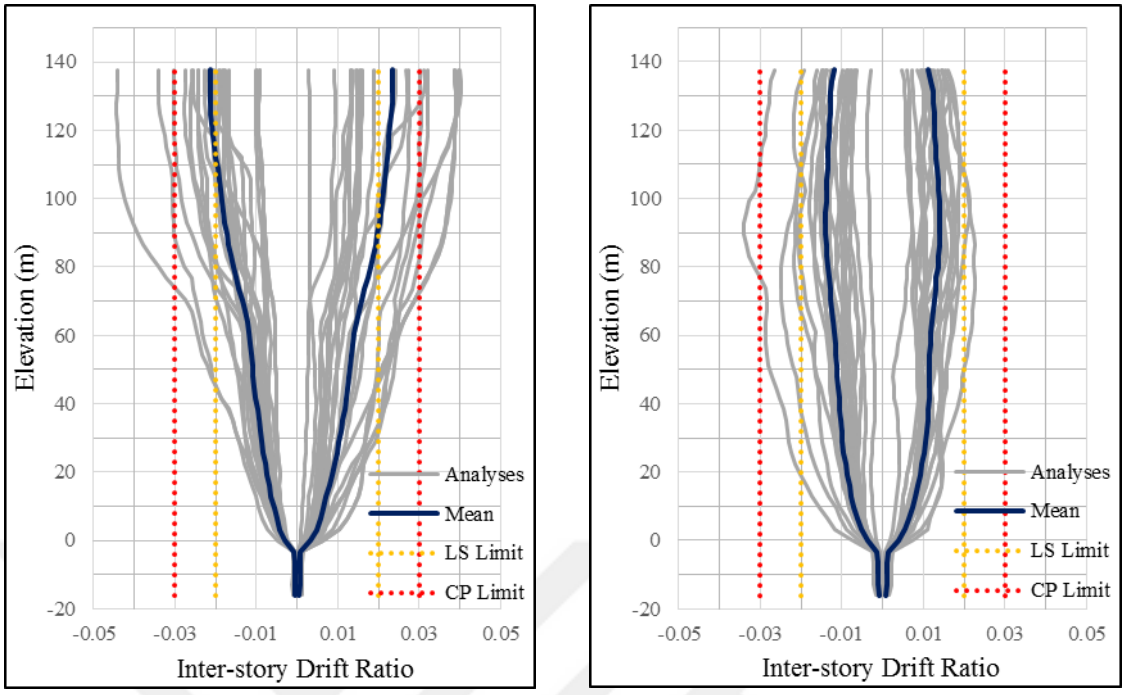

Figure 3.19 NLRHA interstory drift ratio distributions for Tower A (a) DA-X, (b) DA-Y.

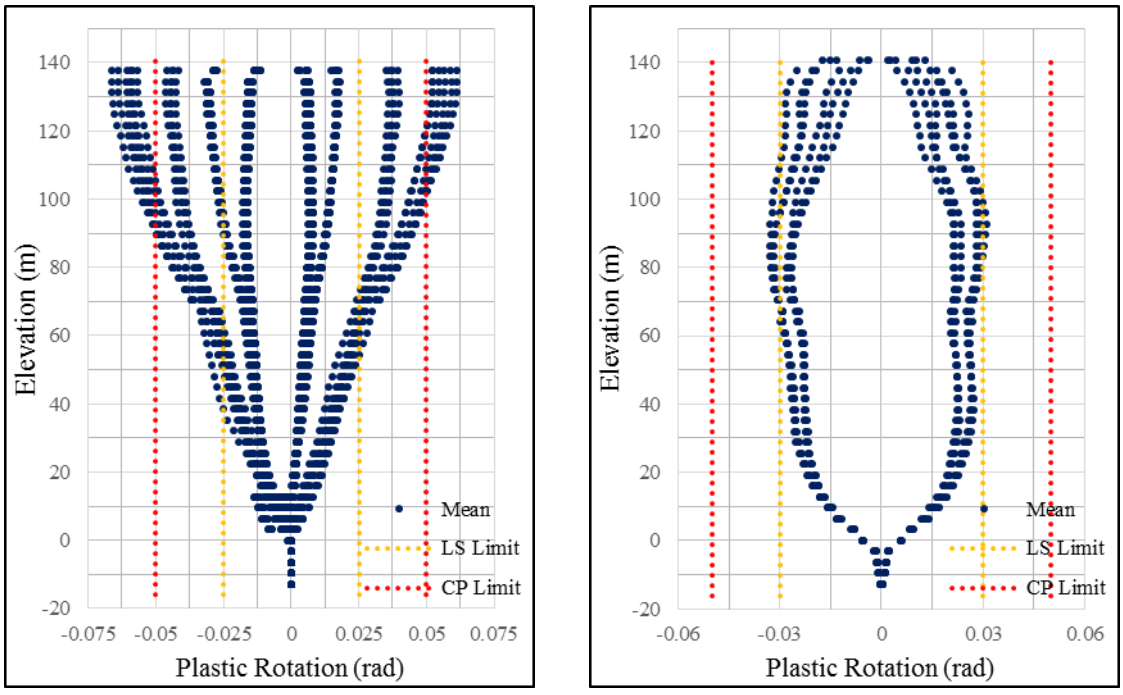

Figure 3.20 NLRHA beam plastic rotations for Tower A for (a) outrigger and perimeter beams, (b) coupling beams.

Although there is no performance limit for shear forces in structural walls, performance based design requires that all structural walls must have adequate shear capacity to in order to achieve reliable performance under earthquakes. According to TEC2017, shear forces considering average of 22 analyses, with an additional one standard deviation should not exceed the capacity of structural walls calculated according to TEC2017 wall shear strength provisions. Since shear (horizontal web) reinforcement of the walls are not is to be designed directly from the analysis results, shear forces obtained from the analyses are compared with maximum permissible wall shear capacities, which are calculated considering average shear stress limit $0.85\sqrt{f_{ce}}$ for walls (TEC2017). Accordingly, shear checks of the structural walls are presented in Figure 3.22 for selected walls (Figure 3.21) of Tower A.

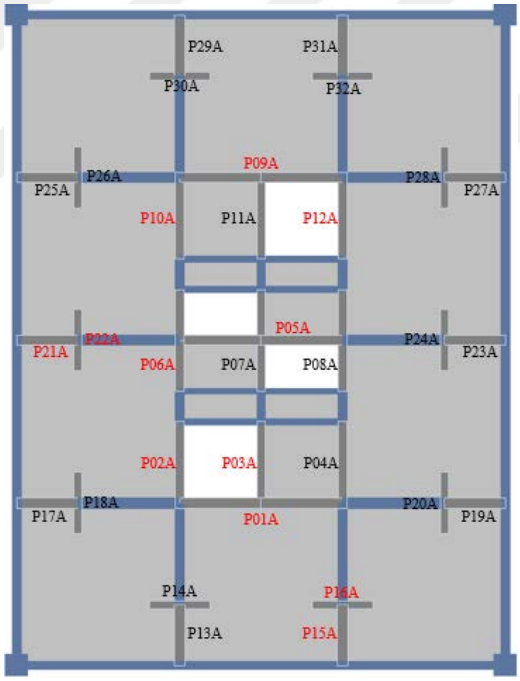

Figure 3.21 NLRHA structural wall shear force control locations for Tower A

According to Figure 3.22, all perimeter T-shaped wall components have sufficient maximum shear capacities. However, shear forces at components of core walls P01A, P05A and P09A exceed the code-prescribed shear stress limit; therefore, these walls require revision of wall thickness. The rest of the core walls components (P02A, P03A, P06A, P10A and P12A), although are close to the upper shear stress limit, have adequate maximum shear capacities.

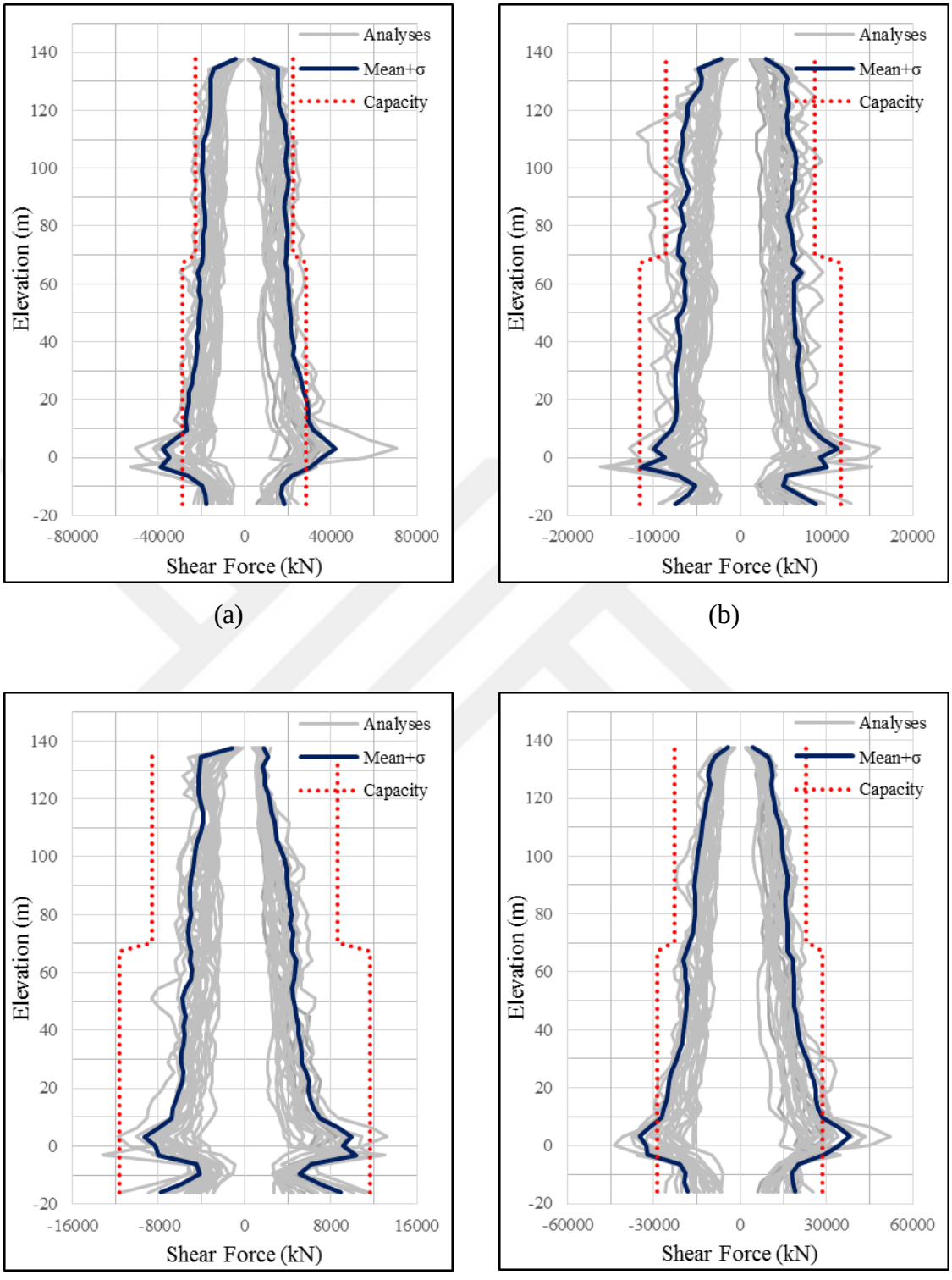

Figure 3.22. NLRHA structural wall shear force distributions for Tower A at (a) P01A, (b) P02A, (c) P03A, (d) P05A, (e) P06A, (f) P09A, (g) P10A, (h) P12A, (i) P15A, (j) P16A, (k) P21A, (l) P22A.

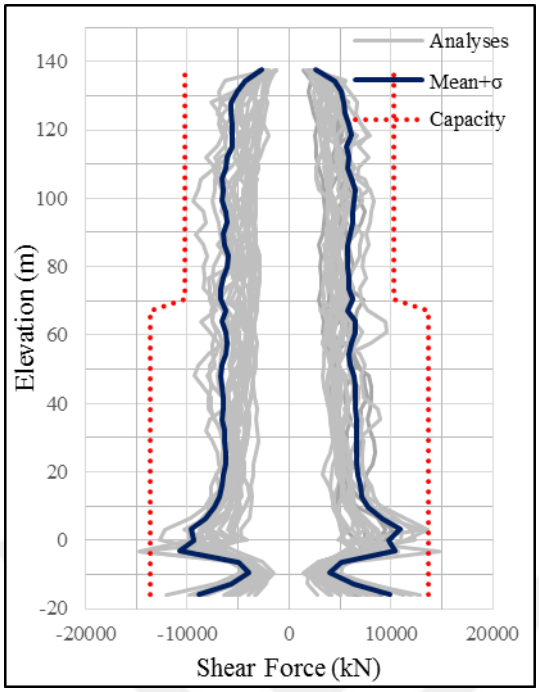

(e)

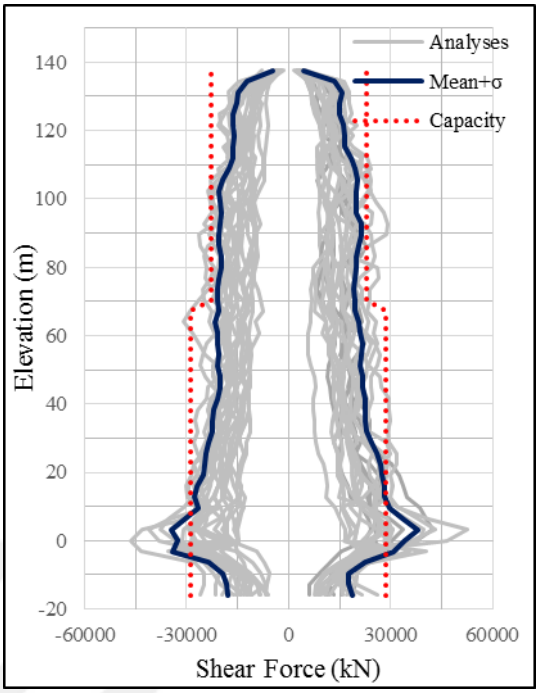

(f)

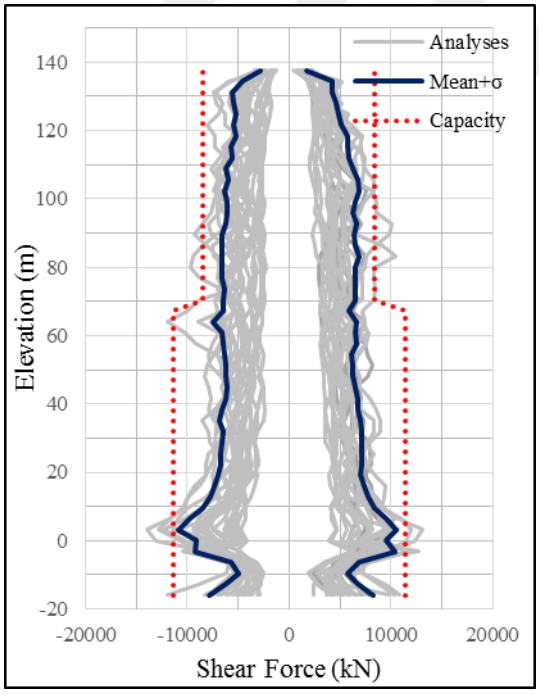

(g)

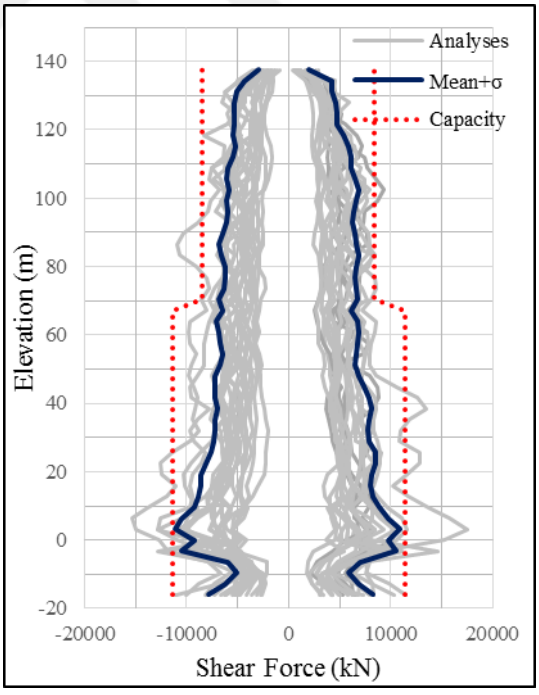

(h)

Figure 3.22. NLRHA structural wall shear force distributions for Tower A at (a) P01A, (b) P02A, (c) P03A, (d) P05A, (e) P06A, (f) P09A, (g) P10A, (h) P12A, (i) P15A, (j) P16A, (k) P21A, (l) P22A (cont.).

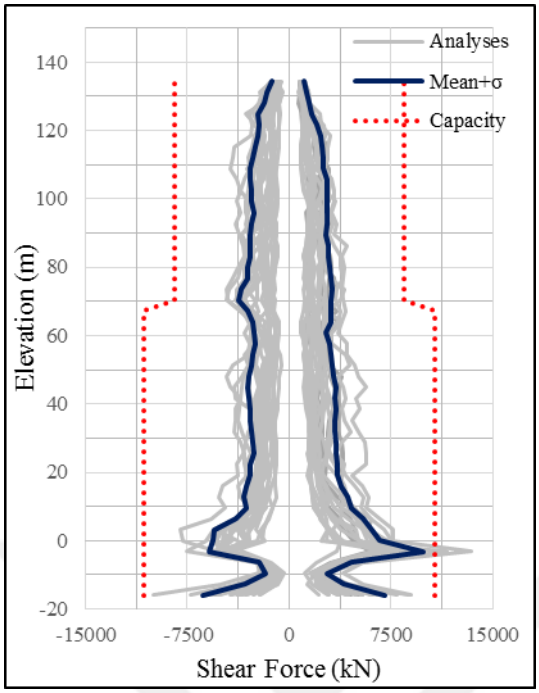

(i)

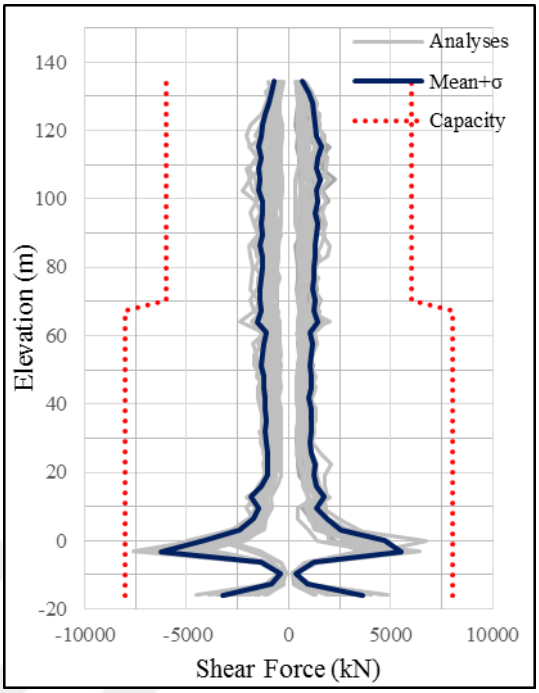

(j)

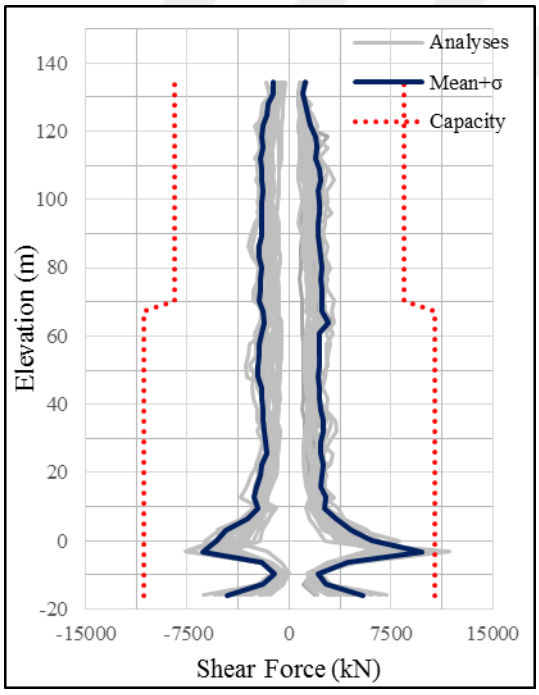

(k)

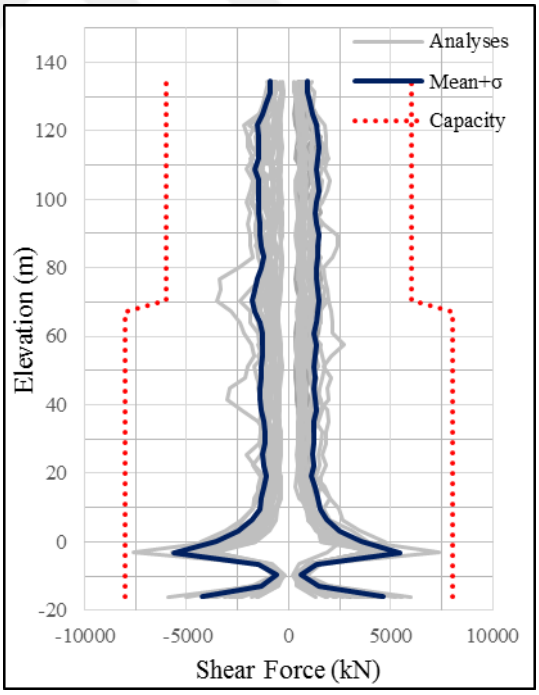

(l)

Figure 3.22. NLRHA structural wall shear force distributions for Tower A at (a) P01A, (b) P02A, (c) P03A, (d) P05A, (e) P06A, (f) P09A, (g) P10A, (h) P12A, (i) P15A, (j) P16A, (k) P21A, (l) P22A (cont.).

For performance based evaluation of nonlinear flexural deformations in structural walls, wall longitudinal strains in compression and tension are checked at critical locations on the walls. These critical points are defined as the two ends (on the cross-section) of all structural wall components. Strain gage results of 22 analyses, as well as their average, are presented in Figure 3.24, for critical locations (Figure 3.23) on selected structural walls of Tower A. Performance limits for longitudinal strains are defined according to Table 3.9, as defined in TEC2017. As shown in Figure 3.24, all of the average strain values obtained from NLRHA are well below IO limit, as is typical for all wall sections in the structure. Therefore, structural walls in Tower A satisfy IO performance criteria, considering flexural strains.

Table 3.9. Strain performance limits for materials.

	Reinforcing Steel (Tension)	Confined Concrete (Compression)
IO	0.0075	-0.0025
LS	0.0240	-0.0135
CP	0.0320	-0.0180

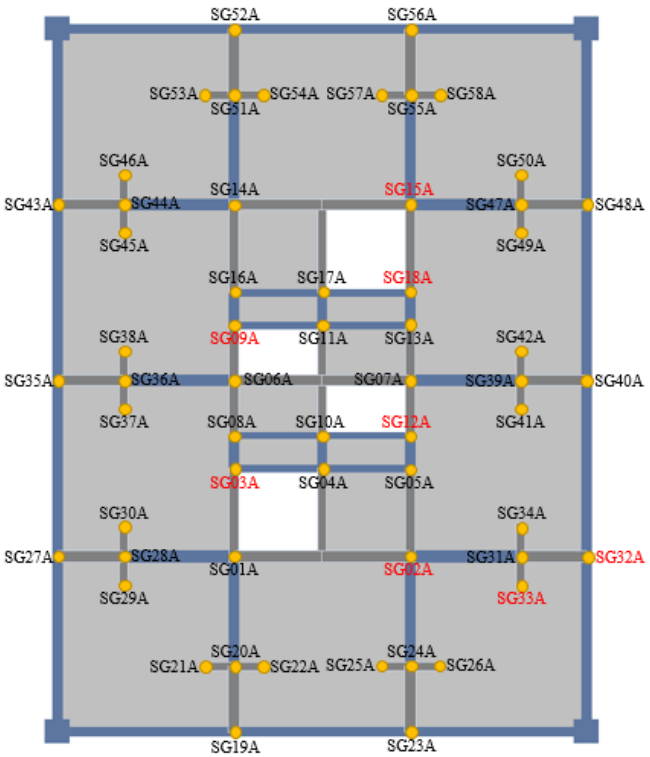

Figure 3.23. NLRHA strain gage location for Tower A.

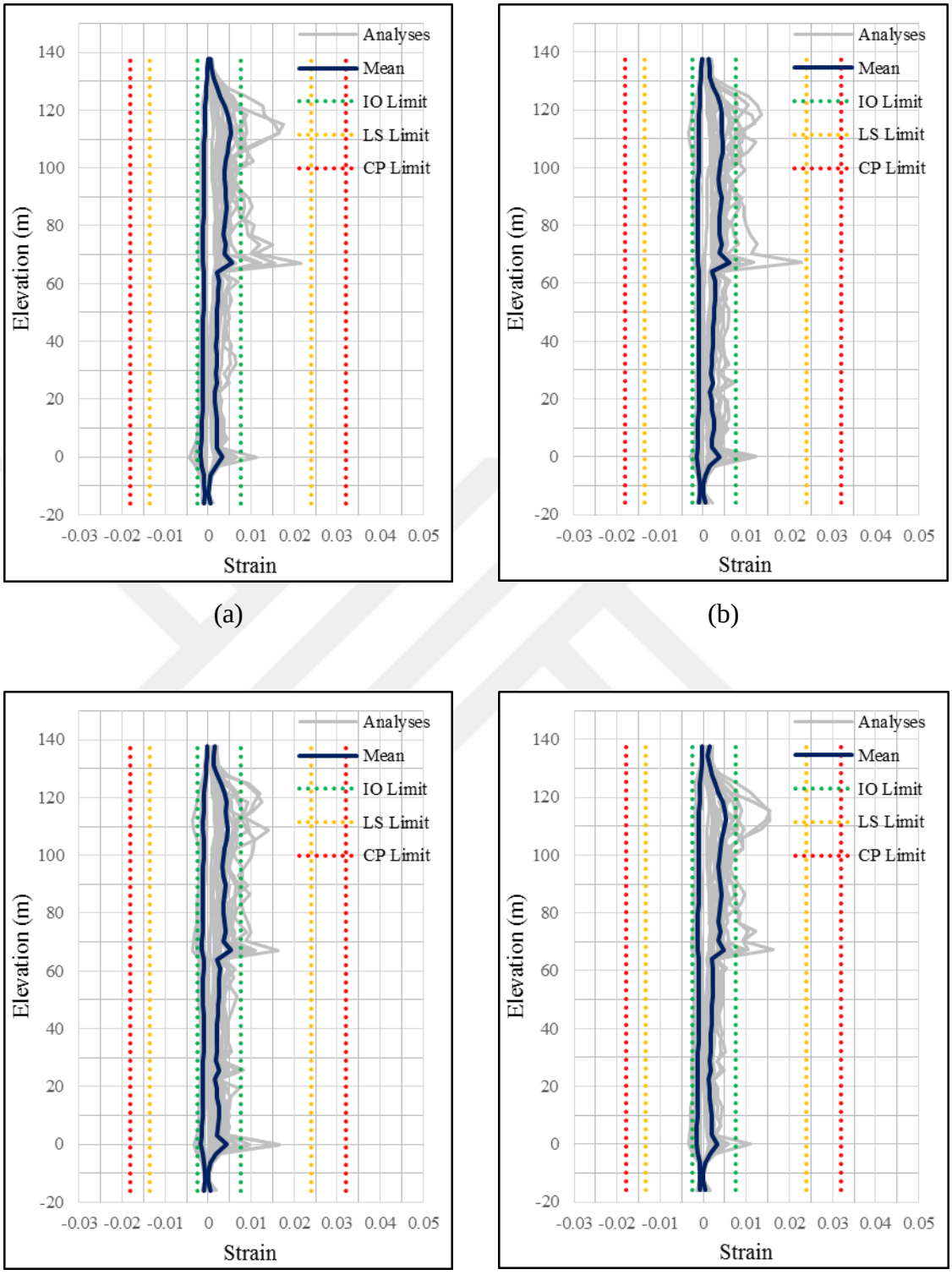

Figure 3.24. NLRHA strain distributions of structural walls for Tower A at (a) SG02A, (b) SG03A (c) SG09A (d) SG12A (e) SG15A (f) SG18A, (g) SG32A, (h) SG33A.

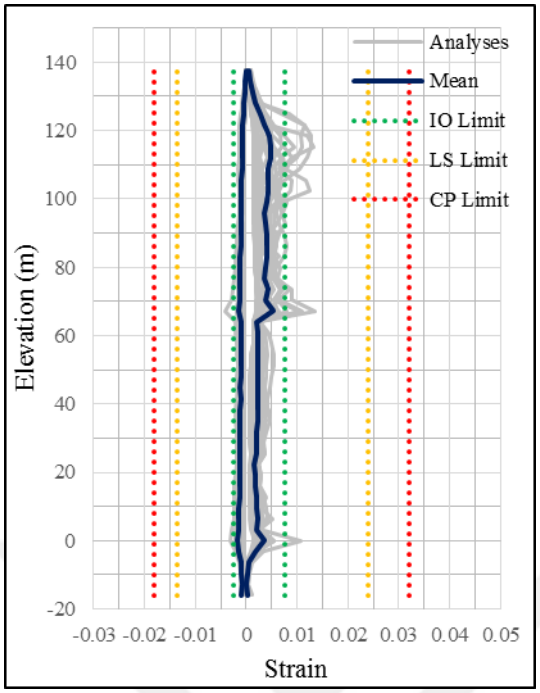

(e)

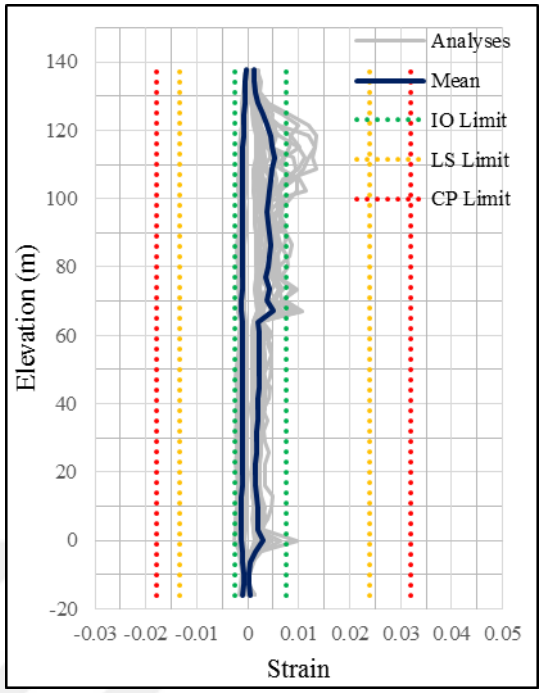

(f)

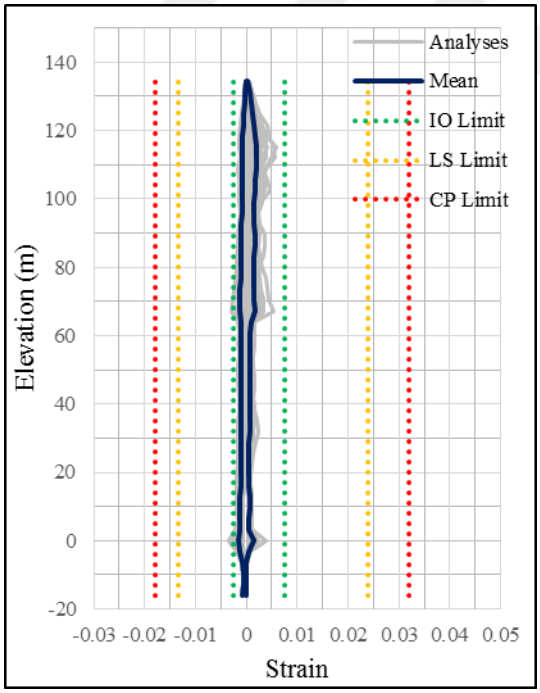

(g)

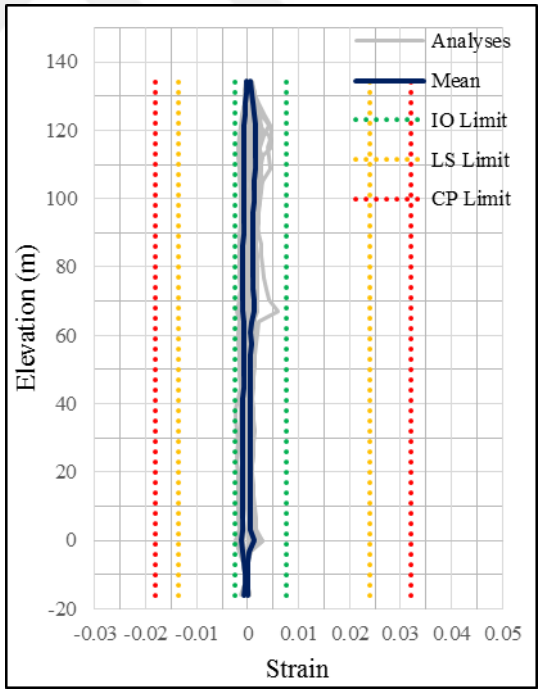

(h)

Figure 3.24. NLRHA strain distributions of structural walls for Tower A at (a) SG02A, (b) SG03A (c) SG09A (d) SG12A (e) SG15A (f) SG18A, (g) SG32A, (h) SG33A (cont.).

3.4.3. Comparison of Single and Double Model Responses for Tower A

In this section, average results of critical response quantities, obtained using double, single-fixed, and single-free models of Tower A are compared. Comparisons of interstory drift ratios, beam plastic rotations, wall shear forces, and wall longitudinal strains are presented in Figure 3.25 to Figure 3.29. As shown in the figures, it is observed that response quantities obtained using double tower model are typically underestimated by the single-tower model with fixed end restraints at the connecting podium levels, whereas the results of the single-tower model with free end restraints are much closer to those of the double-tower model. Overall, NLRHA results show that the single-free model provides results for critical response quantities associated with the seismic performance of the individual tower structure, which are reasonably representative of the results of the comprehensive double-tower model.

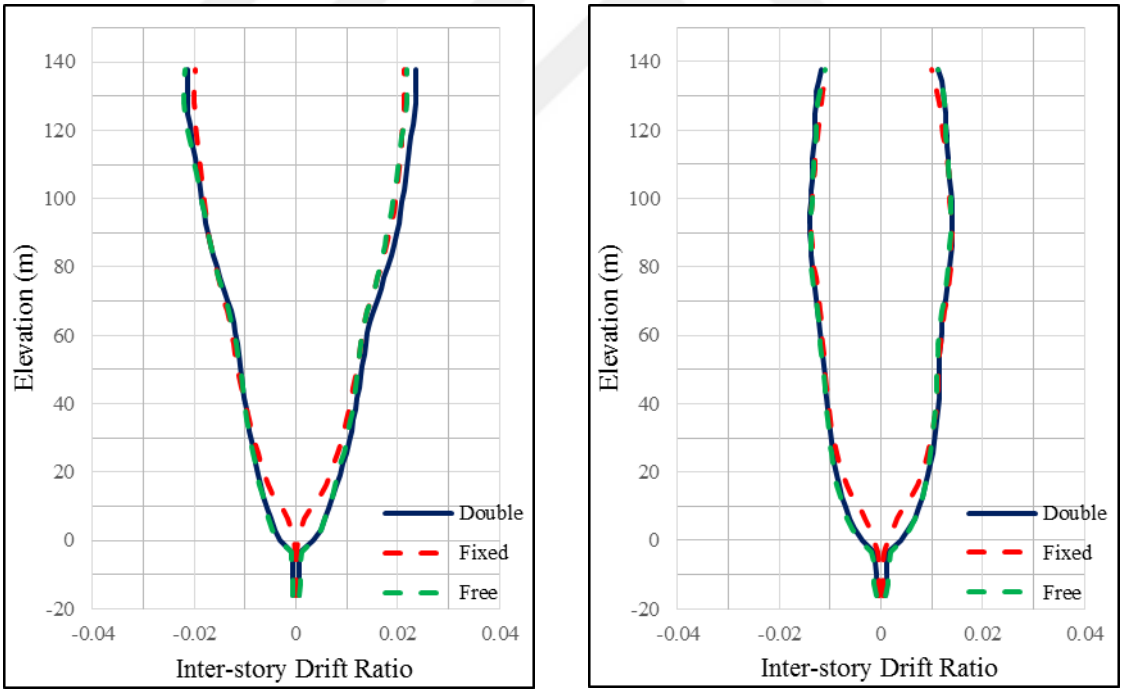

Figure 3.25. Comparison of NLRHA interstory drift ratio distributions for double, fixed and free models of Tower A at (a) DA-X, (b) DA-Y.

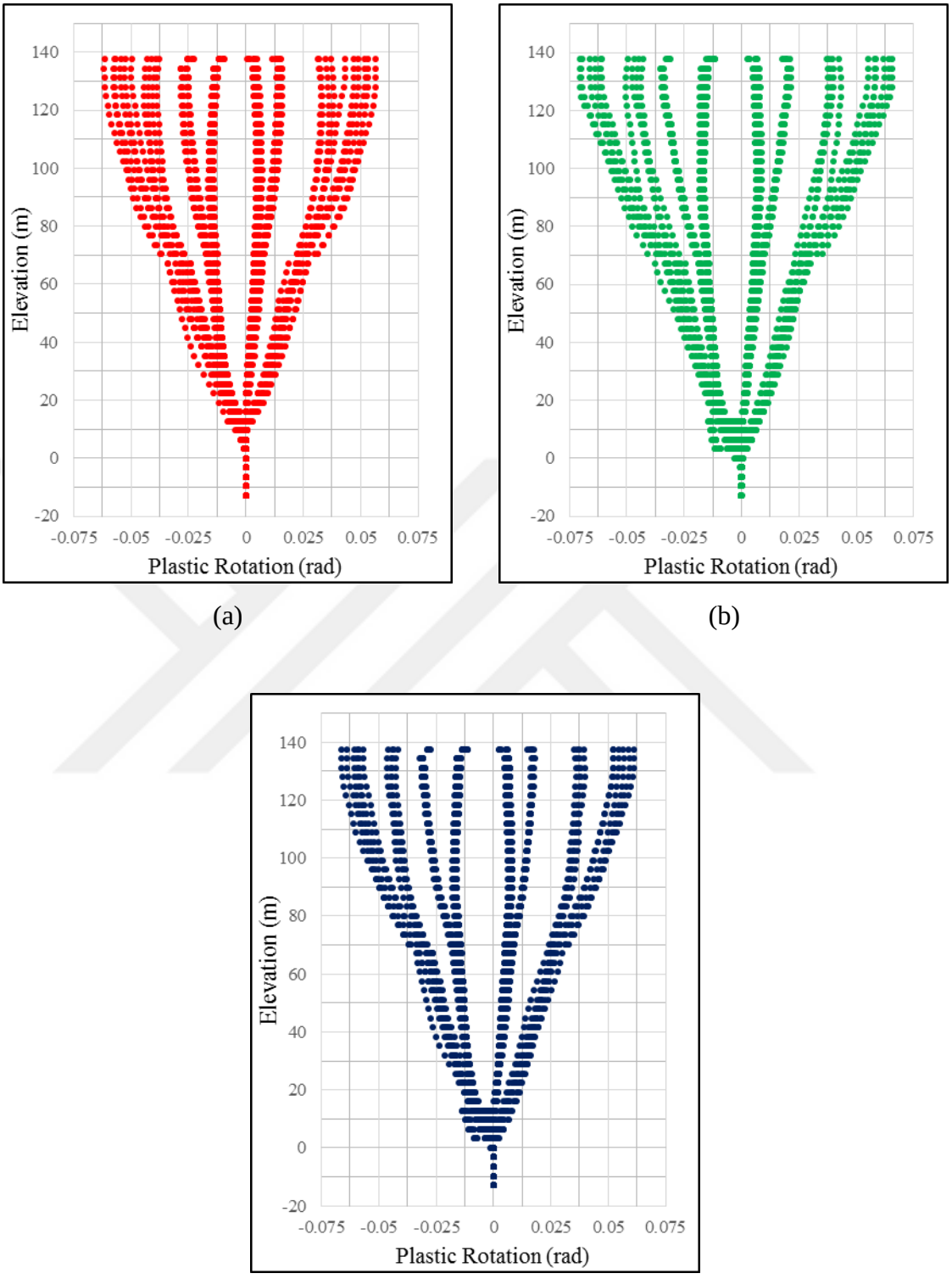

Figure 3.26. Comparison of NLRHA outrigger and perimeter beams plastic rotations for (a) fixed, (b) free, (c) double models of Tower A.

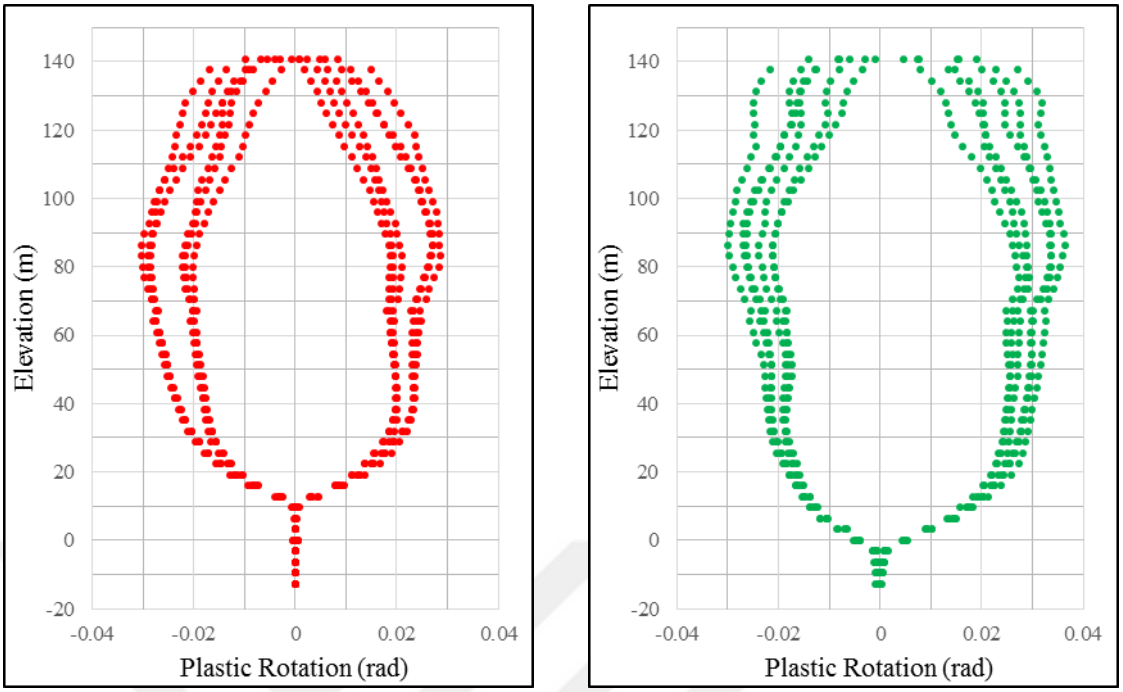

(a) (b)

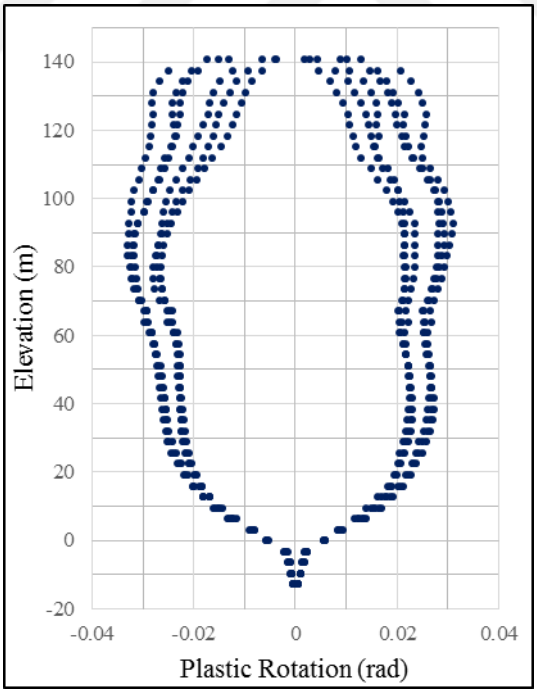

(a)

Figure 3.27. Comparison of NLRHA coupling beam plastic rotations for (a) fixed, (b) free, (c) double models of Tower A.

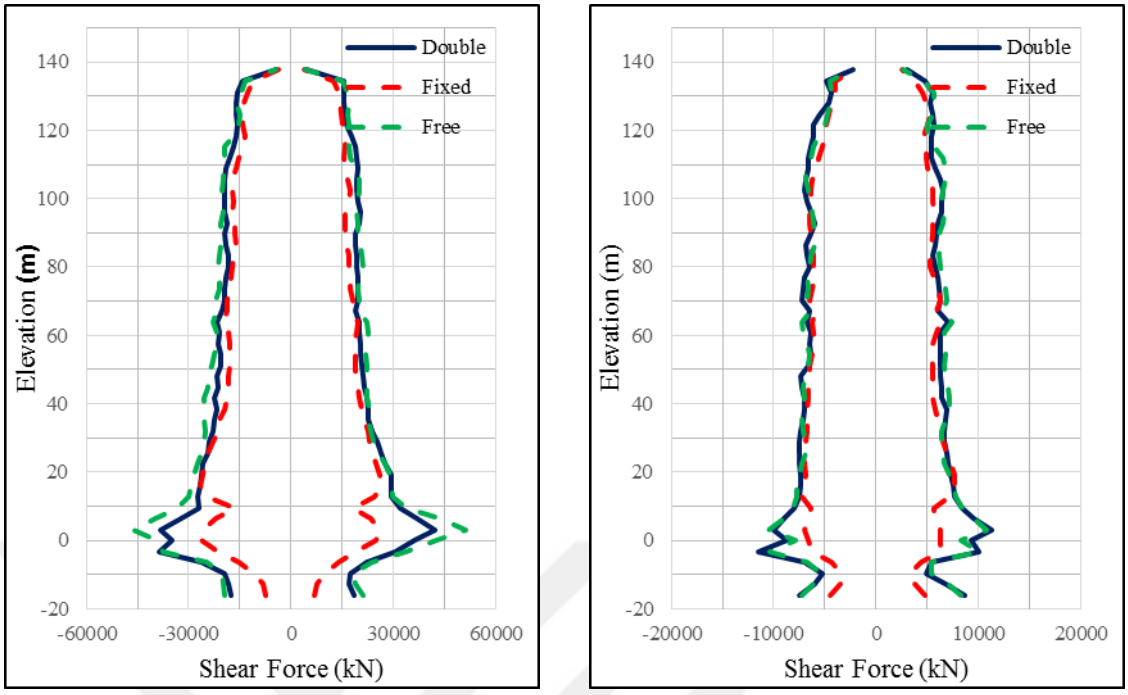

(a)

(b)

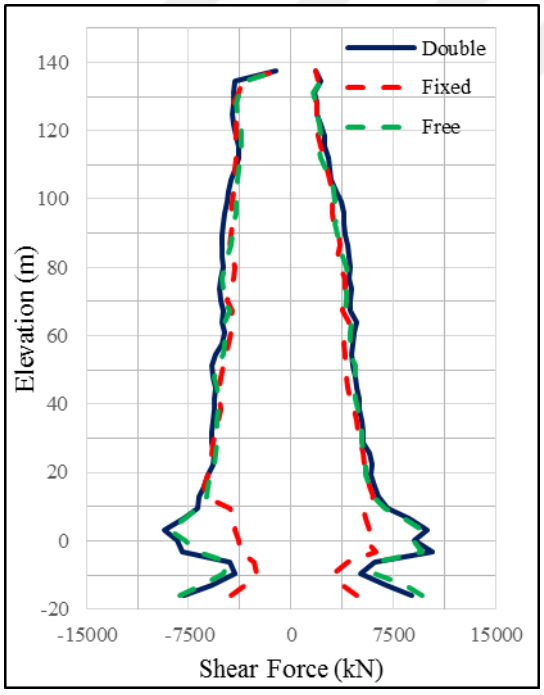

(c)

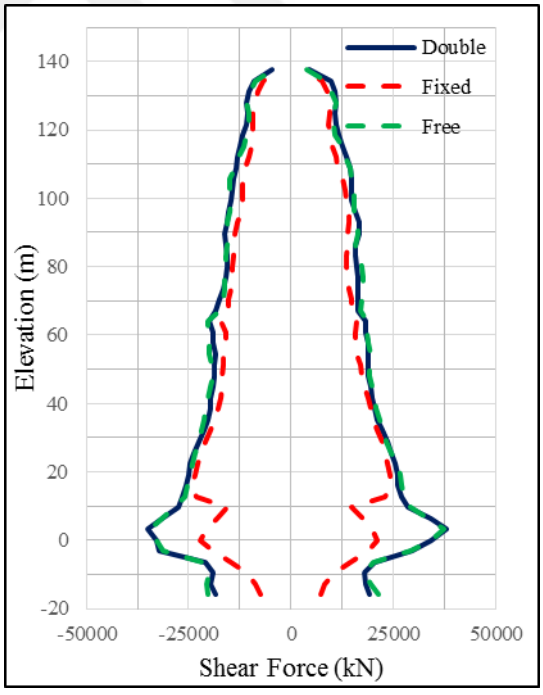

(d)

Figure 3.28. Comparison of NLRHA structural wall shear force distributions for double, fixed and free models of Tower A at (a) P01A, (b) P02A, (c) P03A, (d) P05A, (e) P06A, (f) P09A, (g) P10A, (h) P12A, (i) P15A, (j) P16A, (k) P21A, (l) P22A.

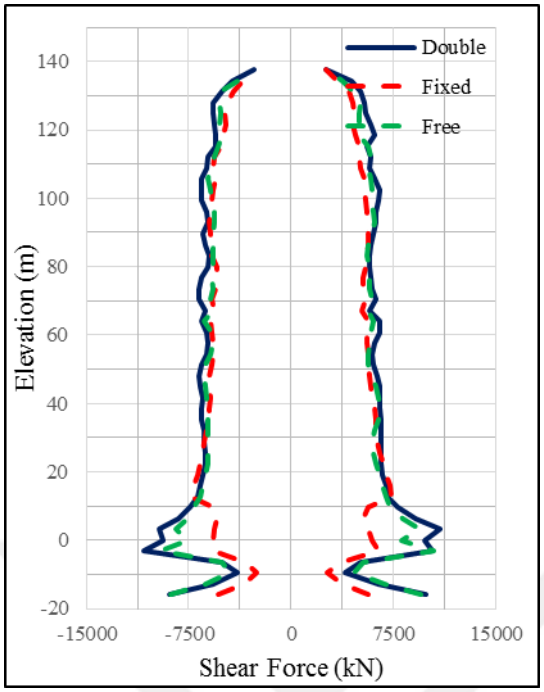

(e)

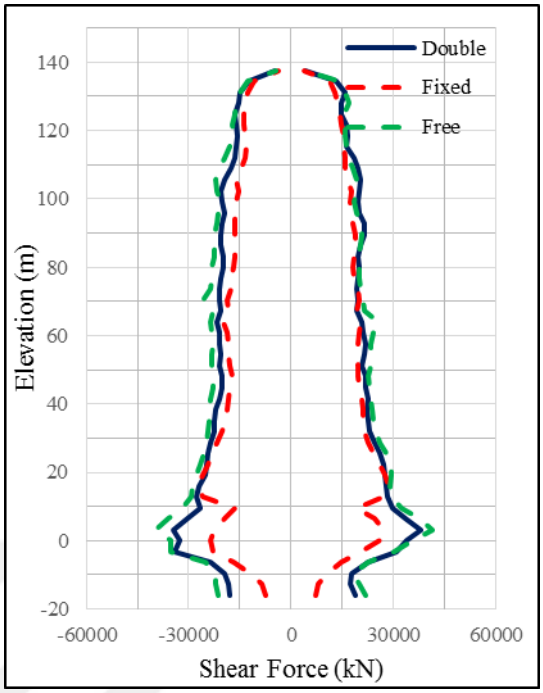

(f)

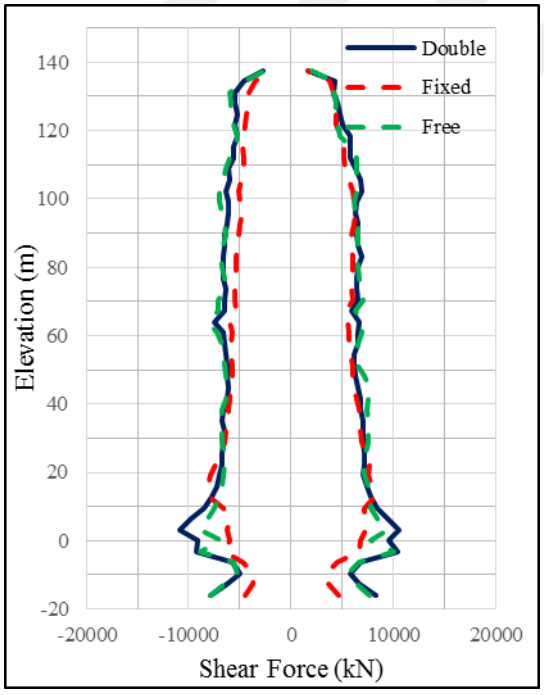

(g)

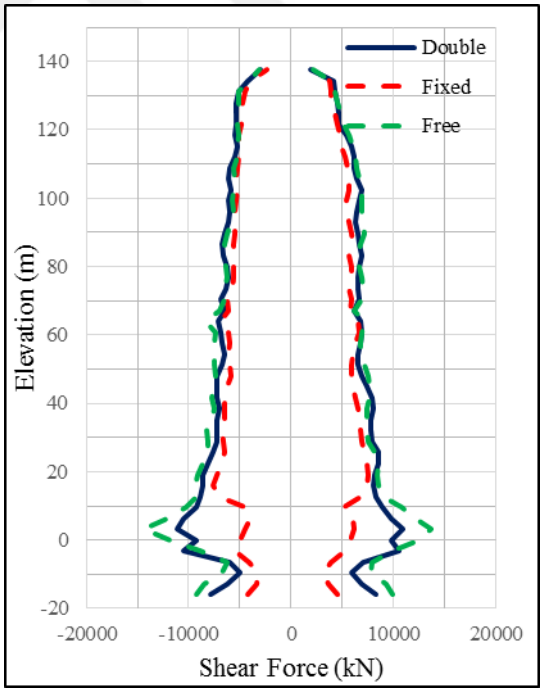

(h)

Figure 3.28. Comparison of NLRHA structural wall shear force distributions for double, fixed and free models of Tower A at (a) P01A, (b) P02A, (c) P03A, (d) P05A, (e) P06A, (f) P09A, (g) P10A, (h) P12A, (i) P15A, (j) P16A, (k) P21A, (l) P22A (cont.).

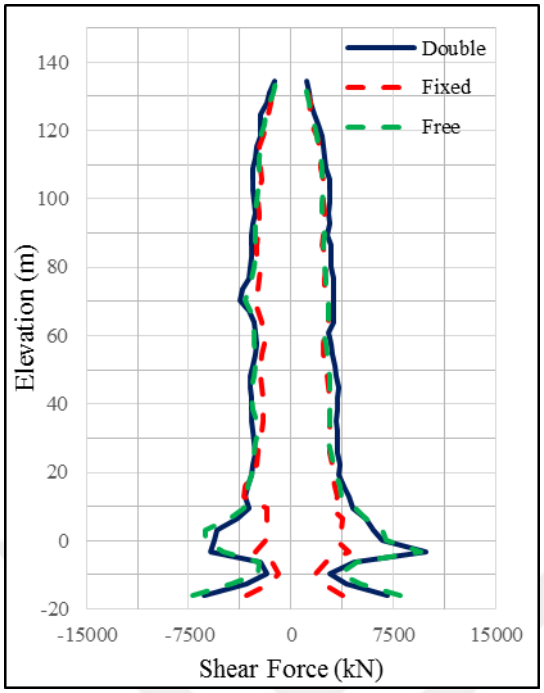

(i)

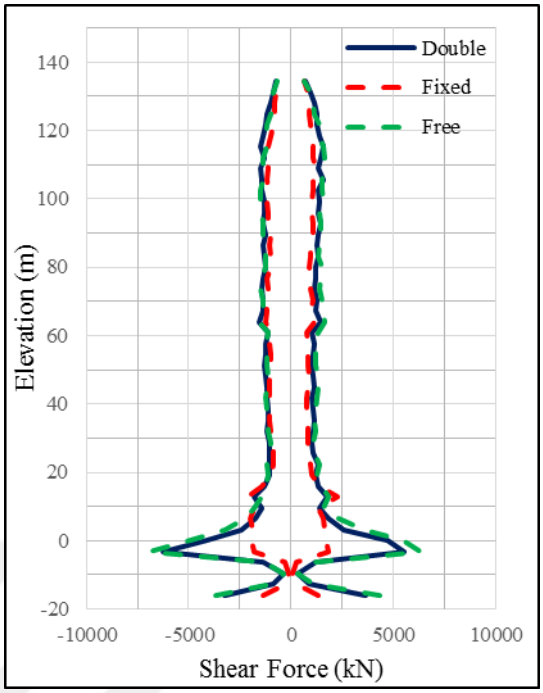

(j)

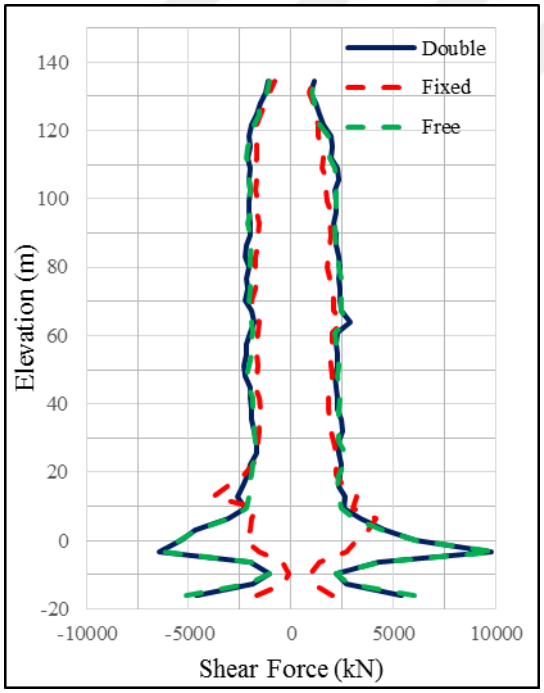

(k)

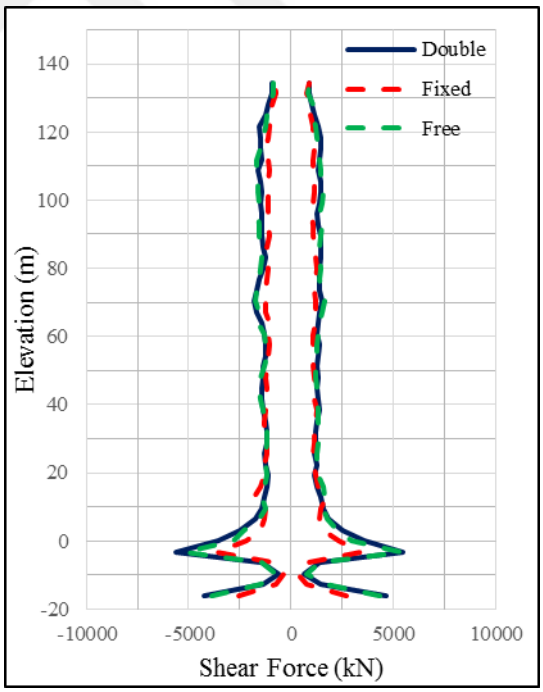

(l)

Figure 3.28. Comparison of NLRHA structural wall shear force distributions for double, fixed and free models of Tower A at (a) P01A, (b) P02A, (c) P03A, (d) P05A, (e) P06A, (f) P09A, (g) P10A, (h) P12A, (i) P15A, (j) P16A, (k) P21A, (l) P22A (cont.).

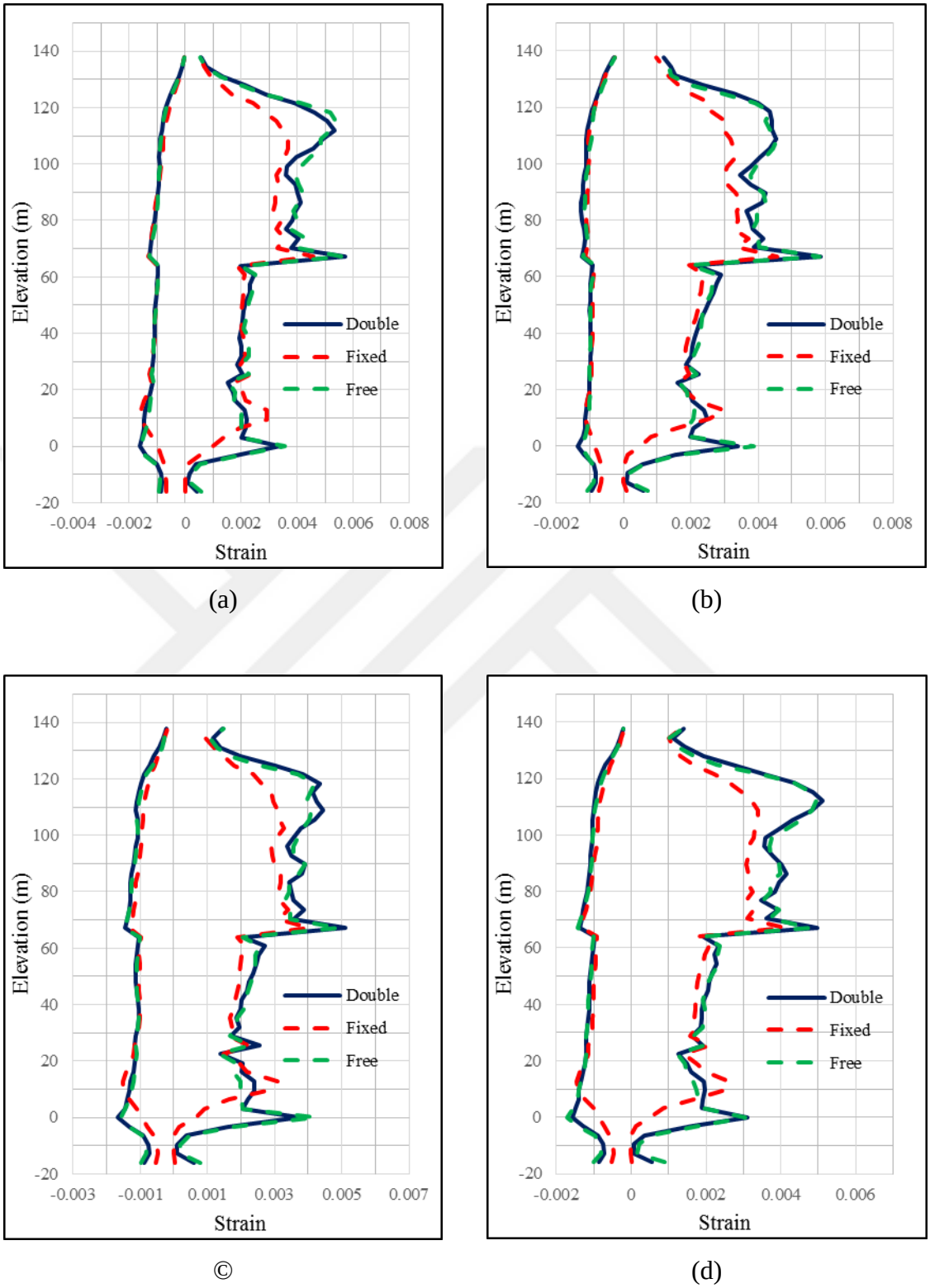

Figure 3.29. Comparison of NLRHA strain distributions of structural walls for double, fixed and free models of Tower A at (a) SG02A, (b) SG03A, (c) SG09A, (d) SG12A, (e) SG15A, (f) SG18A, (g) SG32A, (h) SG33A.

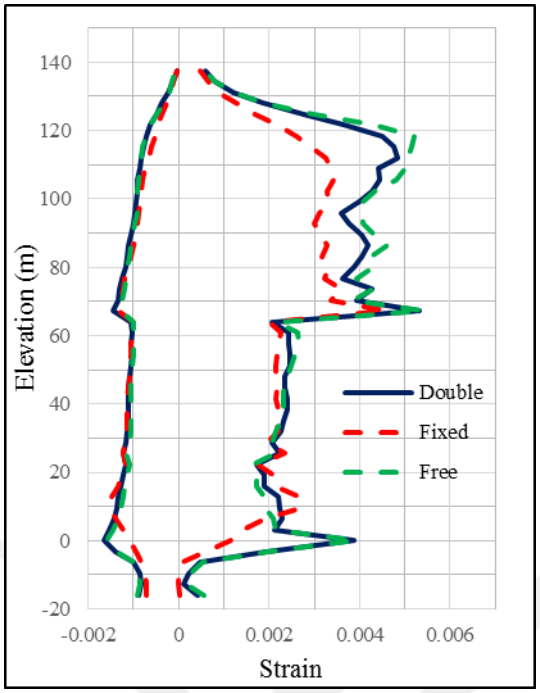

(e)

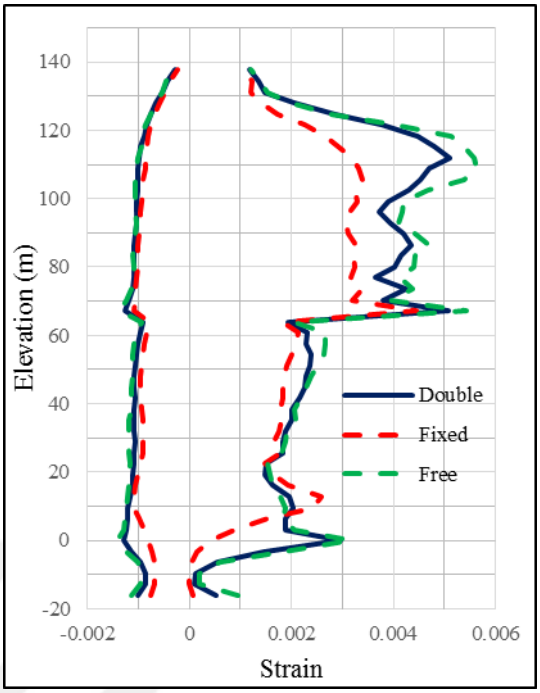

(f)

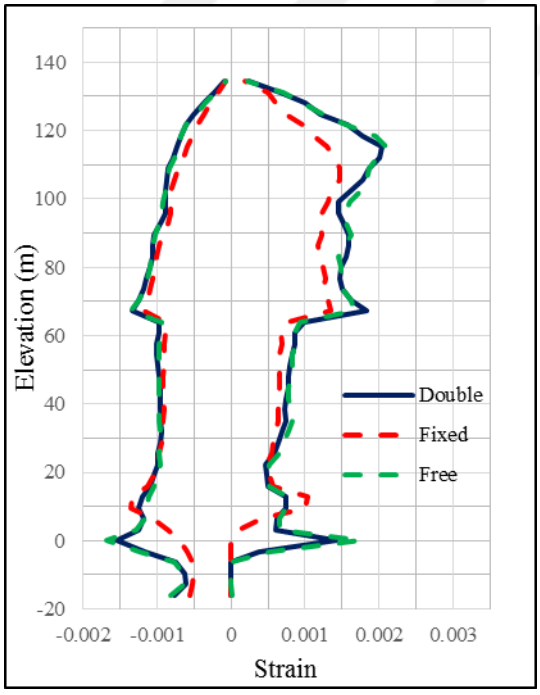

(g)

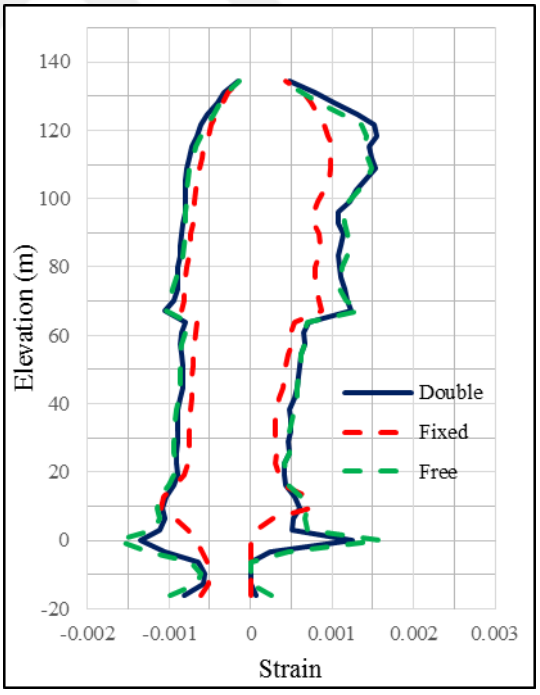

(h)

Figure 3.29. Comparison of NLRHA strain distributions of structural walls for double, fixed and free models of Tower A at (a) SG02A, (b) SG03A, (c) SG09A, (d) SG12A, (e) SG15A, (f) SG18A, (g) SG32A, (h) SG33A (cont.).

4. SUMMARY AND CONCLUSIONS

4.1. Overview

In this study, a hypothetical structure with multiple towers on a common base is analyzed, considering interaction effects between two towers. Linear and nonlinear models of the structure are generated. For linear elastic response analysis of the structure, various analysis methods including response spectrum analysis, modal response history analysis, and direct integration response history analysis, are performed using the software CSI ETABS. For nonlinear response and seismic performance assessment of the structure, nonlinear response history analyses are conducted using Perform 3D software.

Diaphragm effects on the connected podium floors due to the interaction behavior are compared, considering results of different analysis approaches. In plane tensile and shear force distributions developing in the diaphragms are evaluated and corresponding reinforcement designs to achieve sufficient diaphragm capacity are presented. Furthermore, feasibility of relatively simple modeling and analysis approaches, using partial models of the multiple tower structure together fixed or free boundary conditions at locations where the connecting podium floors intersect, is investigated, in order to produce a safe design approach against podium diaphragm effects and to obtain reliable seismic performance predictions for the individual towers.

4.2. Conclusions

Under the light of the analysis results obtained using different modeling approaches and analysis methods used in this study, the following conclusions can be drawn:

- When results of linear elastic analysis methods (RSA and LMRHA) conducted using both double (combined double tower) and single-fixed (single tower with fixed end restraints) model results are compared, RSA provides diaphragm force resultants that are only approximately 10% larger than LMRHA at critical podium levels. The difference between results of the two analysis methods increase to 25% only for

diaphragm shear forces obtained using the double model, yet these diaphragm shear forces are relatively small in magnitude.

- When linear elastic analysis results using the double and single-fixed models are compared, it is observed that the single-fixed model can provide diaphragm tension forces that are up to 75% higher that the double model results, independently from the analysis method used (RSA or LMRHA). However, this percent difference increases to more than 100%, when diaphragm shear forces are considered, also because the diaphragm shear force magnitudes are small.

- When results of NLRHA obtained using double and fixed models are compared, it is observed that the fixed model can provide diaphragm force resultants at critical sections that are almost twice those calculated using the double model.

- NLRHA of the double model of the structure gives approximately 20-30% higher diaphragm tensile forces compared to RSA of the double model. On the other hand, in case of diaphragm shear forces, NLRHA results obtained using the double model are almost twice those obtained from RSA at critical sections. Although NLRHA gives higher diaphragm forces, the total amount of required diaphragm reinforcement for tension is 5% to 15% less than RSA, since expected material strengths are used for design based on NLRHA results. Additionally, diaphragm shear forces obtained in both analyses do not exceed concrete shear strength limits, not necessitating any diaphragm shear reinforcement.

- Differently from the double model, when fixed model is used in the analysis, NLRHA can give 50% higher diaphragm tensile forces compared to RSA. On the other hand, diaphragm shear forces from NLRHA are approximately twice those obtained by RSA, similarly to the double model. When required reinforcement amounts against diaphragm tension are compared, NLRHA results using the fixed model require approximately 10% larger amount of reinforcement, compared to RHA of the fixed model.

- Interestingly, the amount of diaphragm reinforcement obtained from NLRHA of the double model, which is the most robust and reliable analysis approach, is less than the reinforcement amount obtained from RSA of the single fixed model, which is the simplest analysis approach that can be used for diaphragm design. This happens mostly because the fixed model overestimates the diaphragm effects in the connecting podium floors, and also because the design based on NLRHA uses expected material strengths, rather than reduced design strength values for the materials.

- NLRHA results show that the single-free (single tower with free end restraints) model provides results for critical response quantities associated with the seismic performance of the individual tower structures (interstory drifts, wall strains, wall shear forces, beam plastic rotations, etc.) that are close to results of the double model.

- Overall, out of phase response of multiple towers may cause additional problems at critical podium diaphragms between towers that must be considered in design stage. Taking into consideration of analysis durations, and modeling complexity, it is recommended to use single-tower models with free end restraints for design of the individual towers, and single-tower models with fixed end restraints for design of the podium slabs for in-plane axial load and shear forces, whenever comprehensive analyses using a combined multiple-tower model is not possible.

4.3. Recommendations for Future Studies

The following recommendations can be made for future studies related with the scope of this thesis:

- The methodology presented must be applied to different structural configurations, with variable differences in the dynamic characteristics of the individual tower structures, for the results of this study to be generalized. As well, sensitivity of the results to differences in the levels of seismic hazard can be investigated.

- As a simple modeling methodology, instead of assigning fixed end restraints at the continuous boundaries of the structure, use of linear springs and the method of

calibration for the spring stiffness values can be investigated. Furthermore, modeling approaches that consider soil-structure interaction and incorporate foundation flexibility into the analysis can be adopted.

- Instead of using elastic shell elements with effective axial rigidities, in-plane behavior of slab elements can be modeled using fiber section models, in order to obtain more realistic axial stiffness values for the diaphragm members and to evaluate the diaphragm performance using a nonlinear approach.

REFERENCES

Applied Technology Council, 2010, *Modeling and Acceptance Criteria for Seismic Design and Analysis of Tall Buildings*, ATC72-1, Pacific Earthquake Engineering Research Center, California.

ASCE/SEI Seismic Rehabilitation Committee, 2014, *Seismic Evaluation and Retrofit of Existing Buildings*, ASCE/SEI41-13, American Society of Civil Engineers, Reston, VA.

Behnamfar F., Dorafshan S., Taheri A., Hashemi B. H., 2015, "A Method for Rapid Estimation of Dynamic Coupling and Spectral Responses of Connected Adjacent Structures", *The Structural Design of Tall and Special Buildings*, Vol. 25, pp: 605-625.

Chopra A. K., 1995, *Dynamics of Structures, Theory and Applications to Earthquake Engineering*, Prentice Hall, Englewood Cliffs, New Jersey.

Computers and Structures Inc., 2006, *Perform 3D Nonlinear Analysis and Performance Assessment for 3D Structures, User Guide, Version 4*, Computers and Structures Inc., Berkeley, California.

Computers and Structures Inc., 2006, *Perform Components and Elements for Perform 3D and Perform Collapse, Version 4*, Computers and Structures Inc., Berkeley, California.

Computer and Structures, Inc., 2011, Perform 3D V6.0.0: Nonlinear Analysis and Performance Assessment for 3D Structures, California, USA.

Disaster and Emergency Management Presidency, 2017, *Turkish Earthquake Hazard Map* https://testtdth.afad.gov.tr/, accessed at June 2017.

ETABS Ultimate v16.1.0, 2017, Extended 3D Analysis of Building Structures, Computers and Structures, Inc., California, USA.

Mander J. B., Priestley M. J. N., Park R., 1988, "Theoretical Stress-Strain Model for Confined Concrete", *ASCE Journal of Structural Engineering*, Vol. 114, No. 8, pp. 1804-1826.

Naish D., Fry A., Klemencic R. and Wallace J. W., 2009, "*Experimental Evaluation and Analytical Modeling of ACI 318-05/08 Reinforced Concrete Coupling Beams Subjected to Reversed Cyclic Loading*", UCLA SGEL report2009/06, University of California, Los Angeles.

Los Angeles Tall Buildings Structural Design Council, 2015, *An Alternative Procedure for Seismic Analysis and Design of Tall Buildings Located in the Los Angeles Region*, Los Angeles Tall Buildings Structural Design Council, California.

Pacific Earthquake Engineering Research Center, 2010, *Guidelines for Performance-based Seismic Design of Tall Buildings*, Report PEER-2010/05, Pacific Earthquake Engineering Research Center, University of California.

Pasific Earthquake Engineering Research Center, 2013, *Next Generation Attenuation-West2*, http://ngawest2.berkeley.edu/, accessed at June 2017.

Powell, G. H., 2010, *Modeling for Structural Analysis, Behavior and Basics*, Computers and Structures Inc. Berkeley, California.

Turkish Earthquake Code, 2017, *Specifications for Structures to be Built in Disaster Areas*, Turkish Earthquake Code Draft, Disaster and Emergency Management Presidency, Ankara.

Turkish Standards Institute, 1997, *Design Loads for Buildings*, TS498, Turkish Standards Institute, Ankara.

Turkish Standards Institute, 2000, *Requirements for Design and Construction of Reinforced Concrete Structures*, TS500, Turkish Standards Institute, Ankara Turkey.

Qi Xiaoxuan, Chen Shuang, 1996, “Dynamic Behavior and Seismic Design of Structural Systems Having Multiple High-rise Towers on a Common Podium,Paper No. 1101”, Sociedat Mexicana De İngenieria Sismica, *Eleventh World Conference on Earthquake Engineering*, Acapulco, Mexico, June’23-28, 1996, Elsevier Science Ltd., California.